

**MECHANICAL AND ELECTROCHEMICAL PROPERTIES OF
INCONEL ALLOY 617 AFTER REFURBISHMENT THROUGH
HEAT TREATMENT**

by
Mahmoud H Kawthar-Ali, BS & MS in Mech Eng

August, 2002

This thesis is submitted to Dublin City University as the fulfillment of
The requirement for the award of degree of

Doctor of Philosophy

Supervisors

Professor M S J Hashmi

Professor B S Yilbas

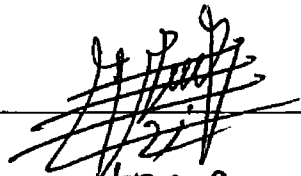
School of Mechanical & Manufacturing Engineering
Dublin City University

DECLARATION

I hereby certify that this material, which I now submit for assessment on the program of study leading to the award of Doctor of Philosophy is my own work and has not been taken from the work of others save and to the extent that such work has been cited and acknowledged within the text of my work

Signed

Date


August 12, 2002

ID No 97971154

ACKNOWLEDGMENT

First and foremost, all praise is to the Almighty, ALLAH Who gave me the courage and patience to carry out this work

My deep appreciation goes to my Ph D thesis advisors Professor M S J Hashmi (Dublin City University, Ireland) and Professor B S Yilbas (King Fahd University of Petroleum and Minerals, Saudi Arabia) for their valuable guidance throughout all phases of this work, for checking and developing the research material, for offering valuable suggestions and for their critic reading of the manuscript. They were always kind, understanding and sympathetic to me. Working with them were indeed a wonderful and learning experience, which I thoroughly enjoyed.

Sincere and many words of thanks are to my father. Last but not least, I owe my beloved family, an expression of gratitude for their patience, encouragement, moral, and material support which made this work possible.

TABLE OF CONTENTS

DECLARATION	2
ACKNOWLEDGMENT	3
ABSTRACT	5
CHAPTER 1	6
INTRODUCTION	6
SCOPE OF THE PRESENT WORK	15
CHAPTER 2	16
LITERATURE REVIEW	16
Summary Of Literature Review Associated With The Present Work	61
CHAPTER 3	62
EXPERIMENTAL WORK	62
Microstructural analysis	62
Mechanical Tests	62
Electrochemical Analysis	63
Experimental Conditions and Apparatuses	63
CHAPTER 4	78
RESULTS AND DISCUSSIONS	78
CHAPTER 5	112
CONCLUSIONS AND RECOMMENDATION FOR FUTURE WORK	112
RECOMMENDATION FOR FUTURE WORK	115
REFERENCES	116
PAPERS IN CONFERENCES AND JOURNALS	126

Title of Thesis Mechanical And Electrochemical Properties Of Inconel Alloy 617 After Refurbishment Through Heat Treatment

Name of Student Mahmoud Hashim Kawthar-Ali **Student No** 97971154

ABSTRACT

The transition piece in gas turbine is an important component, which joins the combustion chamber to the turbine nozzles. These pieces are made from an alloy that resist high temperature and thermal loading and being considerably expensive. The high operating temperature and thermal fatigue limit the lifetime of such component. Consequently, the life extension of the alloy through sound refurbishment process is in demand. The refurbishment of Inconel 617 alloy after 37000 hours of operation in the field is considered through heat treatment process. Tensile and fatigue properties, as well as microstructures and elemental composition of the alloy before and after the heat treatment process are investigated. In addition, the electrochemical response of the heat-treated alloy is investigated through potentiodynamic surface testing. The heat treatment process is carried out at 1175 °C for one and two hours in air free furnace. It is found that the heat treatment of the alloy for one hour partially improves the cavitations at grain boundaries and the fatigue response of the workpiece partially improves. Further, dimples at grain boundary facets was noticed after the heat treatment which is an evident of ductility of the workpieces. Moreover, the corrosion resistance improves considerably for the workpieces subjected to one-hour heat treatment. Consequently heat treatment of the Inconel 617 alloy after long term of operation improves slightly its properties and partial regaining of the alloy properties thought heat treatment with temperature rang and the duration employed in the present work is visible.

CHAPTER 1

INTRODUCTION

In the history of the development of gas turbine, when goals were either high efficiency or high work output for a given size, the designer moves to higher operating temperature. This is the historical fundamental reason for the development of superalloys. Hence, superalloys development was a response to the need for materials, which have high creep and fatigue resistance at elevated temperatures. Superalloys are expensive materials because of rareness of the raw material and the involvement of manufacturing process. Currently, there are wide use of superalloys in petrochemical industries as well as power generation plants where huge quantities of superalloy pieces are being withdrawn due to the utilization of their useful life. These pieces are expensive and their reutilization is in demand. The development of sound refurbishment technique will allow the reutilization of these pieces and hence saving the limited raw supply and money.

Superalloy is an alloy developed for elevated temperature service where relatively severe mechanical stress is encountered and where surface stability is often required. Superalloys are mainly divided into three classes: nickel-base superalloys, cobalt-base superalloys, and iron-base superalloys. They have a face-centered cubic (fcc, austenitic) structure. Normally commercial nickel and cobalt-base superalloys contain substantial alloying additions in solid solution to provide strength, creep resistance, or resistance to surface degradation. In addition, nickel-base superalloys contain elements that, after suitable heat treatment or thermo-mechanical processing, result in the formation of small

coherent particles of an intermetallic compound Mott and Nabarro [1] concluded that both solid solution hardening and precipitation hardening of superalloys are due to internal strains generated by inserting either solute atoms or particles in an elastic matrix In this work we are concerning with nickel-based superalloy

Nickel-base superalloys are vitally important to modern industry because of the ability to withstand a wide variety of severe operating conditions involving corrosive environment, high temperature, high stresses and combination of these factors The chief alloying elements of nickel base superalloys are chromium, cobalt, molybdenum and aluminum The major contribution to the strength of precipitation-hardened nickel-base superalloy is provided by coherent stable intermetallic compounds such as γ' [$\text{Ni}_3(\text{Al},\text{Ti})$] and γ'' [$\text{Ni}_3(\text{Cb},\text{Al},\text{Ti})$] Other phases like carbides such as M_{23}C_6 and M_6C or borides such as M_3B_2 provide significant effects on creep rate, rupture life and rupture strain through their influence on grain boundary properties [2]

Nickel base superalloys are widely used in the gas turbines industry In gas turbines the parts are subjected to combine effects of mechanical and thermal stresses, high temperatures and corrosive environments The output and efficiency of the turbine system increases as the hot gas temperature increases at turbine inlet Consequently, an improvement of the turbine is dependent on the development of materials, which can resist high stresses and heavy corrosive effects at elevated temperatures

Inconel 617 alloy is a face-centered-cubic solid solution nickel-based superalloy, which contains chromium, cobalt, molybdenum, and aluminum Inco Alloy International [3] invented Inconel 617 alloy in the 1970 Solid solution strengthening is provided by

the cobalt and molybdenum. The aluminum and chromium provide oxidation resistance at high temperatures, and the high nickel and chromium contents enable the alloy to resist a variety of oxidizing media [4]. Its carburization resistance at high temperatures is superior to that of Inconel 600, Inconel 601, and Inconel 625 [5]. Strengthening of the alloy during exposure to temperature was found to result primarily from the precipitation of $M_{23}C_6$ type carbide. The phase provides effective strengthening because it precipitates in discrete particles and remains stable at temperatures to 1093 °C. The amount of gamma prime formed is not sufficient to cause appreciable hardening, but it does provide some strengthening at 649 to 760 °C [6]. The combination of high strength and oxidation resistance at elevated temperatures makes the alloy attractive for gas turbine engine, industrial furnace components and applications where high-temperature corrosion resistance is important. The alloy is especially useful at temperatures in excess of 980 °C.

The Gas Turbine like any other heat engine, is a device for converting part of a chemical energy (fuel) into useful available mechanical power. It does this in a manner similar in many ways to the system used by the four stroke cycle reciprocating internal combustion engine. The main difference is that work is accomplished in an intermittent manner in the reciprocating engine, whereas the turbine power process is continuous throughout.

Figure 1.1 shows a simple illustration of gas turbine in its power generation (or mechanical drive) in which air is drawn into the compressor, usually through an air filter situated in a "filter house" to remove any harmful solid particles from the air stream.

This air is then compressed to a designed value by a multi-stage axial or centrifugal compressor. The hot, compressed air is then fed to the combustion system where it mixes with injected fuel. Here the fuel burns and adds its energy to the air. The combustion process rises the air temperature to a flame zone value between 1370 °C and 1760 °C, which is immediately reduced to usable values by the mixing of secondary air that enters the combustion chamber through properly placed holes. This hot, high pressure gas mixture is then ducted to the turbine section where it is allowed to expand down to exhaust temperature. In the expansion process, enough energy is removed from the gas to drive the compressor, the unit driven auxiliaries such as the accessory gear box, fuel pump, cooling water pumps, lube oil pumps, etc. and the load (i.e. alternator, compressor, pump etc). The used gas is then allowed to flow to the exhaust stack system. Since there is still much heat energy in this gas, it can be put to use in a variety of ways, such as air or water heating process drying or as hot air feed supply to a separately fired boiler, waste heat recovery boiler. Any of these heat recovery methods helps to increase the overall thermal efficiency of the turbine cycle.

Several types of compressors are available for Gas Turbine applications. They are centrifugal, Axial Flow and the Intermeshing Lobe Types. All have been used by different manufacturers. All the large turbine uses axial flow type primarily for its ability to pump large volumes of air at better efficiency levels than either the centrifugal or lobe types. Axial flow compressors are so designed that the air moves axially through the blading with essentially no radial travel. This type of compressor is made up of rows of air-foiled shaped blades with each set of rotating blades followed by a set

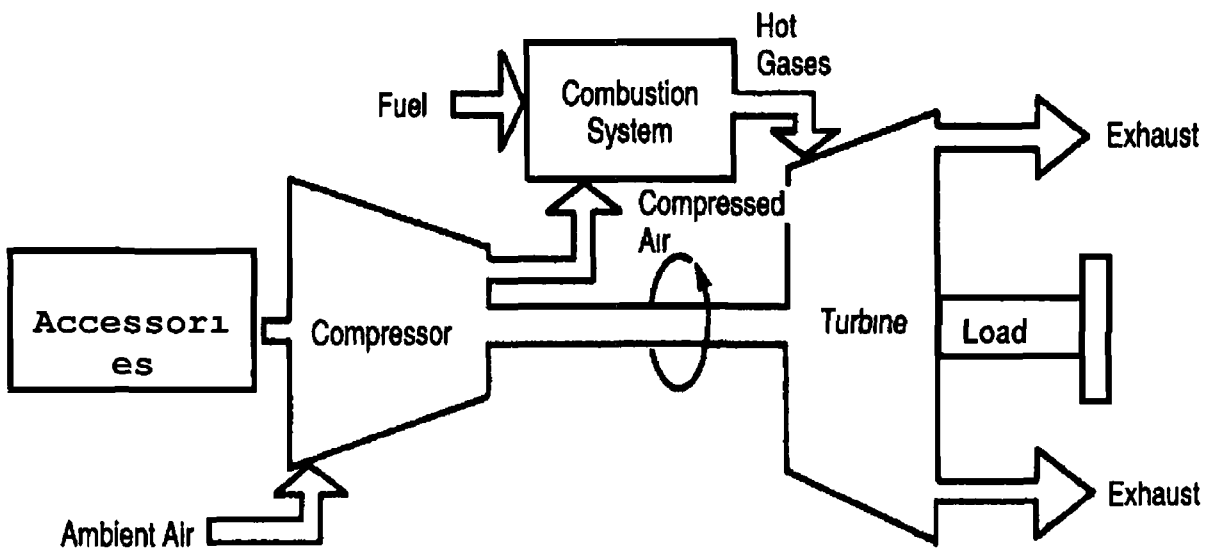


Figure 1 1 Schematics of a gas turbine

of similar stationary blades. Most commercial compressors are designed to divide the pressure rise about equally between rotor and stator.

It is within the turbine section of a gas turbine that part of the thermal energy contained in the hot gas provided by the combustion system is converted into mechanical energy. Sufficient mechanical energy should be taken out of the gas stream to supply the power necessary to drive the axial-flow main compressor, the turbine unit driven auxiliaries (i.e. lube oil and fuel pumps etc), and provide power to overcome bearing frictional losses. Yet reasonable amount of enough excess energy is still available to do an external work (i.e. drive a generator, load compressor etc).

Two main types of turbine designs are used for energy conversion. They are called Reaction and Impulse designs. In the Reaction type, the hot gas is allowed to expand in both the rotating and stationary blades. This is an efficient method of extracting work from gas stream but since not much pressure drop can be used per stage, many stages are required. In the Impulse type the pressure drop occurs in the stationary elements with only a small percentage taking place in the rotating parts. This type has the advantage of being able to do more work per stage hence fewer stages than the Reaction type. It also permits larger pressure and temperature drops to occur in the stationary parts and not in the more highly stressed and difficult to cool rotating elements. The hot gas is delivered to the turbine from the combustion chambers at a temperature and flow required by the load. During its flow through nozzles and buckets (turbine blades) the gas loses both heat and pressure until it is discharged from the final stage at exhaust stack pressure and temperature. In the meantime it has given up enough energy to the turbine rotor to provide the necessary mechanical power.

The combustion zone of a turbine is the space required for the actual burning of the fuel and the subsequent dilution by secondary air from flame temperatures of 1759 °C down to usable values 950 °C. This is normally done in a group of combustion chambers which is usually inside the machine package. The combustion zone comprises an outer casing an inner casing (or 'liner') and the necessary air and gas passages see figure 1.2. As shown in the figure, combustion takes place inside the inner casing. The walls of the casing are cooled by streams of air which are made to flow through louvres punched in the wall material. This air stream flows close to the wall and thus keeps the material cool, and so reduces thermal stress. The hot diluted air flow to the transition piece where it is directed to the first turbine nozzles.

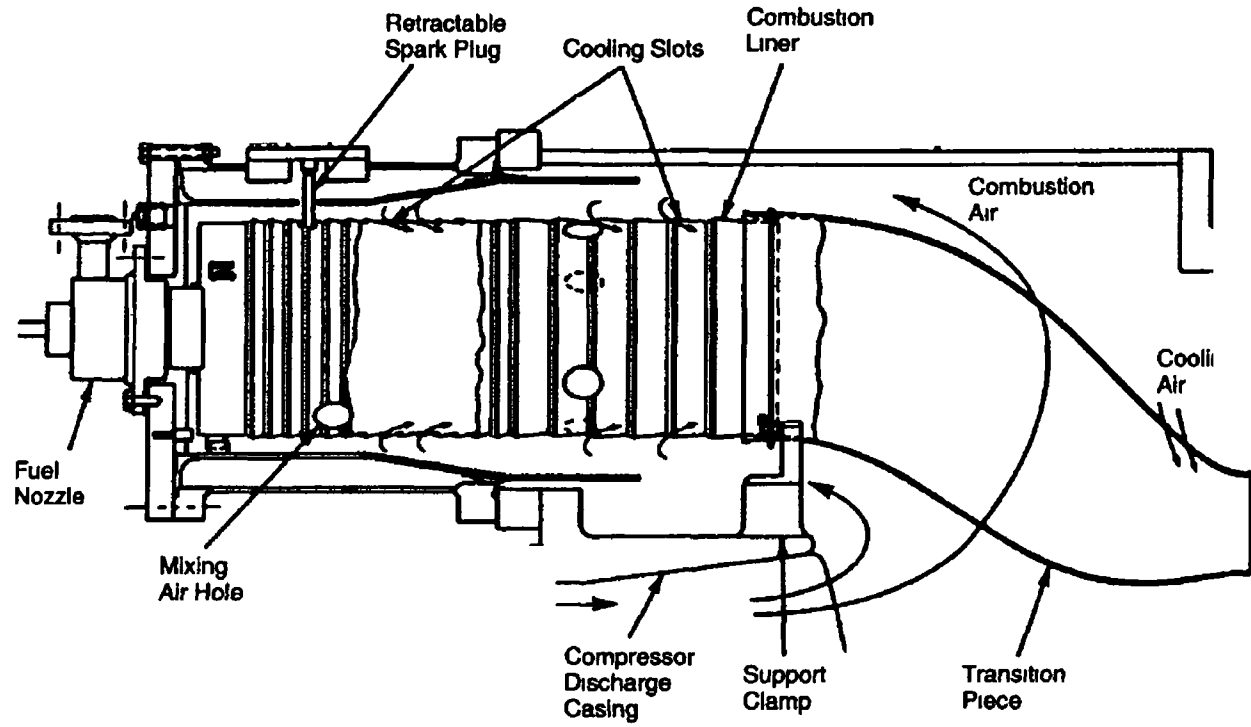


Figure 1 2 Combustion chamber and transition piece

As stated above temperature limitations are the most crucial limiting factors to gas turbine efficiencies. Materials and alloys that can operate at high temperatures are very costly-both to buy and to work on. The combustor liner, transition piece and turbine blades are the most critical components to achieve high-performance and long-life gas turbines. The extreme conditions of stress, temperature, and corrosion make these components materials challenging. The failure mechanism of those materials is related primarily to creep and corrosion and secondarily to thermal fatigue. Further, oxidation, hot corrosion, low cycle fatigue and alloy service aging are the most significant wear and tear mechanisms of the gas turbine hot path component.

SCOPE OF THE PRESENT WORK

The present study is conducted to investigate the mechanical and metallurgical behavior of Inconel 617 alloy used as a transition piece in gas turbine engines, for 37000 hours, after refurbishment by heat treatment process. The workpieces are heat treated at 1175 °C for two different periods. The tensile and fatigue properties of the workpiece before and after the heat treatment are compared to evaluate the effectiveness of the refurbishment. Scanning Electron Microscope (SEM) was used to obtain the microphotographs of workpiece cross-sections and fractographs of fractured surfaces. Energy Disperse Spectroscopy (EDS) is carried out to determine the elemental composition across workpiece cross sections and fractured surfaces. Moreover, the electrochemical response of the heat-treated surface is investigated through potentiodynamic polarization measurements in de-aerated 0.1 N H₂SO₄ and 0.005 N NaCl aqueous solution at 25 °C. Further, the mechanical properties (tensile and fatigue strength) of the alloy were examined after the electrochemical tests.

CHAPTER 2

LITERATURE REVIEW

Considerable research studies were carried out to explore metallurgical, mechanical and electrochemical properties of Inconel alloy. Creep tests were conducted to examine the microstructural changes in Inconel 617 at 1000 °C and 24.5 MPa load by Shigemitsu Kihara et al [7]. The following were found:

- 1) Fine intragranular carbides which are precipitated during creep were effective in lowering the creep rate during the early stages of the creep regime (within 300 h).
- 2) Grain boundary carbides migrate from grain boundaries that were under compressive stress to grain boundaries that were under tensile stress. The rate of grain boundary carbide migration depends on grain size.
- 3) $M_{23}C_6$ type carbides, having high chromium content, and M_6C type carbides, having high molybdenum content, co-existed on the grain boundaries. $M_{23}C_6$ type carbides, however, were quantitatively predominant. Furthermore, M_6C occurred less frequently on the tensile boundaries than on the stress free grain boundaries.
- 4) The grain boundaries on which the carbides were dissolved start to migrate in the steady state creep region. The creep rate gradually increases with the occurrence of grain boundary migration.
- 5) The steady state creep rate depended not so much on the morphological changes of carbides as on the grain size of the matrix.

Laboratory study was performed by W. L. Mankins et al [6] to determine the effects of long-time (215 to over 10,000 h) exposure to temperatures up to 1093 °C on the microstructure and phase stability of Inconel 617 superalloy. Further the microstructures

were correlated with mechanical properties to investigate the strengthening response exhibited by the alloy during high-temperature exposure. The major phase presented in the alloy after exposure to all temperatures from 649 to 1093 °C was found to be $M_{23}C_6$. The phase precipitated as discrete particles and remained stable at all temperatures. No M_6C or MC carbides were found. A small amount of gamma prime was found in samples exposed at 649 °C and 760 °C . PHACOMP analysis indicated 0.63 pct gamma prime could form. No topological close-packed phases such as δ , γ and ϵ were found. Strengthening of the alloy during exposure to temperature was found to result primarily from the precipitation of $M_{23}C_6$. The phase provided effective strengthening because it precipitated in discrete particles and remained stable at temperatures up to 1093 °C. The amount of gamma prime formed was not sufficient to result in appreciable hardening, but it did provide some strengthening at 649 to 760 °C.

A study was made by Kazuaki, et al. [8] to investigate the effects of thermal aging and stress change on the creep rate of Inconel 617 at temperatures above 900 °C. It was found that the creep curve varied sensitively with thermal aging. At 900 °C and under high stress thermal aging increased the creep rate of both the transient and steady state. With decreasing the stress at 900 °C or increasing the test temperature the steady-state creep rate became insensitive to thermal history. The irregular creep curve was shown to alter its shape by thermal aging to the classical type using four different heats of Inconel 617. Further, prestraining under high stress was found to influence the creep rate in the subsequent creep test under lower stress. Following the stress reduction the creep rate initially decelerated and then asymptotically approached to the value obtained without

prestraining. From a practical view point, a distinguished feature was that the influence of stress drop on the creep rate became obscure with decreasing the amount of prestrain to the practical strain range less than 0.1%.

The study was conducted by Kazuaki Mino et al. [9] to investigate the effect of grain boundary migration and recrystallization on the creep strength of Inconel 617 at 1000 °C. Changing grain boundaries caused dissolution of carbide, resulting in carbide free zones behind them and in the recrystallized grains. Notable grain boundary migration and recrystallization were observed preferentially on longitudinal grain boundaries in the specimens crept by more than approximately 10% (tertiary stage). In the practical strain range of up to 7%, the frequency of their occurrence was quite small to prove any consideration of their influence on the creep strength. However, decarburized specimens being free from grain boundary carbide exhibited significant grain boundary migration. A reduction of the creep strength by decarburization was explained in terms of a diminishing of grain boundary carbide and an enhancement of grain boundary migration, which was considered as the recovery process. For the specimens given a slight cold rolling of 7.5%, partial recrystallization was observed by a short time annealing at 1000 °C and not only decreased the strengthening by cold work, but also degraded the strength by the associated microstructural changes, i.e., coarsening of carbide and formation of new grains.

Whittenberger et al. [10] studied the microstructures and tensile properties of Inconel 617 after subjected to molten salt, its vapor, and vacuum for periods up to 10,000 h at 820

°C The microstructures were characterized, and samples were tensile tested at temperatures between -196 °C and 926 °C Neither the structure nor mechanical properties revealed evidence of additional degradation due to exposures to the salt Although some loss in tensile properties was noted, particularly at -196 °C, this reduction could be ascribed to the influence of simple aging at 820 °C

Whittenberger et al [11] compared the tensile properties and the microstructures of several heat-exposed and tested superalloys with those determined for as-received alloys The tensile properties at -196 °C to 926 °C of approximately 1.3-mm thick wrought sheet Co-base Haynes alloy 188 and Ni-base Haynes alloy 230 and Inconel 617 were determined following heat treatment in air and vacuum for periods of up to 22500 hours at 820 °C Substantial changes in structure were generated by prior exposures, including precipitation of second phases For heat treatment in air, oxide scale and surface-connected grain boundary pits/oxides was noticed Compared to the properties of as-received alloys, prior exposure tended to decrease the yield strength and the ultimate tensile strength, with the greatest reductions at -196 °C and 25 °C The most dramatic influence of heat treatment was experienced in the low-temperature residual tensile elongation, where decreases from 40 to 5% at -196 °C were recorded

The effect of gamma prime depletion on the creep behavior after high temperature treatment of Inconel alloy was investigated by Pandey and Satyanarayana et al [12] They showed that gamma prime depletion in the air exposed samples caused a weakening effect leading to enhanced creep rate

High temperature creep and tensile properties of Inconel alloy was examined by Chavaz et al [13] They developed data for the creep and tensile properties of the alloy at elevated temperatures

The etching properties of Inconel alloy due to low-cyclic fatigue at high temperatures were investigated by Komazaki et al [14] A chemical etching technique was utilized to detect the fatigue damage They showed that the density of slip bands increased with increased fatigue life and demonstrated the applicability of the etching technique to fatigue damage evaluation

Evaluation of gas turbine transition-piece after 20000 and 37000 hours of service was studied by Swaminathan et al [15] They indicated that the primary cause of cracking was the increase in net section stress, which exceeded the creep strength of the panel

Ennis et al [16] studied the density, thermal expansivity, thermal diffusivity, and thermal conductivity of carburized high-temperature nickel and iron based alloys The study was part of a program to qualify the materials for applications in the high-temperature reactor Standard measurement techniques were used He concluded that for the nickel-base alloys Inconel 617 and Hastelloy X the changes in the physical properties in the range of carbon contents that gave acceptable mechanical properties were not significant The physical properties of the iron-base alloy Incoloy 800 H were found to be more sensitive to the degree of carburization Significant changes in the density (which decreased with increasing carbon content) and the thermal expansivity (which also decreased with increasing carbon content) were determined The measurements of

thermal diffusivity were subject to relatively large scatter due to the inhomogeneous structure of the carburized alloys, only for Incoloy 800H was a small systematic decrease in diffusivity were found with increasing carburization

Venkatesh et al [17] investigated the strain hardening of Inconel 690 alloy during tensile deformation at temperatures between 200 and 1200 °C They indicated that the third stage of hardening Inconel alloy at temperatures between 600-700 °C and single stage hardening between 750-1200 °C could be described by Bodner-Partom and/or Kock/Mecking dislocation-dislocation interaction model

Ennis et al [18] studied the influence of both thermal exposure and carburization at 800 °C and above on the room temperature tensile properties of Incoloy 800 H, Inconel 617, Hastelloy X and Nimonic 86 and the results have been compared with data available in the literature It was shown that the room temperature ductility of Incoloy 800 H was much less sensitive to carburization than that of the nickel-base alloys This was attributed to greater volume fraction of carbide formed in the nickel-base alloys particular bulk carbon content Also they found that, the nickel-base alloys carbide fractions were higher than in iron-base alloys due to the lower solubility of carbon and to the formation of M_6C carbides

The creep, corrosion, and thermal cycling of nickel alloys in combustion chamber of gas turbine were investigated by Solberg et al [19] They indicted that increased ductility due to high temperature was because off the combination of increased surface cracking, reduce internal creep cavitation

The microstructures and mechanical properties of laser welded Inconel alloy was investigated by Hirose et al [20]. They observed interdendritic gamma phase in the fusion zone of the laser welded samples.

Kleinpass et al [21] conducted total strain controlled in-phase and out-of-phase thermo-mechanical fatigue (TMF) tests on Inconel 617 between temperatures of 850 °C, and 200 °C. The different mechanical strain amplitudes, the cyclic stress-strain response, the change of the microstructure and the development of damage were analyzed. The initial values of the induced stress amplitudes and plastic strain amplitudes, and the amount of cyclic hardening increased with the total mechanical strain amplitude. The observed cyclic hardening resulted from strong dislocation-dislocation and dislocation-particle interactions during plastic deformation at lower temperatures. The dislocation-particle interactions being enhanced by the precipitation of small semi-coherent carbides at elevated temperatures of the TMF cycles. For each type of TMF tests the lifetime behavior could be adequately described by the combination of the relationships of Basquin and Coffin-Manson. At equal total mechanical strain amplitudes in-phase tests always yield smaller lifetimes than out-of-phase tests. The difference between the two types of TMF-tests rises with increasing lifetime. This behavior was caused by different accumulation of creep damage, which was privileged by tensile stresses at high temperatures.

Boursier et al [22] investigated the correlation between Stress Corrosion Cracking (SCC) susceptibility and creep strain-rate at 360 °C on six mill-annealed tubes of

superalloy 600 of different chemical compositions, mechanical properties and grain sizes. The tubes with high creep strain-rate exhibited the greatest susceptibility to stress corrosion cracking and several tubes with low creep strain-rate demonstrated a low susceptibility, but one slow-creeping tube evidenced a relatively easy cracking. Heat treatment at 700 °C, which resulted in an increased creep rate, was found to improve stress corrosion cracking resistance. Further, they concluded that the lack of correlation between creep and stress corrosion cracking might be a consequence of differences of metallurgical structure contribution to creep and/or of an influence of primary water on the creep rate of alloy 600.

Sung et al [23] conducted constant elongation rate tests to evaluate the effect of heat treatment on the intragranular stress corrosion cracking susceptibility of alloy 600 in 140 °C and 50 percent caustic solution at 900 mV versus saturated calomel electrode. The results showed that heat treatment at low temperature for a long time led to a material that was not susceptible to caustic intragranular cracking.

Popov et al [24] estimated the effectiveness of under potential deposition (UPD) of Pb on type 718 superalloy in reducing the corrosion rate and degree of hydrogenation ingress. Cracking hazards created by the permeation and accumulation of hydrogen in the bulk of type 718 alloy limits its practical use. Polarization experiments demonstrated that a UPD of Pb effectively inhibited H discharge by 67 percent. In addition, the H permeation rate through type 718 superalloy membrane was diminished by 70 percent. The inhibition effect observed was due to UPD of Pb on the alloy substrate, which altered

the chemical properties of the substrate and reduced coverage of H on the surface. It was found that the H penetration decreased in the bulk of the alloy as a result of the suppressed H absorption.

England et al [25] examined the oxidation behavior of some commercially available nickel-based superalloy foils and the electronic resistance of the oxide scale formed. Haynes 230, Inconel 625, Inconel 718, and Hastelloy X foil specimens were oxidized in air for several thousand hours at temperatures of 800 to 1100 °C. Haynes 230 was found to exhibit the slowest oxidation kinetics of the alloys studied. Cr₂O₃ was the major oxide phase in the oxide scale of all the alloys, and manganese chromites were found in all alloy scales except Inconel 718. Electron probe microanalysis showed that the concentration of Mn in the oxide scale was much higher than in the alloy, suggesting selective oxidation of Mn. Measurements of the electronic resistance of the oxide scale in air at temperatures up to 800 °C showed that the scale from Haynes 230 had the lowest area-specific resistance.

Dunn et al [26] investigated the influence of the chromium-depleted mill-finished surface of alloy 825 (UNS N08825) on the localized corrosion resistance of proposed nuclear waste container material. Solutions based on the ground water at Yucca Mountain, Nevada, but with an increased concentration of chloride, were used for the tests. The results showed that the breakdown and repassivation potentials for the mill-finished surface were more active than those for polished surfaces. Further, it was found from potentiodynamic polarization tests that pits could be initiated on the chromium-

depleted surface at potentials of 220 mVSCE in a solution containing 1,000 ppm Cl at 95 °C. A similar pit initiation was identified by potentiostatic tests for the mill-finished surface. However, in order to sustain stable pit growth beyond the chromium-depleted layer under long-term potentiostatic tests, a higher potential of 300 mVSCE was required. Moreover, it was also found that an increase in surface roughness decreased the localized corrosion resistance of the material.

Shaikh et al [27] measured the hardness of the nickel based superalloy Inconel 625, aged at 625, 700, and 760 °C for different periods of time ranging from 1 to 335 hours. Peak hardening occurred much earlier at 760 °C than at 700 °C, but the peak hardness was higher at 700 °C than at 760 °C. Precipitates observed to exist in specimens aged at 760 °C for a longer time were confirmed to be γ'' precipitates of $\text{Ni}_3(\text{Nb},\text{Mo})$ type. The results indicate that nucleation occurs heterogeneously on dislocations and stacking faults. Although longer aging caused somewhat uniform nucleation, it still took place preferentially on the secondary defects. At 700 °C, γ' precipitates were observed in addition to γ'' precipitates.

Chang et al [28] studied the effect of a modified heat treatment (MHT) and the standard heat treatment (SHT) on the damage tolerance of alloy 718 turbine disk material in the temperature range of room temperature to 650 °C. The microstructure developed through the MHT sequence was damage tolerant over the temperature range considered. Shot peening led to a distinct improvement in the low-cycle fatigue crack initiation life of the MHT material relative to the SHT material at 650 °C. The serrated grain boundaries

formed through controlled precipitation of grain-boundary δ -phase were beneficial to elevated-temperature fatigue crack growth rates. The δ -phase precipitates that formed at an angle to the grain boundaries did not cause the material to be notch sensitive.

Goods et al [29] used constant extension rate testing to examine the interaction between deformation and exposure of a nickel-based alloy to an oxidizing molten salt environment. He used fracture strain, reduction in area and ultimate strength (UTS) as indicative measuring parameters of the susceptibility of the alloy to environmental degradation. Good tested Inconel 625 LCF specimens at 600 °C in the salt medium and at initial strain rates between 4 times 10^{-8} and 2 times 10^{-5} sec⁻¹. They found that the structure of the oxide film on specimens tested in the molten salt was affected by the imposed continuous deformation. Deformation resulted in an oxide film that was twice as thick as that formed on unstrained salt-exposed surfaces. Further, deformation resulted in significant cracking in the surface oxide. Metallographic observations suggested that some of this cracking initiated quite early in the mechanical tests. Specimens tested in the salt medium exhibited an increase in ductility, as measured by reduction in area and fracture strain, relative to control specimens tested in air, while strength was unaffected.

The effects of heat treatment and applied potential on the stress corrosion cracking (SCC) behavior of Alloy 600 in thiosulfate solution were investigated by Tsai et al [30]. The Electrochemical Potentiokinetic Reactivation (EPR) tests and modified Huey tests showed that a thermal stabilization treatment (990 °C/5 mm + 705 °C /15 h) could eliminate the sensitization of Alloy 600 and result in a lowering of the degree of sensitization as compared with other heat treatments. Electrochemical polarization curves

showed that Alloy 600 could passivate in thiosulfate solution and exhibited two anodic peaks located around -500 and +100 mV (SCE), respectively, independent of the heat treatment. The polarization curves also showed that Cr played an important role in the electrochemical behavior of Alloy 600 in thiosulfate solution. Under applied potential conditions, intergranular stress corrosion cracking (IGSCC) was observed in sensitized and stabilized Alloy 600 in 0.01 M thiosulfate solution at 95 °C. The severity of IGSCC was less after the stabilization heat treatment than after the sensitization heat treatment. In these conditions the susceptibility of IGSCC was strongly affected by the applied potential. In general, the crack initiation time decreased with increasing applied potential in the anodic potential region.

Heck et al [31] concluded in a study that Inconel 783 superalloys had low coefficient of thermal expansion (CTE) than Inconel 718. He stated that to achieve low CTE, alloys based on Ni-Fe-Co compositions require Cr content be maintained at low levels. Added Cr lowers the curie temperature and thereby increases thermal expansion rate over a wider temperature range. The necessary lack of Cr minimizes resistance to both general oxidation and stress-accelerated grain boundary oxygen enhanced cracking (SAGBO). Increased amounts of Al in alloys strengthened by γ' alone also promotes SAGBO. Alloy 783 was the culmination in the development of an alloy system with very high aluminum content that, in addition to forming γ' , causes β aluminate phase precipitation in the austenitic matrix. He discovered that this type of structure could be processed to resist both SAGBO and general oxidation, while providing low thermal

expansion and useful mechanical properties up to 700 °C. The high Al content also reduces density to 5 percent below that of superalloys such as Inconel alloy 718.

Yang et al [32] investigated the integrity of the passive film formed on an untreated alloy 600 in thiosulfate solution, conducted by adding small amounts of dilute chloride ions. In the range of 1 to 0.001 M sodium thiosulfate, the linearity of corrosion potential as a function of the concentration of chloride ions was determined. He found that the chloride content required to generate pitting decreased as the logarithm of the deaerated thiosulfate concentration decreased. For untreated UNS N06600 alloy (alloy 600), ductile fractures were shown by fractography. For sensitized alloy 600, intergranular stress corrosion cracking or intergranular attack were observed. Further, he correlated the fracture mechanism and the active loop regime, where vigorous dissolution reactions were produced during repassivation.

Szklarska et al [33] measured the rate of crack growth in alloy 600 in high-temperature lithiated hydrogenated water at various potentials and pH levels. He found that the mode of cracking depended on temperature and pH of the solution. It was observed that intragranular and transgranular corrosion occurred at 350 °C and 250 °C, respectively. Crack formation occurred at the corrosion potential and at potentials in the active and transpassive regions, but crack formation did not occur in the passive potential region.

Lim et al [34] studied microscopically the microstructural and compositional changes in sensitized Ni-base Alloy 600 after laser surface melting. Three different zones of a laser-melted zone (LMZ), a heat-affected zone (HAZ), and an unaffected bulk zone were analyzed separately. It was found that two different shapes of the precipitated Cr carbides were produced along the grain boundaries in the alloy with Cr depletion occurring along the grain boundaries. Dislocation density was very low in the HAZ. The carbides were completely dissolved at the grain boundaries close to the LMZ and partially dissolved at the boundaries far from the LMZ. The cells formed in the LMZ had the same phase as that of the matrix. Cr was segregated in the cell and grain boundaries in the LMZ, but Fe was not. In addition, the microstructure of the LMZ comprised fine cells with the fine precipitates of a TiN type along the cell and grain boundaries.

Chen et al [35] studied the precipitation of second phases in Incoloy 909 using optical microscopy, scanning electron microscopy, and transmission electron microscopy. Incoloy 909 was a chromium-free, Fe-Ni-Co based superalloy used for aeroengine applications. Incoloy 909 was known to have significantly improved notch rupture strength compared to the earlier superalloy Incoloy 907. Although this improvement was attributed to the increased Si content, the mechanism involved was not fully understood. Analytical electron microscopy was used to determine the compositions and crystal structures of several second phases. From the results, a time-temperature-transformation diagram was constructed. It was found that the Si addition promoted the precipitation of an Fe₂Nb type Laves phase during casting and thermal processing, as well as the

formation of an Si rich orthorhombic phase at high aging temperatures. Both types of precipitate were considered to improve the rupture properties of the alloy.

McIntyre et al [36] exposed specimens of Inconel 600 (I-600), Inconel 690 (I-690), Incoloy 800 (I-800) and Monel 400 (M-400) to high temperature steam generator water conditions typical of those which might be found when the secondary coolant pH was allowed to fall into the acid regime. He analyzed the specimens by surface and electrochemical techniques, either directly following exposure in the acid medium steam generator coolant or after adjusting the coolant pH and chemistry to near-normal steam generator conditions. The initial acid exposure resulted in the growth of a chromium-rich surface corrosion product film on all alloys (except M-400) and the precipitation of nickel-rich sulphates. Following the return to a higher pH, the alloy again had chromium-rich surface oxides, but also exhibited sulphide crystallites adhering to the base oxide, particularly for I-600. The tendency to retain these sulphides was attributed to the porosity of the protective oxide through which nickel was transported to the solution. The conversion of sulphate-sulphide was believed to occur as the pH was raised to normal alkaline conditions. In the case of M-400, a chromium oxide layer was not available to restrict the transport of nickel to the solution. As a result, a thick layer of sulphide crystals grows on the surface of the M-400 alloy even when subjected to a mild acid pH excursion. Even trace concentrations of sulphide/sulphate under normal pH control were shown to react with alloys whose oxide films appeared permeable to nickel transport.

Acoff et al [37] studied the features of migration that were unique to constitutional liquid film migration (CLFM) of Nickel-base alloy 718. His experiment consisted of heat-treating rods of alloy 718 to promote the trapping of niobium carbide particles on the grain boundaries. He subjected the samples to wasothermal treatments above their constitutional-liquidation temperature, which produced CLFM of the grain boundaries. The movement of the liquid films away from their centers of curvature, the formation of a new solid solution behind the migrated liquid films, and the reversals of curvature of the migrated liquid films confirmed that CLFM was the phenomenon observed. The concentration of niobium behind the migrated liquid films for wasothermal treatments below the solidus temperature was shown to be greater than the niobium concentration in the matrix. Further he concluded that above the solidus temperature, there was no increase in niobium concentration.

Shankar et al [38] studied the microstructure and mechanical properties of Inconel alloy 625. He used a tube from an ammonia cracker, which was service-exposed for approximately 60000 h to 600 °C. The alloy showed higher strength and lower ductility compared to the virgin material in the solution-annealed state. Precipitation of intermetallic γ'' and $\text{Ni}_2(\text{Cr},\text{Mo})$ phases and intragranular carbides were found to be responsible for higher strength of the service-exposed alloy. He subjected the service-exposed alloy to thermal aging treatments at 650 °C and 850 °C above the service temperature of the exposed alloy. This subsequently led to the dissolution of the intermetallic phases that in turn increased the ductility of the alloy. Post-service aging of the alloy at 923 °C for short durations resulted in the dissolution of the $\text{Ni}_2(\text{Cr},\text{Mo})$ -

phase. The dissolution of the $\text{Ni}_2(\text{Cr,Mo})$ -phase exhibited significant influence upon yield strength but negligible effect on ductility. Prolonged aging of the alloy for 500 h at $650\text{ }^\circ\text{C}$ resulted in the precipitation of intermetallic delta-phase. Post-service aging of the alloy at $850\text{ }^\circ\text{C}$ promoted the dissolution of both γ'' and $\text{Ni}_2(\text{Cr,Mo})$ phases formed during service. Longer duration aging at $850\text{ }^\circ\text{C}$ led to the precipitation of the delta-phase with an associated increase in strength and loss in ductility. Re-solution annealing of the service-exposed alloy at $1150\text{ }^\circ\text{C}$ caused the dissolution of the strengthening phases. When the re-solution annealed alloy was subjected to prolonged exposure at $650\text{ }^\circ\text{C}$, the yield stress was found to increase rapidly with aging time with attendant loss in ductility due to the precipitation of γ'' .

Wang et al [39] studied the effects of grain boundary carbides on the tensile and impact properties of Inconel 600 at $25\text{ }^\circ\text{C}$ and $-196\text{ }^\circ\text{C}$. Wang concluded that unlike type 316 stainless steel, which could be severely embrittled, grain boundary carbides cause only a significant loss in the reduction of area, but otherwise, little effect on other tensile properties. Deep grain boundary cracks were observed on the fracture surfaces. Charpy V-notch impact specimens were not completely fractured, even at $-196\text{ }^\circ\text{C}$ in samples with grain boundary carbides.

Altın et al [40] investigated the carbon deposition on nickel, cobalt, molybdenum, and iron-based alloy foils during thermal stressing of a JP-8 fuel at $500\text{ }^\circ\text{C}$ wall temperature and 34 atm for 5 hours at a fuel flow rate of 4 ml/min. Temperature-programmed oxidation (TPO) analysis and SEM examination showed that the amount

and the nature of the carbonaceous deposits on the foils depend strongly on the chemical composition of the foil surface. He found that the amount of carbon deposited on metal foils decreased in the order Inconel 600 greater than Havar greater than Fecralloy greater than Waspaloy greater than Hastelloy-C greater than MoRe greater than Inconel 718. The presence of minor components, such as Ti, Al, and Nb, in the alloys appeared to be responsible for reducing carbon deposition from jet fuel thermal stressing. This effect could be attributed to the formation of a passive layer on alloy surfaces that limited the access of deposit precursors to base metals, Ni, Fe, and Co, that catalyze deposit formation.

Antunes et al [41] studied the influence of ΔK , loading frequency, stress ratio and temperature on the high temperature fatigue crack growth rate of nickel base superalloys. This study was based on fatigue tests carried out in corner crack specimens of Inconel 718 at 600 °C and at room temperature. He used three stress ratios (R equals 0.05, 0.5 and 0.8) and loading frequencies ranging from 0.00017 to 15 Hz. For frequencies below 0.25 Hz, the load wave shape was trapezoidal with different dwell times at maximum load. At relatively high frequencies, the propagation was cycle dependent, while for lower frequencies it was time dependent. At intermediate frequencies a mixed crack growth occurred. In addition, he found that the increased of R increases the transition frequencies, (i.e., extends the time dependent crack growth to higher frequencies) and produced an increase of cyclic crack growth rate for all regimes of crack growth. In the time dependent regime, a higher variation was observed, that can be explained by an acceleration of oxidation damage promoted by the increase of maximum stress.

Dong et al [42] investigated the effects of sulfur, with content variations of 15 to 175 ppm, on the stress-rupture and tensile properties in nickel-base alloy 718. The stress-rupture life decreased dramatically with increasing sulfur content. This was especially noticeable in the ductility loss at 650 °C. Dong indicated that Auger electron spectroscopy of stress-rupture tested specimens provided direct evidence of sulfur and phosphorus segregation to grain boundaries and carbide/matrix interfaces. He found that the stress-rupture life and fracture morphology were both correlated with the segregation of sulfur at grain boundaries in alloy 718. Further, sulfur was also preferentially segregated at the carbide matrix surfaces, and phosphorus was found to be distributed on grain boundaries. However, the phosphorus segregation did not correlate with stress-rupture behavior. Sulfur contents in the range of 15 to 50 ppm had little effect on the stress-rupture life. However, the stress-rupture life decreased dramatically with increasing sulfur content above 50 ppm.

The structural characterization of an aged Inconel 718 previously quenched from 990 °C was investigated by Slama et al [43]. He utilized X-ray diffraction, transmission electron microscopy and micro-hardness during the study. The X-ray diffraction patterns revealed the co-existence of the simple cubic, the tetragonal and the orthorhombic structures. These structures correspond respectively to the γ' , γ'' and δ phases. Through a detailed study of each XRD pattern Slama gave the lattice parameter and the crystalline grain size of the existing phases. Transmission electron microscopy (TEM) observations on thin foils led to identification of the different phases responsible for the various

hardening stages occurring during isothermal tempering performed at 680 °C and 750 °C for 4, 50 and 100 h. The γ' and γ'' phase precipitation were strongly dependent on the aging temperature and time. For 680 °C aging temperature, hardness investigations showed that a first hardening (HV equals 450) occurred when the duration was about 4 h (γ' particle size given by TEM observation was about 5-6 nm). A second hardening (HV equals 500) was shown to occur at 50 h. It corresponds to the precipitation of γ'' phase perfectly coherent with the gamma matrix. For 750 °C aging temperature, the γ'' phase precipitation (coherent with the matrix and the disc shaped with a length of 30 nm) produces a fast hardening after 4 h (HV equals 466). For a longer thermal exposure, the orthorhombic delta phase appeared, reaching a high grain size and fraction volume after 100 h and leading to a drastic micro-hardness decrease. From 30 nm on, the tetragonal distortion of the γ'' particles increased with increasing precipitate size.

In total strain controlled in-phase and out-of-phase thermo-mechanical fatigue (TMF) tests on Inconel 617, Nicrofer 5520 Co with a maximum temperature of 850 °C, a minimum temperature of 600 °C and different mechanical strain amplitudes Kleinpass, Bernd et al [44] analyzed the cyclic stress-strain response, the change of the microstructure and the development of damage. He reported that the initial values of the induced stress amplitudes and plastic strain amplitudes, and the amount of cyclic hardening increased with the total mechanical strain amplitude. The observed cyclic hardening results from strong dislocation-dislocation and dislocation-particle interactions during plastic deformation at lower temperatures the latter being enhanced by the precipitation of small semi-coherent carbides at elevated temperatures of the TMF cycles.

For each type of TMF tests he described the lifetime behaviour by the combination of the relationships of Basquin and Coffin-Manson. It was found that at equal total mechanical strain amplitudes in-phase tests always yield smaller lifetimes than out-of-phase tests. The difference between the two types of TMF-tests rised with increasing lifetime. This behavior was caused by different accumulation of creep damage which was favored by tensile stresses at high temperatures.

Huang et al [45] investigated the oxidation behavior of a new type of wrought Ni-Fe-Cr-Al superalloy in temperature range of 1100 °C to 1300 °C. He compared the results with alloy 214, Inconel 600, and GH 3030. He concluded that the oxidation resistance of the new superalloy was excellent and much better than that of the comparison alloys. Scanning electron microscopy (SEM), electron probe microanalysis (EPMA), and X-ray diffraction (XRD) experiments revealed that the excellent oxidation resistance of the new superalloy was due to the formation of a dense, stable and continuous Al₂O₃ and Cr₂O₃ oxide layer at high temperatures. Differential thermal analysis (DTA) showed that the formation of Cr₂O₃ and Al₂O₃ oxide layers on the new super-alloy reached a maximum at 1060 and 1356 °C, respectively. The Cr₂O₃ layer peeled off easily, and the single dense Al₂O₃ layer remained, giving good oxidation resistance at temperatures higher than 1150 °C. In addition, the new superalloy possessed high mechanical strength at high temperatures. On-site tests showed that the new superalloy has ideal oxidation resistance and could be used at high temperatures up to 1300 °C in various oxidizing and corrosion atmospheres, such as those containing SO₂, CO₂ etc, for long periods.

England et al [46] studied the oxidation kinetics of Haynes 230, Inconel 625, Inconel 718, and Hastelloy X foil specimens. They oxidized the foil specimens in air for several thousand hours in the temperature range of 800 °C to 1100 °C. It was found that the oxidation kinetics of alloys studied obeyed the parabolic rate law. Further, Haynes 230 exhibited the slowest oxidation kinetics of the alloys studied. X-ray diffraction, scanning electron microscopy, and electron probe microanalysis (EPMA) were the principal characterization tools employed. Chromium oxide, Cr₂O₃, was the predominant oxide phase in the oxide scale of all alloys studied. Manganese chromites were also detected in the oxide scales of Haynes 230, Hastelloy X, and Inconel 625. EPMA showed that the concentration of Mn in the oxide scale was much higher than in the alloy, indicating selective oxidation of Mn. The electronic resistance of the oxide scale was measured in air at temperatures up to 800 °C on samples oxidized in air for up to several thousand hours. The oxide scale on Haynes 230 exhibited the lowest area-specific resistance, consistent with its slower oxidation kinetics.

The Hardening behavior due to precipitation of γ' [Ni₃Nb] phase during aging of Ni₁₂₂Cr₉Mo₅Fe₄Nb alloy was studied experimentally by Kusabirakı et al [47]. The alloys were homogenized at 1100 °C for 3.6 ks and quenched in water. The homogenized alloy was aged at temperatures between 620 °C and 800 °C for up to 720 ks. The aging was also carried out at 620 °C to 750 °C for up to 720 ks for the alloys cold rolled with reductions of 4, 10, 30 and 50% after the homogenization. The micro-Vickers (HV) hardness test was made for the aged specimens. TEM was used to study the

microstructures of the specimens. He observed that for the specimens without cold rolling, the hardness monotonically increases with increasing aging time at 620, 670 and 750 °C. On the other hand, the HV hardness increases with increasing aging time and then reaches the maximum values at 36 and 72 ks at 650 °C and 750 °C, respectively. In the specimens with the maximum values of the MV hardness, disk-like γ'' precipitates with diameters of 30 to 35 nm were observed in a gamma matrix. Coarsening of the γ'' phase seems to obey the Ostwald ripening mechanism. The activation enthalpy for the coarsening was obtained to be 418 kJ/mol. For the specimens with cold rolling, over-aging was rather restrained due to fine γ'' particles precipitated along dislocations.

Singh et al [48] studied the corrosion resistance Inconel alloys 600, 601 and Nickel-201 in 0.01-10M H₂SO₄ at 30 °C, 60 °C, and 90 °C. Open circuit potential (OCP) measurements at 30 °C indicated the attainment of a positive OCP for alloy 601 in all concentrations of acid except in 10M H₂SO₄, while alloys 600 and 201 showed negative OCP values even in 0.01M H₂SO₄. Further negative shift in OCP was recorded for alloys 600 and 201 at 60 and 90 °C. However, a positive shift in OCP was noted for alloy 601 in 10M H₂SO₄ at 60 and 90 °C. Corrosion current measurements indicated better corrosion resistance for alloy 601 than for alloy 600, whereas alloy 201 showed poor corrosion resistance in all concentrations of acid. Alloy 601 showed spontaneous passivation from the corrosion potential in 0.01-1.0M H₂SO₄ at 30 °C during potentiodynamic polarisation. In contrast, alloys 600 and 201 exhibited I_{crit} - I_{pass}

transitions before the onset of passivation in all concentrations of acid at all experimental temperatures

Kayano et al [49] conducted a Trans-Varestraint test to examine the solidification cracking susceptibility of Inconel 706 as a function of Ni content in base metal. Three kinds of Ni-base alloys with three different levels of Ni content were used. It was observed that dendrite structure in the fractured surface of the specimen of Trans-Varestraint tested. The quantitative analysis of crack revealed that the solidification crack length and the temperature range in which hot cracking occurred (brittle temperature range, BTR) decreased with the increase of Ni content. Calculation of liquidus and solidus temperature of alloys by thermo-calc data indicated that the solidification temperature range also decreased with increase of Ni content. On the basis of these results, it was deduced that the improvement of the solidification cracking susceptibility with Ni content was attributed to the decrease of the solidification temperature range of alloys.

The strain hardening response of Inconel 690 during tensile deformation between 200-1200 °C was examined by Venkatesh et al [50]. At low temperatures, up to 600 °C, two stages of hardening, dislocation-dislocation and dislocation-solute interactions were observed. Increasing temperatures to 700 °C resulted in the introduction of a third hardening stage, transmission electron microscopy suggesting that this additional hardening stage arised because of a transition in the dislocation arrangement from

random tangles to a cellular substructure. Moreover, at temperatures from 750 °C to 1200 °C, a single hardening stage was observed, this was associated with a cellular/sub-grain dislocation substructure. They reported that the third stage of hardening in Inconel 690 at temperatures between 600 °C and 700 °C and single stage hardening between 750 °C and 1200 °C could be described by the Bodner-Partom (B-P) and/or Kocks-Mecking (K-M) dislocation-dislocation interaction model. Furthermore, between 750 °C and 950 °C the hardening behavior could be described by the modified K-M dislocation-constant periodic barrier size interaction model. At higher temperatures, greater than 950 °C, the modified K-M model could be utilized through inclusion of an experimentally determined strain dependent barrier spacing.

Vishnudevan et al [51] evaluated the corrosion behavior of Inconel 600 and 601 alloys by DC polarization method in orthophosphoric acid solution of concentrations 0.5 N to 15 N. He observed a passivation range from plus 200 mV to plus 800 mV for 601 alloy. In the case of Inconel 600 a less passivation range in comparison with Inconel 601 was observed. In addition, the passivation current was found to be higher than that of 601 alloy. TAFEL polarization study indicated that Inconel 601 alloy was more corrosion resistant than Inconel 600.

Chen et al [52], studied The segregation behavior of boron at grain boundaries in two Inconel 718 plus based alloys with different B concentrations. Alloys, one

containing 11 ppm of B and the other 43 ppm of B, were homogenized at 1200 °C for 2 hours followed by water quenching and air cooling. Using secondary ion mass spectrometry they reported that a strong segregation of boron at grain boundaries was observed after the heat treatment in both alloys. The segregation was found mainly to be of non-equilibrium type. Further, the homogenized samples were annealed at 1050 °C for various lengths of time. During annealing, Boride particles were observed to first form at grain boundaries.

Patel et al [53] evaluated the effect of steam on oxidation and corrosion of three superalloys (X-45, Inconel-617 and IN-738LC). He exposed the materials to steam environment at 840 °C. The steam environments used were (a) steam generated from deionized water, (b) steam generated from deionized water with 5 ppm each of NaCl and Na₂ SO₄ and (c) steam generated from deionized water with 50 ppm each of NaCl and Na₂ SO₄. The respective exposure times were 3900, 2950, and 1450 hours. IN-738LC showed severe internal oxidation in steam. In contaminated steam the hot corrosion damage was maximum in Inconel-617. Moreover, X-45 showed less oxidation damage than IN-738LC and less hot corrosion than Inconel-617.

Kawagoishi et al [54] investigated the growth characteristics of a small crack for Inconel 718 at room temperature by rotating bending fatigue. It was found that (1) The crack initiated at the grain boundary and then propagated as a transgranular crack. (2) When the stress level was higher than the fatigue limit, the fatigue life was mainly

controlled by the growth life of a crack smaller than 1 mm (3) The fatigue limit was a limiting stress for the crack propagation (4) At low stress levels the crack growth rate was determined by the stress intensity factor range ΔK , and at high stress levels by the small crack growth law

The welding of wrought Inconel 718 using CO₂ cw and Nd YAG pulsed lasers was investigated from microfissuring and metallurgical aspects point of view by Zhang et al [55] They indicated that the use of Nd YAG pulsed lasers could easily and effectively prevent microfissuring by producing better bead profiles The recrystallization in the heat affected zone of the materials with residual elongated grain significantly reduced susceptibility to microfissuring Metallographic examination suggested that the microfissures occurred by a segregation mechanism where the pipeline diffusion of niobium along the grain boundary and the delta phase played the dominant roles The microstructures were characterized by transmission- and scanning- electron microscopy, showing that the γ carbide eutectic was suppressed in the fusion zone welded by both CO₂ cw and Nd YAG pulsed lasers owing to rapid solidification The carbides with 0.5-1 micron dimensions were dispersed within and between the dendrites On the other hand, the γ Laves eutectic was suppressed only in the fusion zone welded by CO₂ cw lasers, where the dislocation density was higher than in Nd YAG pulsed laser welds

Chen et al [56] study the dependence of creep fracture of Inconel 718 on grain boundary precipitates As preparation for the study, Inconel 718 was heat treated to obtain various materials with identical grain size and microstructures, but with a different

state of dispersion of delta precipitates at the grain boundary. The density of delta precipitates ρ in different materials was ranged from 0% to about 70%. Creep tests were conducted on these materials at 795 MPa and 625 °C. It was found that both the rupture time and total creep strain decreased with an increase in the value of ρ when its value was below about 45%. However, when the value of ρ was above 45%, both the rupture time and creep strain increased with an increase in ρ to a value much higher than that observed in the material without delta precipitates at grain boundaries. Scanning Electron Microscopy observations of the crept samples and their fracture surfaces showed that the presence of delta precipitates at grain boundaries resulted in the formation of creep voids in all specimens. However, the effect of creep voids on the final fracture of the material was dependent upon the value of ρ . At lower values of ρ , creep voids were observed to be isolated, and the fracture could be due to the propagation of wedge cracks initiated at triple points of grain boundaries. At higher values of ρ , the probability of wedge crack formation might be reduced. The fracture would then be controlled by the growth of cavities coupled with grain boundary sliding, which was observed to be strongly influenced by precipitates at grain boundaries.

Aleman et al [57] study the interface analysis on diffusion bonded of Ti 6242 alloy to Inconel 625 superalloy. The microstructures of the as-processed products were analyzed and the interdiffusion of the different elements through the interface was determined by microanalysis. They reported that starting from Inconel 625, first a γ phase ($\text{Cr}_4\text{Ni}_3\text{Mo}_2$), followed by several phases like NbNi_3 , Ni_3Ti , $\text{Cr}(20\% \text{Mo})$, beta Cr_2Ti , NiTi , TiO , TiNi , and Ti_2Ni intermetallics, just before the Ti 6242 was identified.

In this couple, the diffusion of Ni in Ti was faster than the diffusion of Ti in the superalloy and then a Kirkendall effect was produced. The sequence of formation of the different phases in both couples were in agreement with the respective ternary diagrams. They also showed that the formation of intermetallics could be avoided by using Cu/V interlayer.

The effect of sulfur on the solidification and segregation in Inconel 718 alloy was studied by Sun et al [58]. It was found that sulfur was extremely depleted in the matrix, slightly dissolved in the Laves phase and NbC, and seriously segregated as sulfides. Except for the needle-like Y-phase $(\text{Nb}, \text{Ti})_{2\text{CS}}$, a globular sulfide was newly found to form following the precipitation of the Laves phase. The precipitation of sulfides was speculated to be avoided when the sulfur content was low enough and most of the sulfur in the alloy was dissolved in the Laves phase. Further, sulfur had diverse effects on the solidification behavior of the alloys.

Gao et al [59] studied the crack growth kinetics, surface chemistry, and microstructure in a commercial Inconel 718. The results suggested that environmental enhancement of sustained-load crack growth in Inconel 718 was associated with the formation and rupture of niobium oxides at grain boundary surfaces and was controlled mainly by the rate of oxidation and decomposition of niobium carbides at the grain boundaries. They indicated that initial results from a study of a niobium-free Ni-18Cr-18Fe alloy (its base composition was identical to Inconel 718) confirmed the possible influence of niobium and the proposed mechanism.

The preoxidation condition with low concentration nitric acid permanganate and conventional high concentration alkaline permanganate for steam generator material Inconel 690 and 600 was studied by Wen et al [60]. He performed experiments in three parts, chromium release, measurements of corrosion potentials and polarization curves in NP and AP solutions for Inconel 690 and 600. The results show that AP is more effective than NP in releasing chromium from Inconel 600 oxides while the reverse applies to Inconel 690 oxides. The corrosion potential of Inconel 600 moves in a positive direction when the acidity becomes high NP, while the reverse occurs for Inconel 690. Further, the corrosion increases when the acidity or alkalinity becomes high for both materials.

Schwartz et al [61] evaluated the influence of some specific thermomechanical processing methods on the resulting grain boundary character distribution (GBCD) in FCC materials such as oxygen-free electronic (ofe) copper and Inconel 600. Samples of ofe Cu were subjected to a minimum of three different deformation paths to evaluate the influence of deformation path on the resulting GBCD. These include rolling to 82% reduction in thickness, compression to 82% strain, repeated compression to 20% strain followed by annealing. In addition, the influence of annealing temperature was probed by applying, for each of the processes, three different annealing temperatures of 400 °C, 560 °C, and 800 °C. The observations obtained from automated electron backscatter diffraction (EBSD) characterization of the microstructure demonstrated that among the processes considered, sequential processing is the most effective method to disrupt the random grain boundary network and improve the GBCD. Further, they also

demonstrated that the primary effect of thermomechanical processing is to reduce or break the connectivity of the random grain boundary network

Rong et al [62] developed a universal theoretical method to predict and characterize electron diffraction patterns (EDPs) which contain various variants of precipitate(s) with a matrix. The plane and direction transition matrices for three gamma double prime -phase variants and 12 delta -phase variants precipitated from a gamma matrix in the Inconel 718 alloy were deduced, from which the EDPs for seven low-index zones of gamma matrix containing gamma double prime precipitates were predicted by plotting and were found to be consistent with transmission electron microscopy (TEM) observations. Meanwhile, three variants of delta phase, precipitated from any one of four left brace 111 right brace matrices in 12 possible orientational variants, were also predicted and confirmed by EDPs. Further, their theoretical calculations indicated that the left brace one half 10 right brace -type superlattice reflections in the $\langle 100 \rangle$ zone of the gamma matrix permitted detection of both gamma double prime and delta phase precipitates, but not of gamma double prime phase precipitates. Therefore, the precipitates shown in dark-field images using these superlattice reflections cannot be unambiguously determined to be gamma double prime phase.

Hirose et al [63] applied laser surface annealing to age-hardened Ni base super alloy Inconel 718 using a 2.5 kW CO₂ laser to improve its performance in hydrogen environment. In the solutionized zone the age precipitates of gamma prime and gamma double prime are dissolved in the matrix, and thereby the hardness of the solutionized

zones is reduced to below 250 Hv from approximately 450 Hv of the aged base metal hardness. Further, they found that the ductility of the surface annealed specimen is almost twice that of the base metal in a tensile test under a 29.4 MPa hydrogen atmosphere at room temperature with hydrogen pre-charging.

The applicability of fracture surface roughness measurements to identify the crack propagation mode in nickel base superalloys (transgranular, intergranular or mixed) was studied by Antunes et al [64]. The roughness measurements were used to study the influence of loading frequency and stress state on the fatigue crack propagation mode occurring in Inconel 718 tested at 600 °C. The results obtained indicated that this technique can be used as an alternative or as a complement to standard fractography. The best roughness parameters for identifying the crack propagation mode are average roughness, mean roughness depth and mean height profile peak. Analysis of roughness spectra in terms of the frequency range showed that the amplitude values of the profiles with wavelengths identical to the grain size are significant when propagation is intergranular.

Induction brazing of Inconel 718 to Inconel X-750 using Ni-7Cr-3Fe-3.2B-4.5Si (wt %) foil as brazing filler metal was investigated by Xiaowei et al [65]. Moreover, the influence of the heating cycle on the microstructures of the base material and holding time on the mechanical properties of the brazed joints were also investigated. Brazing was conducted at the temperature range 1100 °C to 1200 °C for 0-300 s in a flowing argon environment. Both interfacial microstructures and mechanical properties of brazed joints

were investigated to evaluate joint quality. The optical and scanning electron microscopic results indicate that good wetting existed between the brazing alloy and both Inconel 718 and Inconel X-750. The diffusion of boron and silicon from brazing filler metal into base metal at the brazing temperature is the main controlling factor pertaining to the microstructural evolution of the joint interface. The element distribution of Cr, Fe, Si, Ni and Ti was examined by energy dispersive X-ray analysis. It was found that silicon and chromium remain in the center of brazed region and form brittle eutectic phases, boron distribution is uniform across joint area as it readily diffuses from brazing filler metal into the base metal. Further, they also found that the microstructures of the base material were not affected by the rapid heating and cooling cycle of induction processing, but the shear strength increased with increasing brazing time. Results show that excellent joint shear strengths of as high as about 503 MPa were obtained when processed at approximately 1150 °C for 300 second.

Parker et al [66] investigated the microstructural changes occurring at the low alloy steel fusion line in nickel based transition welds which are believed to be critical to the development of creep cavities and cracks. The progressive changes in Type I carbides observed following laboratory ageing at 625 °C and from interrupted creep specimens tested at 590-625 °C have been evaluated by optical and electron microscopy. They concluded that general, these carbides appear to be $M_{23}C_6$ type and grow in an approximately elliptical shape with the long dimension in the plane of the interface. The accuracy of these predictions is such that measurements of carbides in service can be used to estimate an equivalent operating temperature.

The high-temperature, isothermal-oxidation behavior of a superalloy was studied in the as-rolled and deformed conditions by Khalid et al [67]. The microstructural changes occurring during the oxidation of samples were examined using optical, scanning electron microscopy (SEM), fine-probe EDS microanalysis, and X-ray diffraction techniques. The topography of the oxide layers formed in the as-rolled and cold-deformed specimens exposed at various temperatures and time intervals is also examined. It was found that a Cr_2O_3 external layer was adherent and uniform on the rolled specimens in comparison to the scattered and preferential oxide developed on the deformed specimens. The latter can be attributed to the concurrent dynamic changes occurring in the deformed substructure that subsequently lead to breaking and spallation of the oxide.

Slama et al [68] investigated the aging of the Inconel 718 previously quenched from 990°C . They indicated that it is characterized by a hardness peak at 650°C , then a maximum in hardness at about 750°C . Over this temperature, the hardness progressively decreases. In the $550\text{-}650^\circ\text{C}$ temperature range, TEM observations have revealed that β precipitates are formed as long platelets parallel between them within the same grain, as well as extremely fine γ' particles responsible for the observed improvement in hardness. For a tempering temperature higher than 650°C , a first hardening occurs after a 4 h treatment, which has been associated with the γ' phase precipitation, with a more or less spherical shape. Beyond this time, a second hardening takes place linked to the γ'' phase precipitation as thin platelet shaped, perfectly coherent with the matrix. The misfit

between the γ' and γ'' phases is about 3% in the $\langle 001 \rangle \gamma'$ direction and lower than 1% in the $\langle 100 \rangle \gamma'$ and $\langle 010 \rangle \gamma''$ directions. During a longer aging at 750 °C, the γ'' platelets progressively dissolve while β precipitates grow.

The solid particle erosion of Inconel 625 rod, 20 mm in diameter, at elevated temperatures was studied by Jip et al [69]. The erosion rate of Inconel 625 decreases up to 450 °C and then increases with temperature. The temperature dependence can be predicted roughly by mechanical energy density, but not by mechanical properties such as tensile strength, yield strength, hardness and elongation. At both room temperature and 850 °C, erosion of the alloy occurs in a ductile manner and the values of velocity exponents are similar, though the eroded surfaces are remarkably different.

Flow reactor experiments were conducted to study carbon deposit formation from decomposition of a jet fuel (JP-8) at 500 °C and 500 psig for 5 h on the surface of two superalloys, Inconel 600 and Inconel X by Altın et al [70]. The deposits collected on superalloy surfaces were characterized by temperature-programmed oxidation, size exclusion microscopy, and energy-dispersive X-ray spectroscopy. Significantly lower deposition on Inconel X compared to that on Inconel 600 was attributed to the presence of minor elemental components, such as Al, Ti, Nb, and Ta in the Inconel X alloy.

Hiroyuki et al [71] investigated oxidation resistance of the TiAl-base alloys at high temperature and compared it to Ni-base superalloy Inconel 713C. The reagent used was a mixture of 40 mass% WO_3 powder with 60 mass% Al_2O_3 powder. The bed was

fluidized by an argon gas flow. Specimens were treated in the bed at 1000 °C for 7.2 ks. The oxidation tests were carried out at 900 °C and 950 °C for 720 ks in air and in a typical exhaust gas atmosphere. An excellent oxidation resistance was obtained and it was attributable to a continuous and sound Al₂O₃ surface layer formed during the treatment. This protective layer acts as a barrier against the formation of a complex oxide scale consisting of a TiO₂ layer and a porous inner layer of TiO₂ and Al₂O₃. The new surface treatment gives an oxidation resistance superior to that of the Ni-base superalloy Inconel 713C up to 950 °C.

Fatigue tests were performed on the compact tension specimens of Type 304 stainless steel and Inconel 718 by Heung-Bae et al [72] to investigate the effects of specimen thickness on crack tip deformation and fatigue crack growth rate (FCGR). Specimens of different thickness were used. The results show that FCGR is a function of specimen thickness, the effect of which is accelerated as specimen thickness increases. Therefore, it is thought that not only applied stress level but also specimen thickness should be taken into account in the measurement of FCGR, which is not considered in ASTM E 647, 1995 Standard test method for measurement of fatigue crack growth rates.

Neville et al [73] studied the erosion-corrosion behaviour of two nominally corrosion resistant alloys (a superduplex stainless steel, UNS S32760 and Inconel 625 (UNS N00625) and a wear-resistant material Stellite 6 (UNS AMS5387). The experiments comprised exposure to an impinging jet of 3.5% sodium chloride solution at 100 m/s, 18 °C and 50 °C in the absence of entrained solids and also with 1000 parts per

million sand particles at 25 m/s and 50 °C. It was found that the passive film on the corrosion resistant materials remains essentially intact under solids-free impingement but that these alloys exhibit active corrosion under liquid-solid impingement and that the direct and indirect effects of corrosion on the erosion-corrosion behaviour of such alloys can be extensive. The study also demonstrated that there is a potential for significant galvanic interactions between materials when under different erosion regimes.

The fatigue crack growth behavior of Inconel 718 was investigated under rotating bending fatigue at room temperature, 300, 500, and 600 °C in air by Chen et al [74]. It was found that the fatigue strength of plain specimens increased considerably in the long-life region at the elevated temperatures, because the early growth of a small crack in the range of 20 to 30 μm was suppressed. However, a crack grew faster at higher temperature after growing beyond about 50 μm due to the decrease of crack growth resistance. The fatigue life in the stable crack growth period can be predicted by the small crack growth law.

Fatigue and creep-fatigue tests were carried out at 850 °C by Yamamoto et al [75] to investigate the creep-fatigue life characteristics of Inconel 738LC. Test results show that the degree of life reduction does not depend on the scale of hold time. To clarify the creep-fatigue damage mechanisms under creep-fatigue loading, in-situ SEM observations were carried out during the tests. In the tensile strain hold test, multi-site grain boundary cracking was observed from the beginning of the test. On the other hand, only a single main crack was observed in the compressive strain hold test. The crack propagates in an

intergranular manner, and it is different from the features observed under cyclic fatigue conditions. Through the detailed observations, it was found that the grain boundary sliding damage occurs at most surface grain boundaries.

Edris et al [76] carried out a detailed microstructural examination of coatings of the Ni-based alloy Inconel 625 deposited onto mild steel substrates using high-velocity oxy-fuel thermal spraying. The deposits were analyzed using X-ray diffraction and optical, scanning electron, and transmission electron microscopy. It was found that the as-sprayed microstructure consisted of Ni-based metallic regions together with oxides exhibiting the Cr_2O_3 and NiCr_2O_4 crystal structures. Although the metallic regions were mainly highly alloyed, the presence of Ni-rich grains was detected in all coatings.

Lopez et al [77] investigated the microstructures developed during diffusion bonding of Inconel 625 and Hastelloy G3 nickel alloys to an AISI 4130 low alloy steel by hot uniaxial pressing, plane strain compression, hiping, and coextrusion. Light microscopy, scanning electron microscopy, and scanning transmission electron microscopy were used to analyze the microstructures. An examination of the steel/superalloy interface revealed that a metallurgical bond is obtained by the interdiffusion of different elements. Carbon diffusion from the steel into the superalloy was found to cause carbide precipitation close to the interface. In all instances, a displacement of the interface between the austenite and the ferrite toward the steel side was evident. Furthermore, it was determined that the microstructural changes observed could impair the corrosion resistance of the superalloy.

Liu et al [78] undertake a systematic research to determine the effect of cold rolling on the precipitation kinetics of δ phase in Inconel 718. He found that above 910 °C, cold rolling promotes the precipitation of delta phase and below 910 °C, the precipitation of δ phase is still preceded by the γ'' precipitation in cold-rolled Inconel 718. Cold rolling promotes not only the precipitation of γ'' phase but also the γ'' yields δ transformation. Further, he reported that the relationship between the weight percentage of δ phase and aging time follows the Avrami equation

The grain structures and microscopic features of a nickel-base Inconel 738LC were examined under various melting and casting conditions by Lin et al [79]. Results show that the grain size of the γ matrix is reduced significantly by a treatment of lowering melt superheat temperature (LMST). By the addition of a trace intermetallic compound Al_xNi_y to the melt together with LMST treatment, a remarkable refinement could be obtained. The grain size over the whole section of castings could be refined to 0.5-0.8 mm, i.e. to ASTM grain size M11-12. In addition, the size of primary MC carbides in the alloy is reduced and the secondary dendrite arm spacing and phase constitution of the alloy are less sensitive to the additions.

Liu et al [80] studied the precipitation of intermetallic phases such as the equilibrium δ phase in Inconel 718 alloy due to cold rolling. The as-received alloy was cold rolled to obtain strips of 10 mm thickness after which the strips were fully solution treated at 1040 °C for 1 h followed by air cool, and then cold rolled by 25%, 40%, 50%,

65% reduction in thickness in multiple passes. The influence of cold rolling altered the morphology of the δ phase and the shape of the δ phase changed from needle to spheroid with an increased in cold rolling reduction.

Keiji et al [81] studied Hydrogen embrittlement and intergranular corrosion of sensitized SUS316 steel and Inconel 600. Intergranular corrosion susceptibility with the strauss test for SUS316 steel increased with sensitized time and reached a maximum at 650 °C, 86.4 ks, then decreased. Intergranular corrosion susceptibility in boiling 40% HNO₃ test for Inconel 600 increased with sensitized time and reached a maximum at 650 °C, 8.64 ks, then decreased. Hydrogen embrittlement susceptibility with the tensile test under cathodic charging on SUS316 steel increased with formation of Cr depleted zones. On the other hand, hydrogen embrittlement susceptibility with the tensile test under cathodic charging on Inconel 600 increased with formation of Cr carbides.

Cherian et al [82] used Scanning Auger electron spectroscopy and x-ray photoelectron spectroscopy analyze discolored gold plating on nickel alloys which have been used as a thermal shield inside nacelle housings for various jet engines. The thin gold film is applied to serve as a low emissivity coating to reflect thermal radiation. Inconel 625 sheet was gold plated and exposed to 590 °C in air for 924 hours to achieve an appropriate service use reference point. The visual appearance of the gold thin-film surface had noticeably dulled after this prolonged exposure. Further, in some cases, several dark spots a few microns in size also appeared on the dulled gold surface. The x-ray photoelectron spectroscopy and Auger electron spectroscopy were used to

differentiate the composition of the gold plated Inconel samples prior to thermal exposure and after the prolonged exposure. Scanning Auger micrographs showed that the composition of the dulled gold surface had changed due to the diffusion of nickel from the substrate alloy through the gold thin film. Nickel was absent at the surface of the unexposed samples while significant nickel concentrations were detected on the discolored gold surface and with the highest nickel levels detected in the dark spots on the gold surfaces. Auger depth profiles made on the exposed gold film verified that a discrete gold layer remained on top of the Inconel with a broad Ni-Cr-Au zone beneath this gold layer.

Ashour et al [83] Investigated the effect of sulfate ions on the crack growth rates (CGRs) of notched specimens of Inconel 600 under constant load in chloride containing aqueous solutions at 250 °C. The intergranular stress corrosion crack growth rates increased in chloride solutions while its hinder with increasing sulfate concentrations. Stress intensity factor (k) for stress corrosion cracking decreased with increasing of aggressivity of chloride ions while increased in the presence of sulfate solutions. At very low concentration of chloride (0.001 m), k-value retardation was observed. It is clear from the results that hydrogen in the aqueous solutions has a deleterious effect on crack propagation. The difference in crack growth rates in chloride ions and in chloride containing sulfate solution at high temperature can be recognized as caused by the difference in local environment conditions at a crack tip. The results indicate that the crack don't propagate under this conditions in the presence of sulfate ions. It is mainly

due to a hinderance of chloride ions adsorption on active sites of the fracture surfaces and the formation of chromium oxide layer which is stable at higher temperature

Hong et al [84] analyze the crystal structure and morphology of the γ'' phase of Inconel 718 superalloy utilizing transmission electron microscopy (TEM) Samples cut from heat-treated material were punched and thinned by twin-jet electropolishing technique The analysis of the diffraction patterns suggested the γ'' phase had a thin ellipsoidal disc shape with its c-axis perpendicular to the discs

Yilbas et al [85] examined the corrosion properties of Inconel 617 alloy, after 37,000 h of operation as a transition piece in the gas turbine engine The workpiece surfaces are treated using an Nd YAG pulsed laser The electrochemical tests are carried out in 0.1 N H_2SO_4 + 0.005 N NaCl deaerated aqueous solution at room temperature It is found that the laser treated workpieces result in improved corrosion rates The locally scattered shallow pits are observed at the workpiece surface after the electrochemical test

Solid-state diffusion bonding of Inconel registered trademark alloy 718 to 17-4 PH registered trademark stainless steel was studied by Guoge et al [86] Mechanical tests and metallographic examinations were used to evaluate the joint quality The effect of bonding pressure on the joint integrity was also assessed In all joints, failure occurred nearly without plastic deformation The thermal residual stress generated from cooling to room temperature was calculated by finite element modeling and the result showed

that the poor joint ductility was not caused by the residual stress, but by the formation of continuous intermetallic films along the interface.

Seawater corrosion behavior of laser surface treated Inconel alloy was investigated by Cooper et al [87]. They showed that corrosive damage was more severe in the WC injected than the TiC injected workpieces and the laser melted workpieces

Pitting corrosion of mill annealed Inconel alloy in aqueous chloride and chloride-thiosulfate solutions at low temperature was studied by Ho and Yu [88]. They indicated that pit density and average pith depth increased with increasing concentration of sodium chloride and temperature of solution.

Ganzalez-Rodriguez and Fionova [89] studied the intergranular corrosion due to structural evaluation. They demonstrated that the correlation existed between intensity of intergranular corrosion of the alloy and the effect of fragmentation of large grains.

Chen et al [90] studied the susceptibility to heat-affected zone (HAZ) cracking during electron-beam welding in two Inconel 718 based alloys doped with different levels of boron. He reported that by lowering the carbon, sulfur, and phosphorous concentrations to be "as low as possible," the occurrence of HAZ cracking was related directly to the level of segregation of boron at grain boundaries, which occurred by non equilibrium segregation during a pre weld heat treatment. Further, the study has demonstrated a direct correlation between the amount of boron segregated at grain

boundaries and their susceptibility to HAZ cracking, in terms of the total crack length and number of cracks observed in the HAZ. The analysis of results suggests that both the melting and re-solidification temperatures of the boron-segregated grain boundaries can be about 100 °C to 200 °C lower than those of the grain boundaries that were susceptible to constitutional liquation of Nb carbides on them, making boron more deleterious in causing HAZ cracking.

The application of a $\text{Ce}(\text{SO}_4)_2$ slurry to two Ni-based, and one Fe-based superalloy is analyzed in terms of oxide morphology and microstructure developed after oxidation in air at 930 °C for 225 hours by Rabbanı et al [91]. He found that, the alloy containing the greatest amount of Al suffered the most internal damage upon application of the $\text{Ce}(\text{SO}_4)_2$ slurry as compared with the control coupon. The oxide/alloy and oxide/gas interfaces were also more convoluted for the Ni-based alloys with the $\text{Ce}(\text{SO}_4)_2$ coating than the control coupons. From inspection of the metallographic cross-sections it is apparent that the $\text{Ce}(\text{SO}_4)_2$ application rendered a thinner oxide on the two Ni-based alloys. Transmission electron microscope (TEM) of the microstructure revealed differences in oxide grain size for the three alloys. The greatest variation was seen in the structure of the oxide formed on Inconel 601 with $\text{Ce}(\text{SO}_4)_2$ application. The grains were 10 times larger on average, and crater-like formations were noted. Considerable plastic deformation in the form of dislocation loops was also present. Precipitates were noted predominately in the oxide grains formed on Incoloy 800, and at grain boundaries for Inconel 601.

Zupanic et al [92] characterizes the structure of continuously cast Ni-based superalloy IN 713C using several microstructural characterization techniques (LM, SEM, TEM, EDS, XRD) They reported that the structure consisted of columnar dendritic γ -grains with apparently fully coherent and rather uniformly distributed γ' precipitates, primary MC carbide and MC/ γ eutectic The eutectic MC carbide contained a considerable amount of Cr resulting in a decrease in the MC lattice constant from 0.441 to 0.435 nm Due to higher cooling rates at continuous casting the microstructural constituents were much finer than in the as-received samples In addition, the continuously cast specimens did not contain the γ - γ' eutectic and some minor phases despite stronger segregation of solute elements The partition coefficients of solute elements Ti, Mo, Nb, Al, Cr, Fe and Ni in the continuously cast IN 713C were 0.55, 0.82, 0.46, 0.99, 0.96, 1.02 and 1.03, respectively

Summary Of Literature Review Associated With The Present Work

The studies reported previously in the open literature are involved with electrochemical, mechanical, and metrological properties of Inconel alloys particularly Inconel 625 and 718. Studies on Inconel 617, however, are limited in number and were dealt mainly with the alloy, which were not subjected to long hours of operation at an elevated temperature. Moreover, Inconel 617 is widely used as hot-path component (i.e. transition piece, liner etc.) in gas turbines, therefore, investigation into electrochemical, mechanical and metrological properties of the alloy after used for long hours of operation is essential. Furthermore, to reduce the maintenance cost and minimize the frequency of the component replacement, investigation into the refurbishment of the components, which are subjected to thermal and mechanical degradation, and their life extension becomes necessary. The present study is conducted in the light of the literature review and the need for the refurbishment of the alloy. Since the alloy has the commercial interest in the industries, no such study is presented extensively in the open literature. Consequently, it become difficult to compare the present findings with the data available in the open literature.

CHAPTER 3

EXPERIMENTAL WORK

To examine the effect of the refurbishment, Inconel 617 workpieces were subjected to mechanical and electrochemical tests as well as microstructural analysis. The equipment used are discussed in the experimental apparatus section in this chapter.

Microstructural analysis

Microstructural analysis is the combined characterization of the morphology, elemental composition and microstructural features through the use of microscope. In the present work the Scanning Electron Microscope (SEM) was used to examine the morphology of the fracture surface. The Energy Dispersive Spectroscopy (EDS) was used to obtain the elemental composition at the fracture surface.

Mechanical Tests

Two types of mechanical test were conducted on the workpieces namely, Tensile and Fatigue tests. Both tests were performed using Instron 8501 machine. The tensile test is the one that is used most commonly to evaluate the mechanical properties of materials. Its main use is the determination of properties related to the elastic design of machines and structures. In addition, the tension test gives information on a material's plasticity and fracture. The chief advantages of the tension test are that the stress state is well established and the test has been carefully standardized. In a tension test workpieces are subjected to a tensile load, which is gradually increased until fracture. The strain caused by the applied load is plotted in an x-y chart.

Fatigue tests are conducted to determine the behavior of materials under fluctuating loads. It is classified as crack initiation or crack propagation test. A specified mean load (which may be zero) and an alternating load are applied to workpieces and the number of cycles required to produce failure (fatigue life) is recorded. The alternating load can be applied in several ways (axial, plane bending, rotating etc.) to the specimens. In this work axial fatigue life test was conducted on the workpieces.

Electrochemical Analysis

Corrosion is defined as the destructive and unintentional attack of a metal. It is an electrochemical process and ordinarily begins at the surface. In here the corrosion rate was determined via potentiodynamic measurements utilizing standard saturated calomel electrode with controlled rate of leakage laboratory test.

Experimental Conditions and Apparatuses

The workpiece elemental composition is given in table 3.1. The workpieces were prepared from the transition piece of a gas turbine engine which had about 37000 hours of operation in the field as shown in figure 3.1. The workpieces were cut in standard size for tensile and fatigue testing and ground down to 2 mm thickness as shown in figure 3.2. They were cleaned chemically and ultrasonically before the heat treatment process. Figure 3.3 shows some of the workpieces after and before the heat treatment and mechanical tests. High temperature furnace was used during the heat treatment process and the high temperature oxidation of workpieces was prevented through placing them in

quartz tubes in the furnace as shown in figure 3.4. In the heat treatment process one temperature level and two heat durations are considered as reflected in table 3.2 below.

Ni	Cr	Co	Mo	Al	C	Fe	Mn	Si	S	Ti	Cu
Balance	22	12.5	9	1.2	0.07	1.5	0.5	0.5	0.008	0.3	0.2

Table 3.1 Chemical composition of Inconel 617 alloy (wt %).

Temperature (°C)	1175	1175
Duration (hours)	1	2

Table 3.2 Heat treatment conditions

Electrochemical tests were carried out using a three-electrode-cell as shown in figure 3.5. The cell accommodated inlet and exit for an inert gas and thermometer. A potentiostat maintaining the electrode potential within 1 mV of a preset value over a wide range of applied current was employed. A computer controlled scanning potentiostat (EG&G model 273) was used for potentiodynamic measurements. A record of current and potential was plotted continuously using an x,y recorder. In the experiment, standard methods were used, i.e. a saturated calomel electrode with controlled rate of leakage was employed as reference electrode, and the electrolyte was an aerated 0.1 N H₂SO₄ and 0.05 N NaCl held at 25 °C. The workpieces were prepared as coupons as indicated in figure 3.6 as well as standard samples as shown in figure 3.2. The coupon workpieces surfaces are masked to expose a surface area of 1 cm². The standard sample surfaces were partially masked by epoxy, provided that the central region of the workpiece (50

mm from the lateral center-line) was exposed to a electrolytic solution. Electrochemical tests are repeated three times and it is observed that in all times the results are identical.

Mechanical properties (fatigue and tensile test) of Inconel alloy were investigated before and after the heat treatment of the workpieces as well as after the electrochemical tests. Table 3.3 reflects the maximum and minimum loads used during mechanical tests. Table 3.4 gives the fatigue test conditions for the as received (untreated) workpieces while tables 3.5 and 3.6 indicate the fatigue test conditions for one and two hours heat treated workpieces, respectively. The mechanical test were repeated three times and the result of the tests are found to be identical.

Figure 3.7 shows the Instron 8501 material testing system used to obtain tensile and fatigue data. The system is a closed loop servo-hydraulic, dynamic, single axis fatigue testing system equipped with a hydraulically actuated self-aligning gripping system. The machine maximum load capacity is ± 100 KN with displacement of ± 75 mm and strain of ± 25 %. To ensure the vertical alignment of the specimen, specially machined metal inserts are used during the tests. Any preloading induced during clamping is adjusted to zero prior to testing by balancing of the load cell after clamping.

All tensile and fatigue tests are carried out using a specialized Fatigue Laboratory Application Software [FLAPS], which provided complete machine control, data acquisition, data reduction and analysis capability. All constant amplitude fatigue tests and position increment tensile tests are designed in FLAPS. Tensile tests are carried out under position control. The software logged position and corresponding load of the test with a constant position increment until fracture occurred at the

ultimate tensile strength The elastic modulus of Inconel 617 is obtained by getting the load and position data throughout the test The final stress value just before the fracture is selected as the tensile strength and the final actuator position gave the corresponding strain

Fatigue tests conducted through FLAPS as follows, initially a ramp to mean load level and then a sinusoidal loading with a frequency of 20 Hz at a stress ratio $R = 0.1$ The maximum cyclic stress ranged approximately from 60% to 80% of tensile strength of the material

	Fatigue
Maximum Load (kN)	26
Minimum Load (KN)	1.5

Table 3.3 Maximum and minimum loads used during mechanical tests

Sample no	Area of cross section (mm ²)	Load _{max} (KN)	Load _{min} (KN)	Fatigue life (cycles)
617-AR-F1	46 3855	15 46	1 546	778,101
617-AR-F2	44 9344	17 97	1 797	190,730
617-AR-F3	44 175	19 14	1 914	235,101
617-AR-F4	45 934	21 44	2 144	142,646
617-AR-F5	47 9552	23 98	2 398	66,217
617-AR-F6	47 3922	25 28	2 528	69,699

KN Kilo Newton

Table 3.4 Fatigue test condition for as received workpieces

2

Sample no	Area of cross section (mm ²)	Load _{max} (KN)	Load _{min} (KN)	Fatigue life (cycles)
617-h1-f1	43.6	14.53	1.453	238714
617-h1-f2	48.5	19.4	1.94	223139
617-h1-f3	51.1	22.14	2.214	105647
617-h1-f4	42.93	20.03	2.00	92142
617-h1-f5	47.86	23.93	2.393	57955
617-h1-f6	40.64	21.68	2.168	40651

KN Kilo Newton

Table 3.5 Fatigue test condition for workpieces heat treated at 1175 °C for 1 hours

Sample no	Area of cross section (mm ²)	Load _{max} (KN)	Load _{min} (KN)	Fatigue life (Cycles)
617-h2-f1	49.2	16.4	1.64	555865
617-h2-f2	44.66	17.86	1.79	120089
617-h2-f3	41.91	18.16	1.82	89691
617-h2-f4	50.50	23.57	2.36	51356
617-h2-f5	45.22	22.61	2.26	59253
617-h2-f6	48.51	25.87	2.59	51222

KN Kilo Newton

Table 3.6 Fatigue test condition for workpieces heat treated at 1175 °C for 2 hours

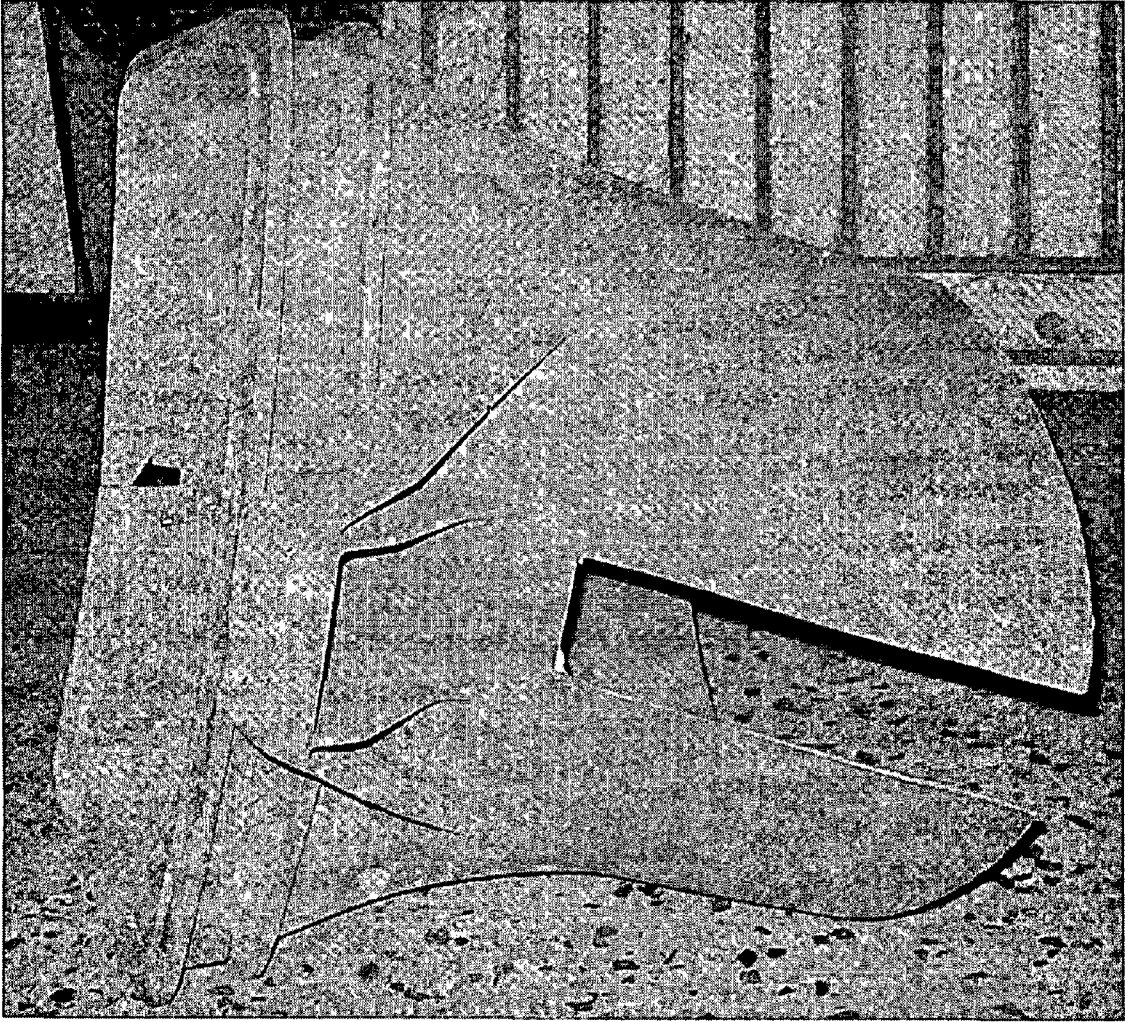
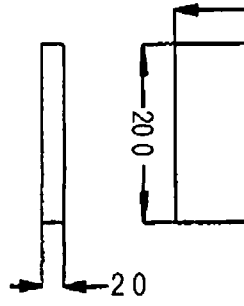


Figure 3 1 Gas turbine transition piece after cutting the workpieces out of it



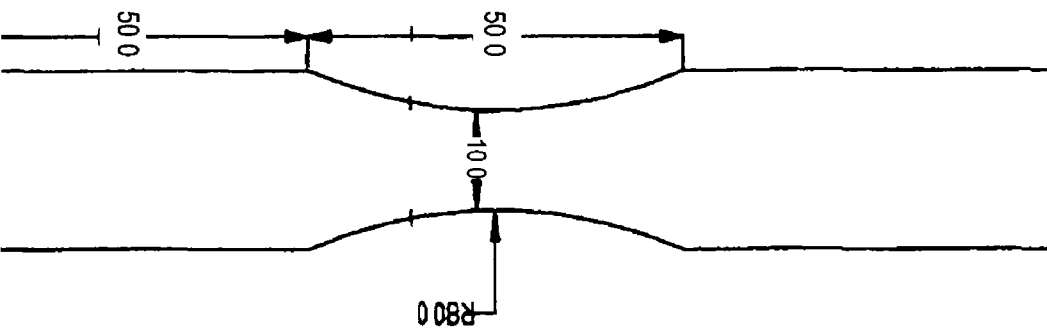


Figure 3 2 Dimensions of the workpiece in mm

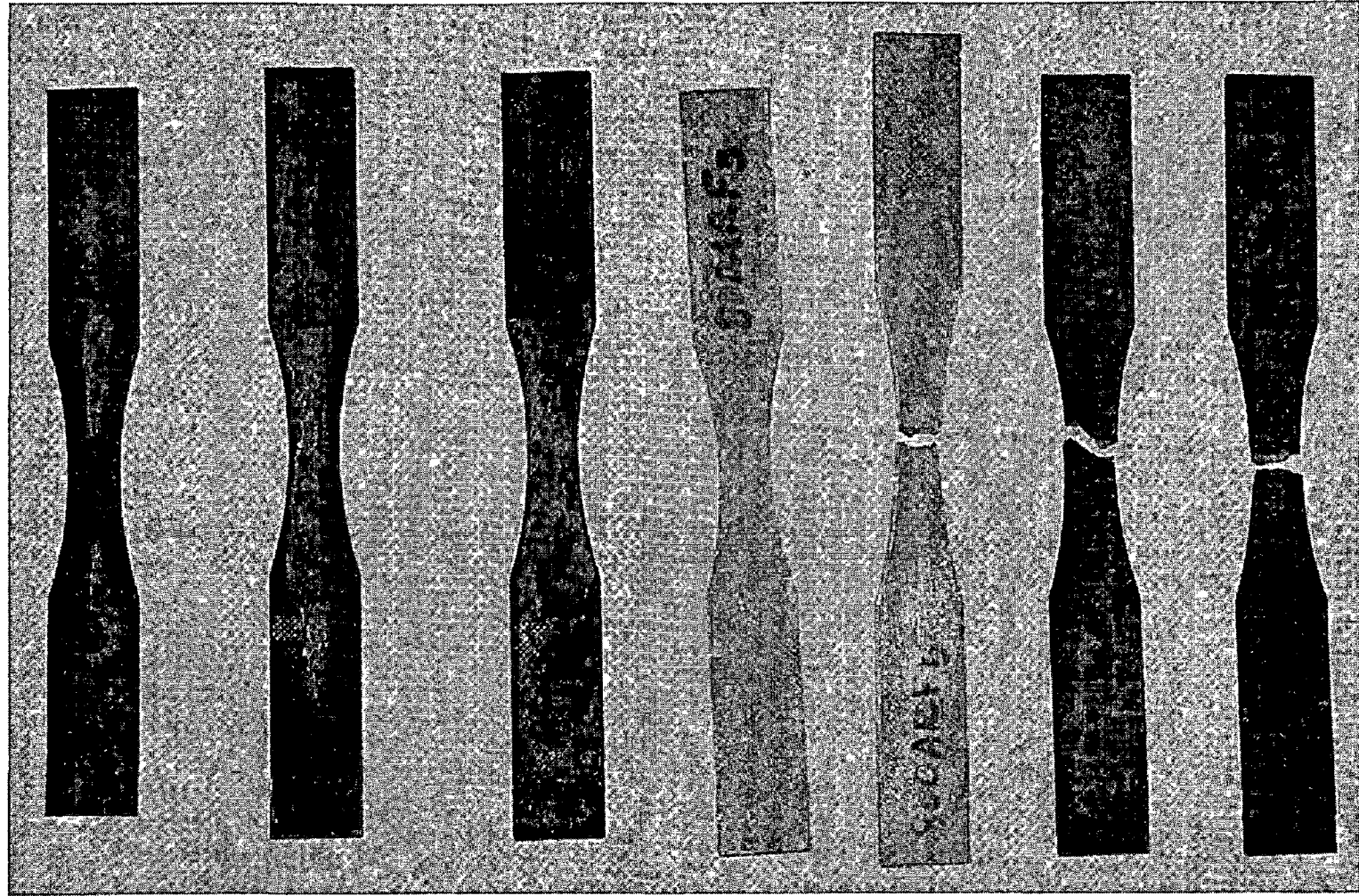


Figure 3 3 Workpieces before and after heat treatment

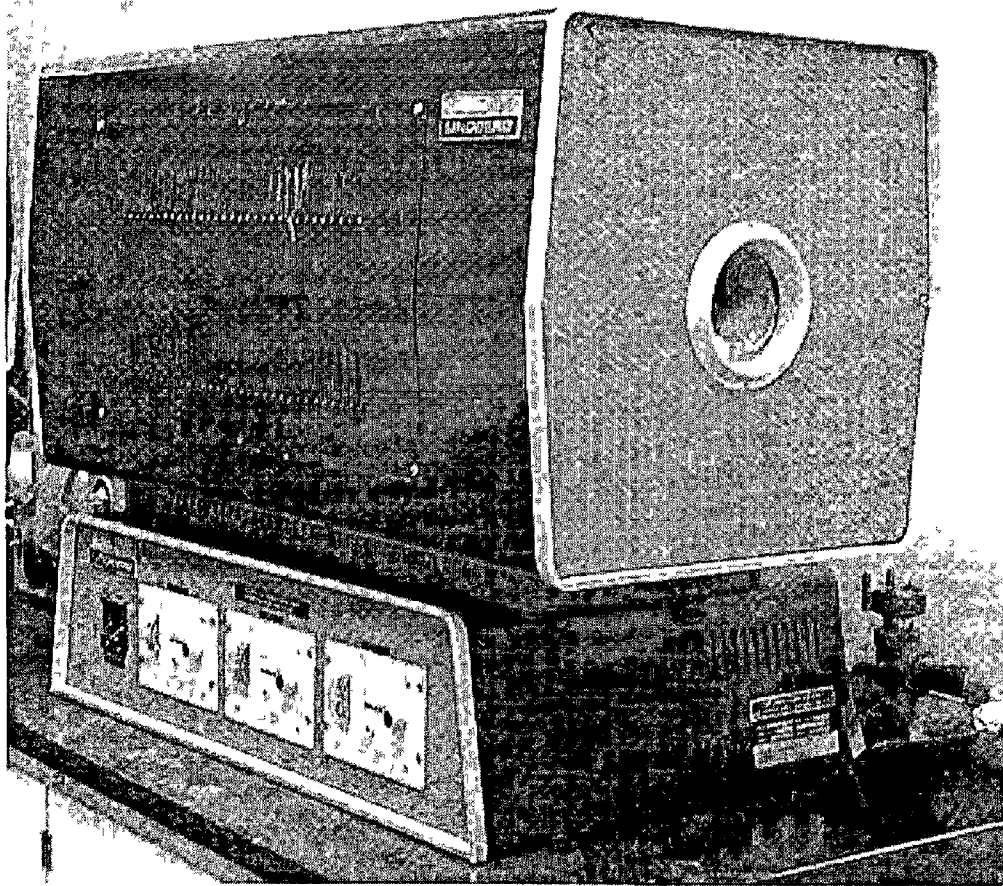


Figure 3 4 High temperature furnace

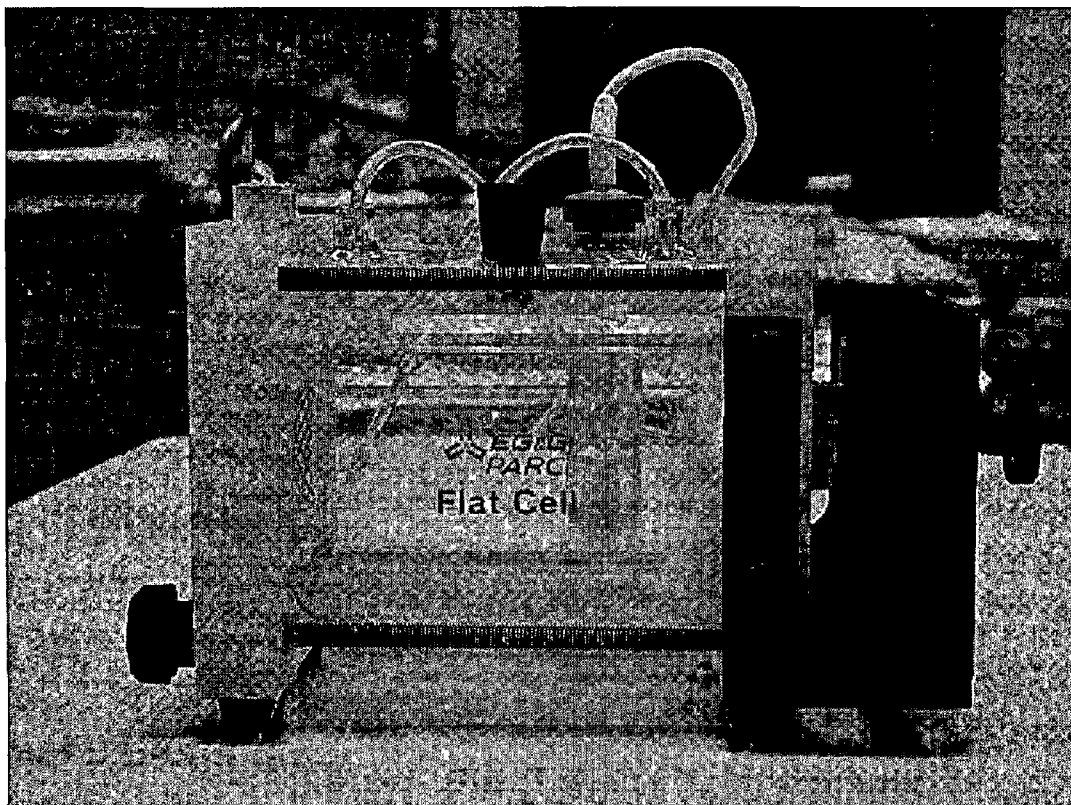


Figure 3 5 Corrosion cell used in the electrochemical tests

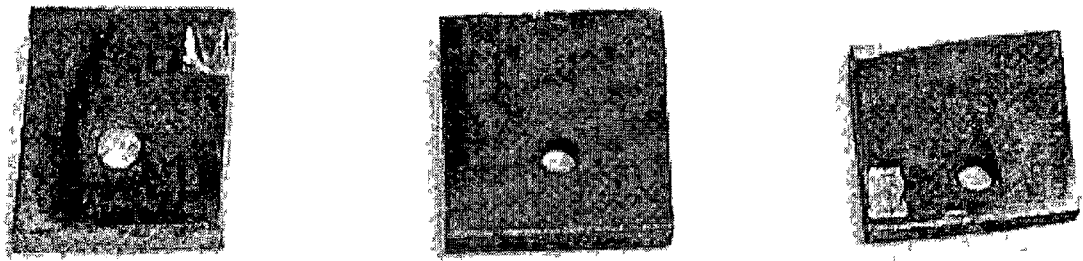


Figure 3 6 Workpieces coupons used in the electromechanical test

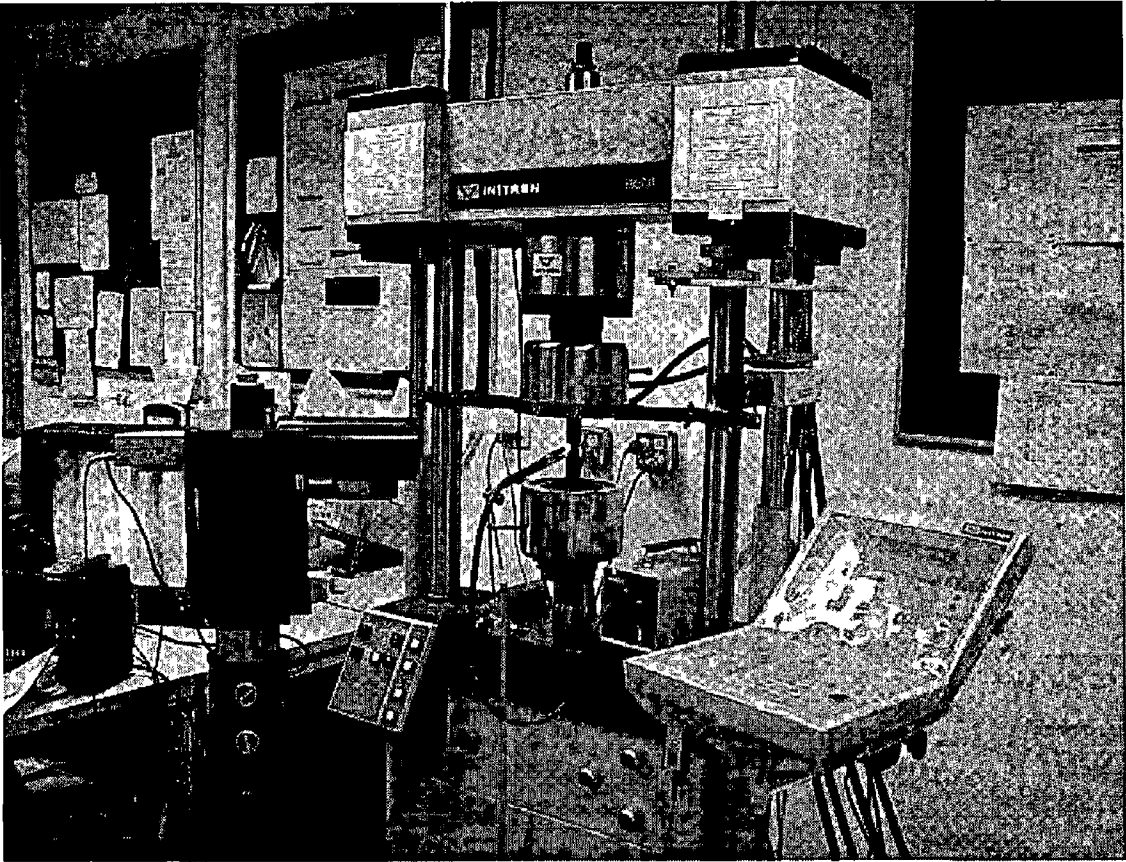


Figure 3 7 Instron 8501 system used for the mechanical tests

SEM is carried out to obtain the micrographs of the cross-section of workpieces and fractographs of fractured surfaces. SEM model JSM-5910 by JEOL was used in this work the picture of which is shown in figure 3.7 and its specification is indicated in table 3.3. The JSM-5910 is a high-performance, scanning electron microscope with a high resolution of 3.0 nm. The Intuitive PC Interface allows the instrument to be easily operated with a mouse only. JSM-5910 five axis, computer controlled, specimen chamber can accommodate a specimen of up to 8-inches in diameter and its standard automated features include Auto Focus/Auto Stigmator, Auto Gun (saturation and alignment), and Automatic Contrast and Brightness. The JSM-5910 features an eucentric stage and a super conical lens.

Resolution	3.0 NM (30kV, WD8mm, SEI)
Accelerating voltage	0.3 to 30 kV (55 steps)
Magnification	x 18 to 300,000 (136 steps)
Filament	Pre-centered W hairpin filament
Objective lens	Super Conical lens
Objective lens apertures	Click-stop type (3-step variable) Fine position controllable in X/Y directions
Maximum specimen size	8-inch (203.2mm) dia. Specimen can be mounted
Specimen stage	5 axis computer controlled Eucentric goniometer X=125mm, Y=100mm, Z=5 to 48mm T= -10 to 90°, R=360° (endless)
Display CRT	17-inch SVGA color monitor

Table 3.7 SEM model JSM-5910 specifications

EDS is carried out to determine the elemental composition across workpiece cross sections and fractured surfaces. The qualitative and quantitative information are most commonly determined for a sample by monitoring the emitted X-rays after sufficient external energy is supplied to excite it. These X-rays may be analyzed either by their wavelength or by their energy. Both approaches have their merits and drawbacks and they are usually seen as complementary. For rapid qualitative and semi-quantitative analysis, however, energy dispersive systems utilizing sophisticated computer analysis routines are preferred. This type of spectrometer is currently being operated with the SEM by additions of specific accessories. This enables SEM to do elemental analysis of a particular element within the scanned area.

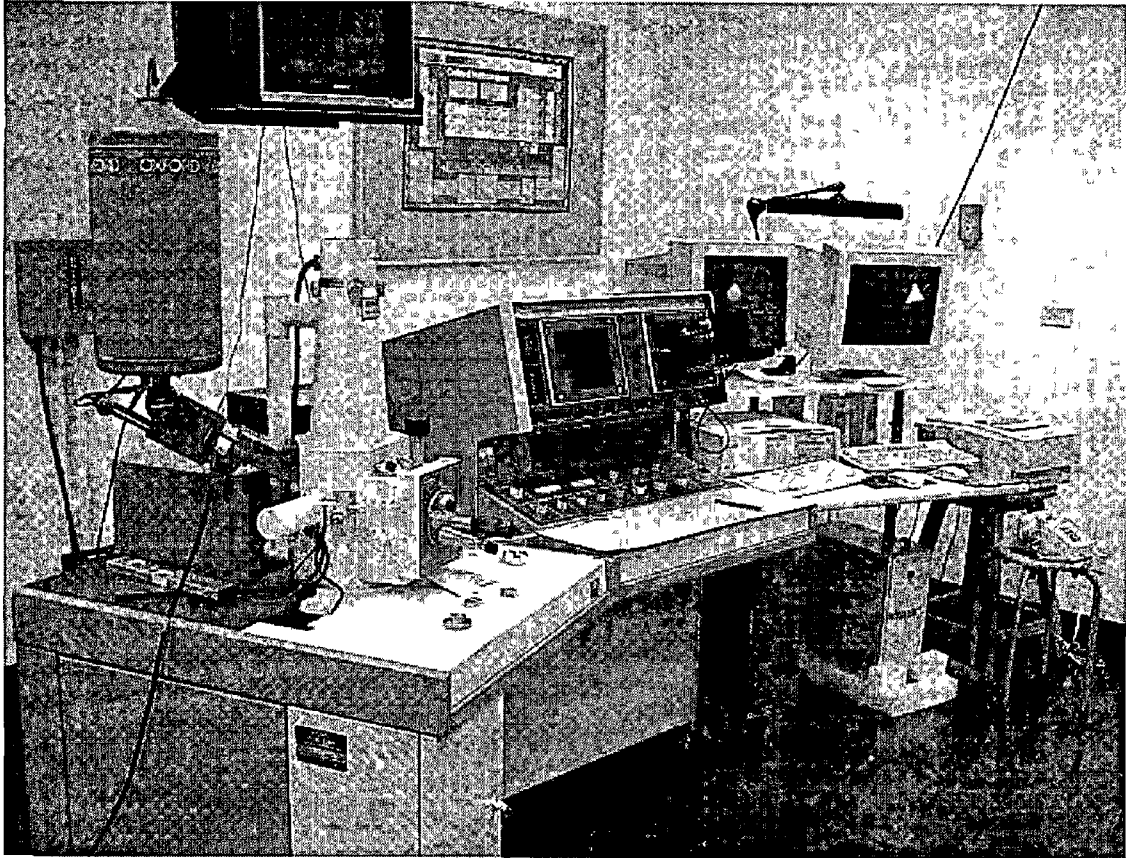


Figure 3 8 Scanning Electron Microscope Model SJM 5910

CHAPTER 4

RESULTS AND DISCUSSIONS

In this chapter the results of the mechanical tests, electrochemical tests, SEM and EDS for the workpieces are presented before and after heat treatment (i.e. refurbishments). It should be noted that the analysis made in this section covers comprehensively the results obtained, therefore, individual test results will be discussed together with other relevant test results.

Heat treatment of Inconel 617 alloy, after about 37000 hours of usage as a gas turbine transition piece is carried out at 1175 °C. Figure 4.1 shows the cross-section of the workpieces before the heat treatment process. The cavitation along the grain boundary is observed for untreated workpiece surface, in which case, agglomeration of grain boundary carbides occurs. The multiple discontinuous creep cracks are also seen. The cavitation at the grain boundary reduces partially after the heat treatment process as depicted in figure 4.2. The EDS data in table 4.1 reveals that the chromium content improves and aluminum degradation slows at grain boundaries after the two hours heat treatment process.

	Al	S	Ti	V	Cr	Fe	Ni
Grain Boundary as received	0.91	7.86	-	0.04	17.37	21.08	52.74
Grain Boundary after one hour heat-treatment	1.01	3.63	-	0.15	22.04	21.29	51.88
Grain Boundary after two hours heat-treatment	2.46	3.48	0.27	0.3	27.97	7.09	58.43

Table 4.1 – EDS results at the grain boundary of the workpieces (% wt)

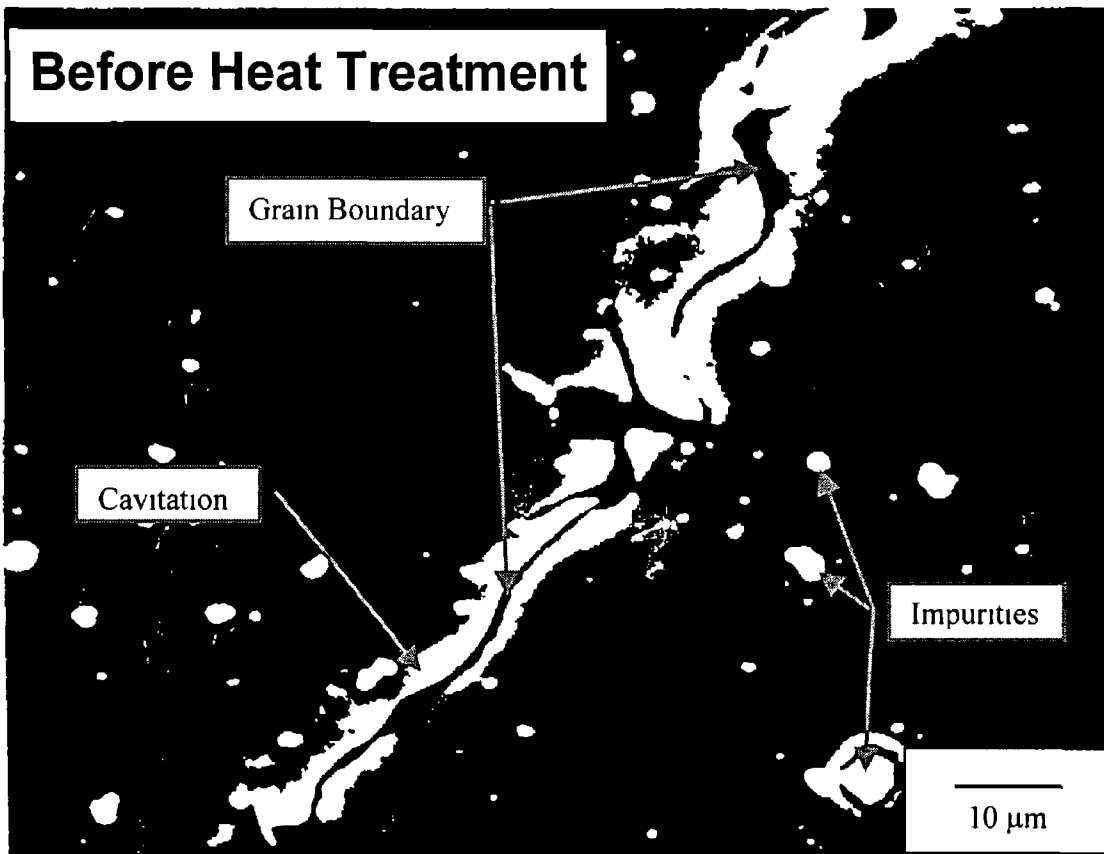


Figure 4 1 Microphotograph at grain boundary before heat treatment

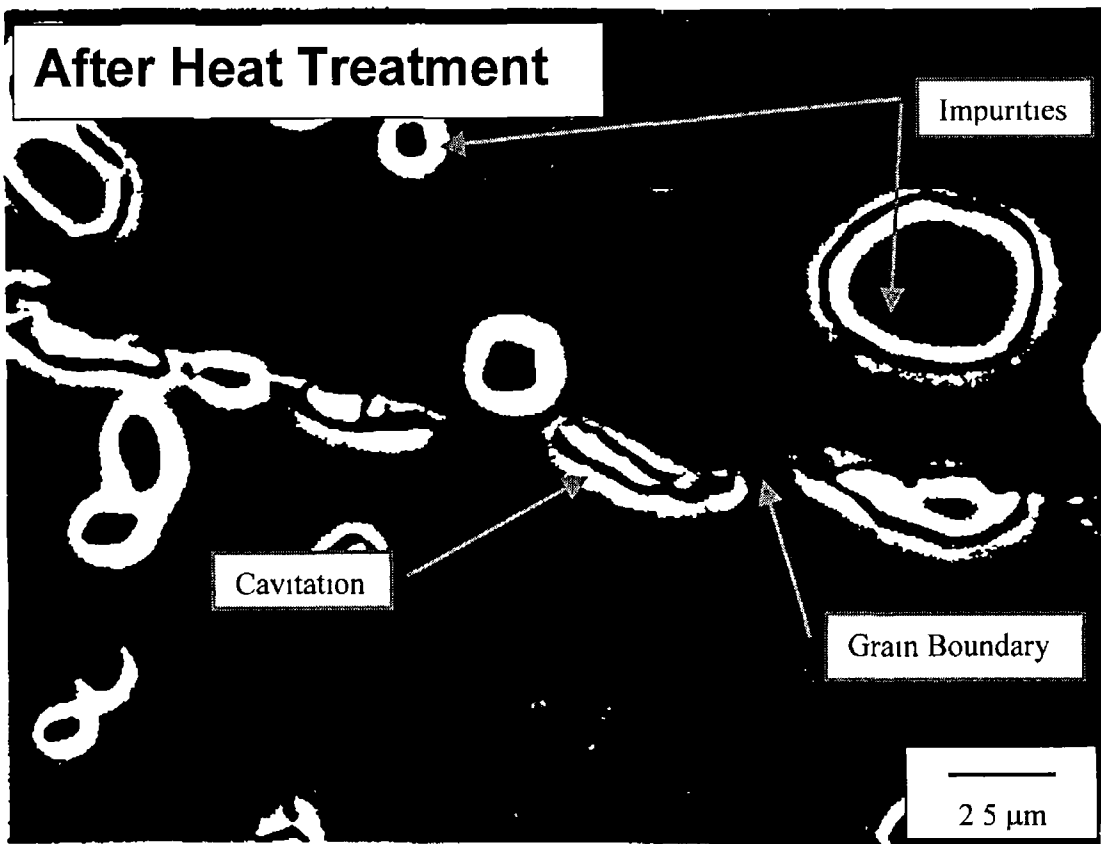


Figure 4 2 Microphotograph at grain boundary after heat treatment of 1 hour

Figure 4 3 shows the fatigue test results before and after the heat treatment process. The fatigue behavior of the heat treated and untreated workpieces appear to be almost the same, i.e. the fatigue properties of the workpiece was not improved considerably by the heat treatment process. This may occur because of the fact that the grain boundaries of the alloy are decorated by large carbide and nitrides. Moreover, the heat treatment results in only partial improvement in the grain boundaries. Consequently, the fatigue behavior of the alloy may not change after the heat treatment process. It should be noted that the grain boundary micro cracks are responsible for an increased effective stress and accelerated the fatigue failure. Moreover, the large grain size accelerates the crack growth as long as it propagates along the same grain boundary in front of the crack tip kinder for further propagation, therefore, the crack propagation diminishes when a subsurface grain boundary is reached. It is expected that the crack propagation from the surface might stop at an early stage in the small-grained workpieces. However, the heat treatment results in locally scattered small grains. Consequently, the effect of grain size on the fatigue response of the heat treated workpiece is not substantial.

Figure 4 4 shows the fatigue test results for the workpieces after and before the electrochemical tests. The fatigue behaviors of the workpieces do not vary considerably, provided that the fatigue properties of the workpieces after electrochemical test are slightly worsens. This is because of the oxide formation in the surface vicinity and micro-pitting at the surface, which can also be seen from figure 4 5, in which the pit sites are shown.

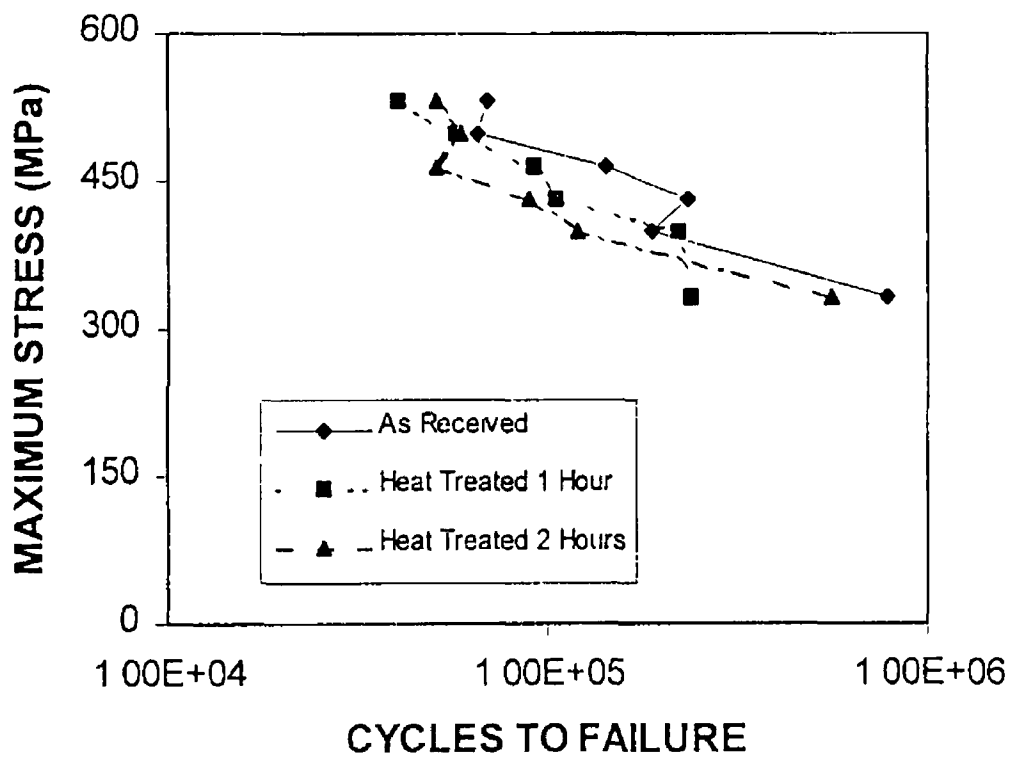


Figure 4 3 Fatigue test result for heat treated and as received workpieces

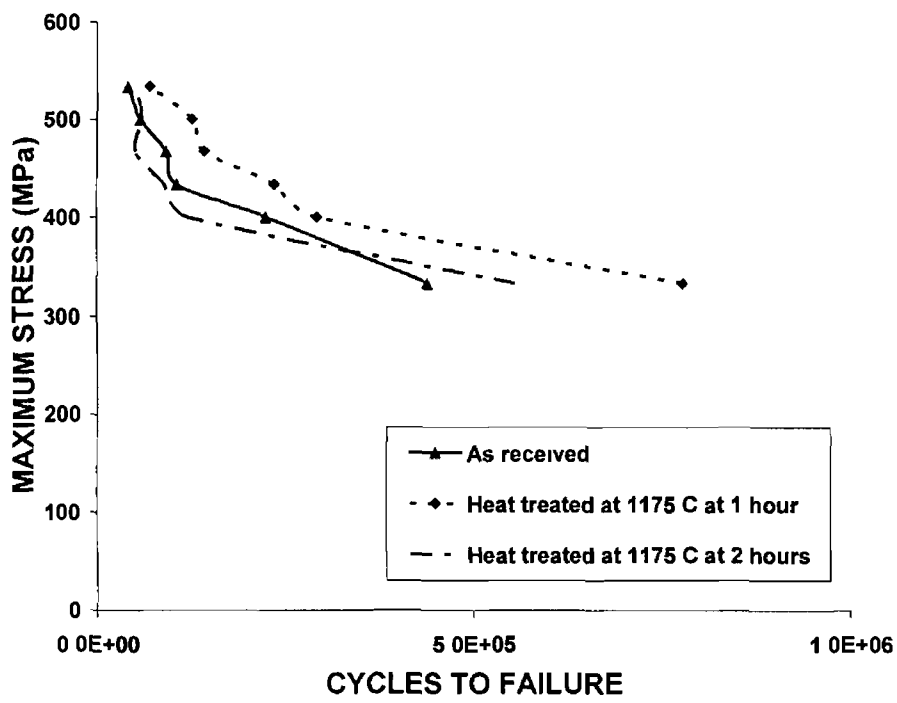
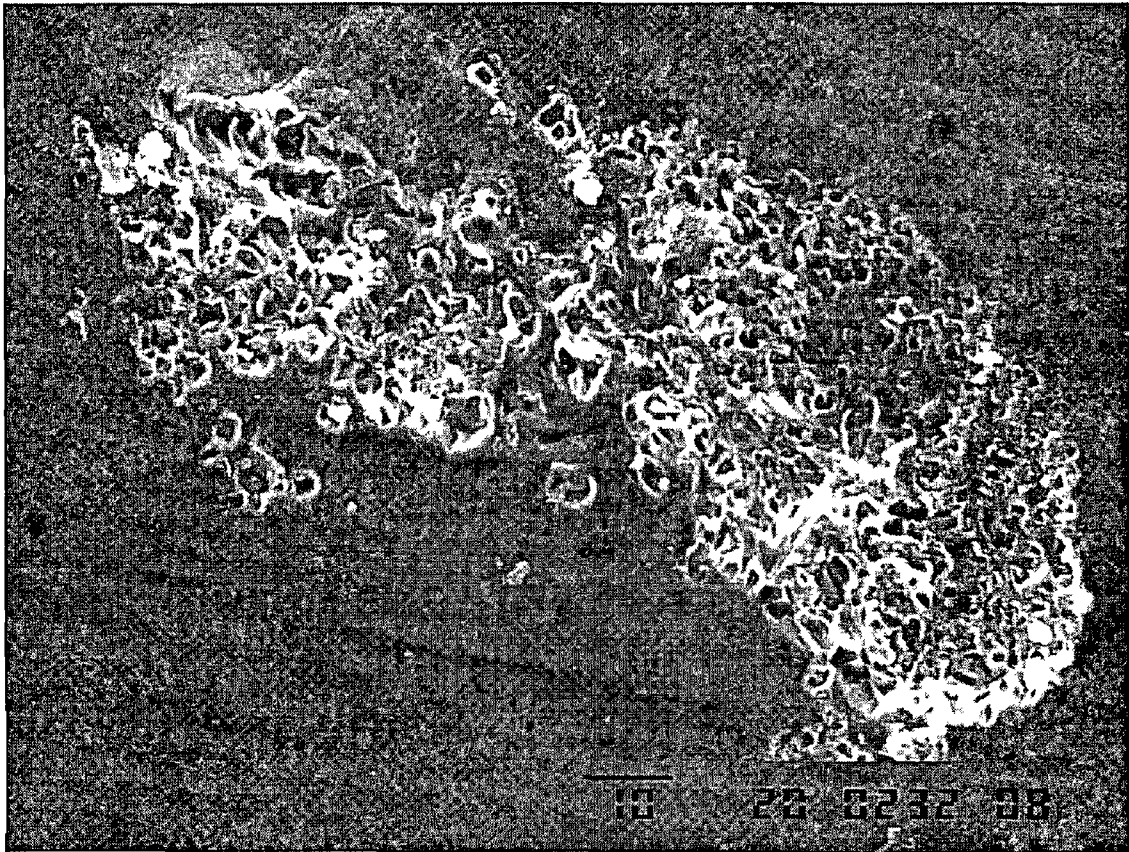


Figure 4 4 Fatigue test results after electrochemical test of the heat treated workpiece



10 μm

Figure 4 5 Micro pits formed at the surface after the electrochemical tests

Figure 4 6 shows the tensile test result before and after heat treatment. Untreated workpieces result in lower strain as compared to those corresponding to heat treatment process. This may occur because that in the case of untreated workpieces, grain boundary carbides exhibit significant grain boundary migration, which in turn enhances the brittleness of the alloy and reduce the strain during the tensile tests. However, heat treatment process decarburize the specimen partially, which is partially free from grain boundary carbides. This enhances the ductility of the alloy and improves the tensile strength through reducing the stress accumulation at the grain boundary. Moreover, the high degree of surface cracking is due to surface oxidation as evident from figure 4 7. Increased ductility occurs due to combination of increased surface cracking and reduced internal creep cavitation as consistent with the early work [19]. Figure 4 8 shows the tensile test results corresponding to heat-treated and untreated workpieces after the electrochemical test. When comparing the electrochemically treated workpieces with untreated, it can be observed that the electrochemically treated surfaces result in slightly less tensile strength. This is because of the partially surface oxidation and increased surface pitting after the electrochemical tests.

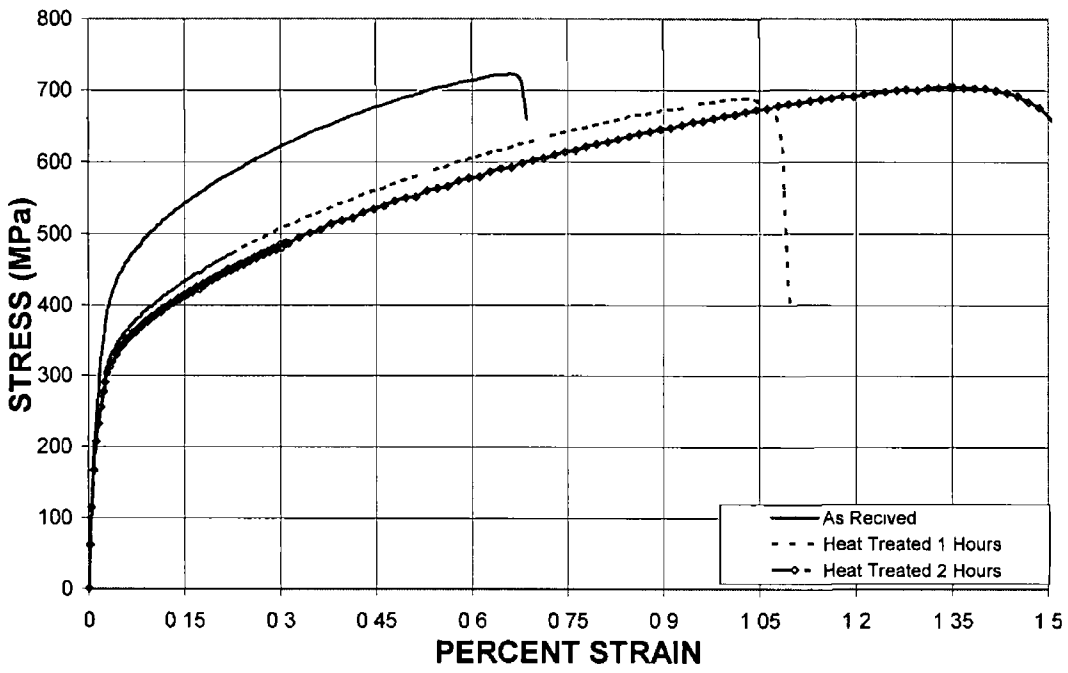


Figure 4 6 Tensile test result for heat treated and as received workpieces

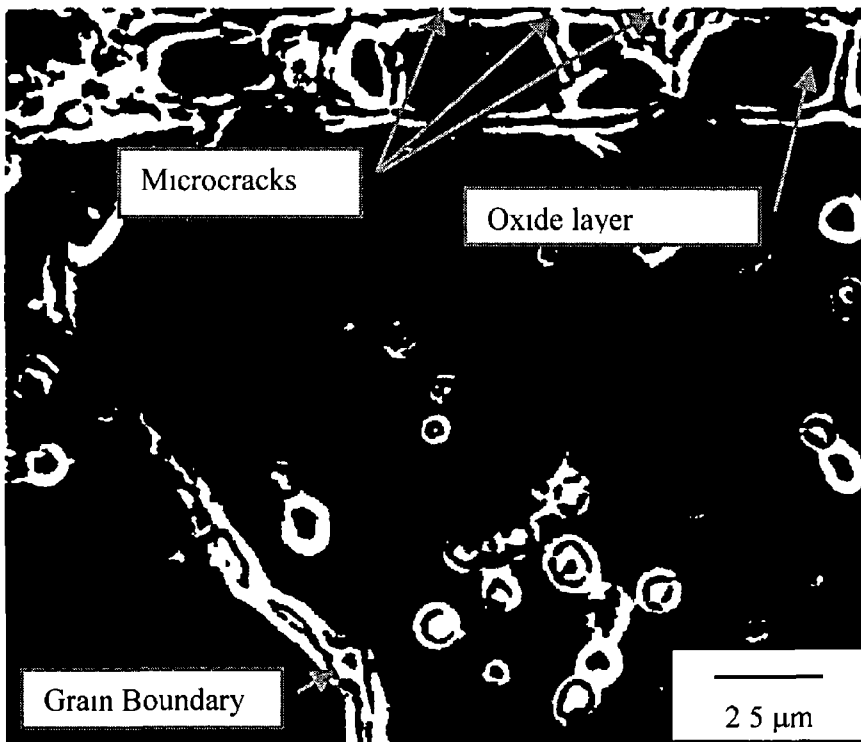


Figure 4 7 Workpiece cross-section close to surface

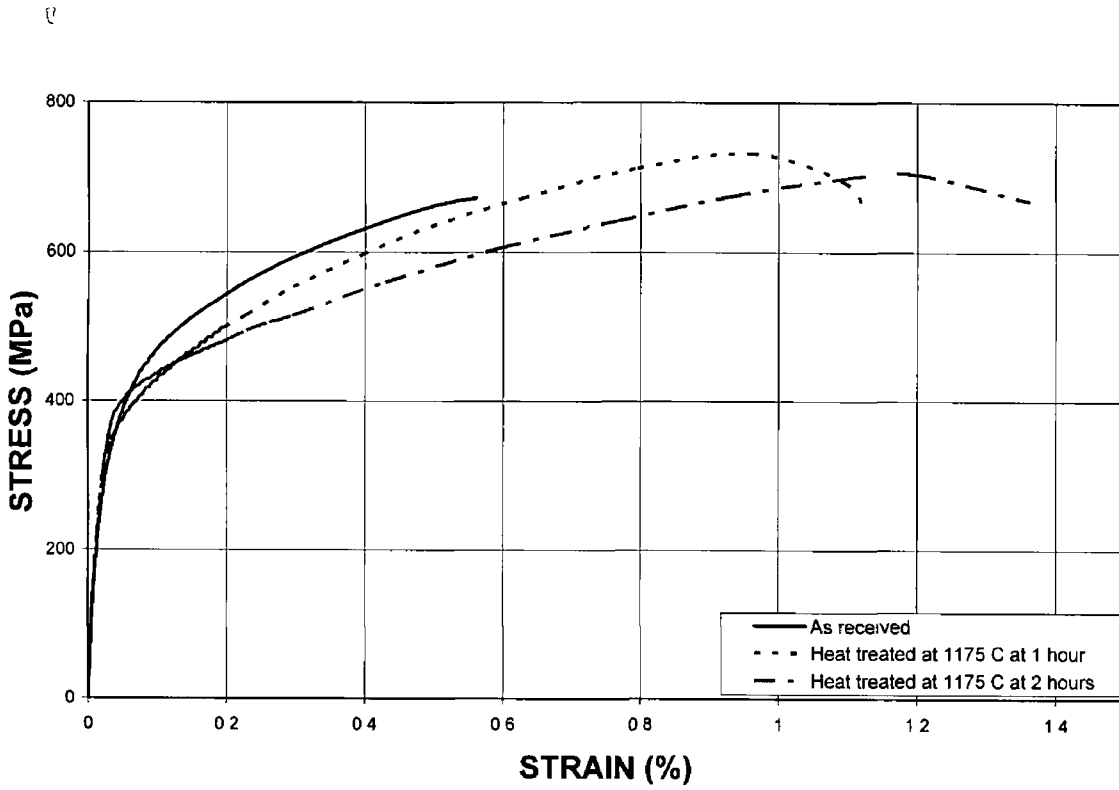


Figure 4 8 Tensile test results after electrochemical test of the heat treated workpiece

Figures 4 9 and 4 10 show the fractographs of workpiece surfaces after tensile and fatigue tests respectively. The tensile fractographs show grain-boundary facets. The existing of the dimples in many areas of grain boundary facets indicates the ductility. The large grain size and presence of cavities facilitates the propagation of the intragranular portions of the fracture. However, at high magnification the transgranular portions of the fracture surface may exhibit dimples. The dimple size varies as evident from figure 4 9b. In this case, micro-void coalescence produces shear dimples with characteristic elongated shape. Moreover, the larger dimples probably formed at carbide or nitride particles. This is presumably initiated by a large inclusion.

When examining figure 4 10a associated with the fatigue fractographs, fracture occurs entirely by micro void coalescence. The variety of sizes of dimples existed. Some feature resembles cleavage facets, since the low degree of flatness is existed, which is normally a characteristic of cleavage. The dimples are the characteristic of fast fracture. High magnification of fatigue-fracture surface is shown in figure 4 10b. The array of regular fatigue striations is visible at the transgranular facets. The secondary cracks at the roots of striations are visible.

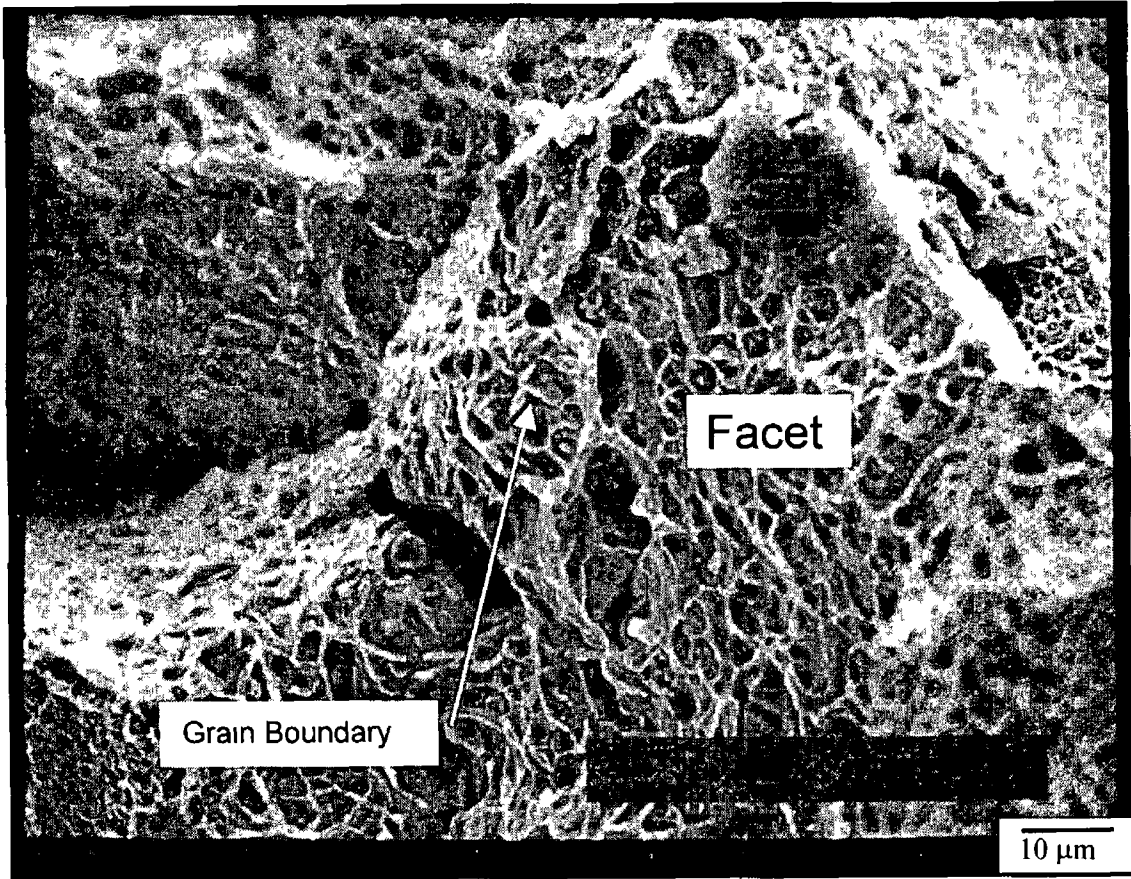


Figure 4 9a Fractured surface after tensile of one hour heat treated workpiece

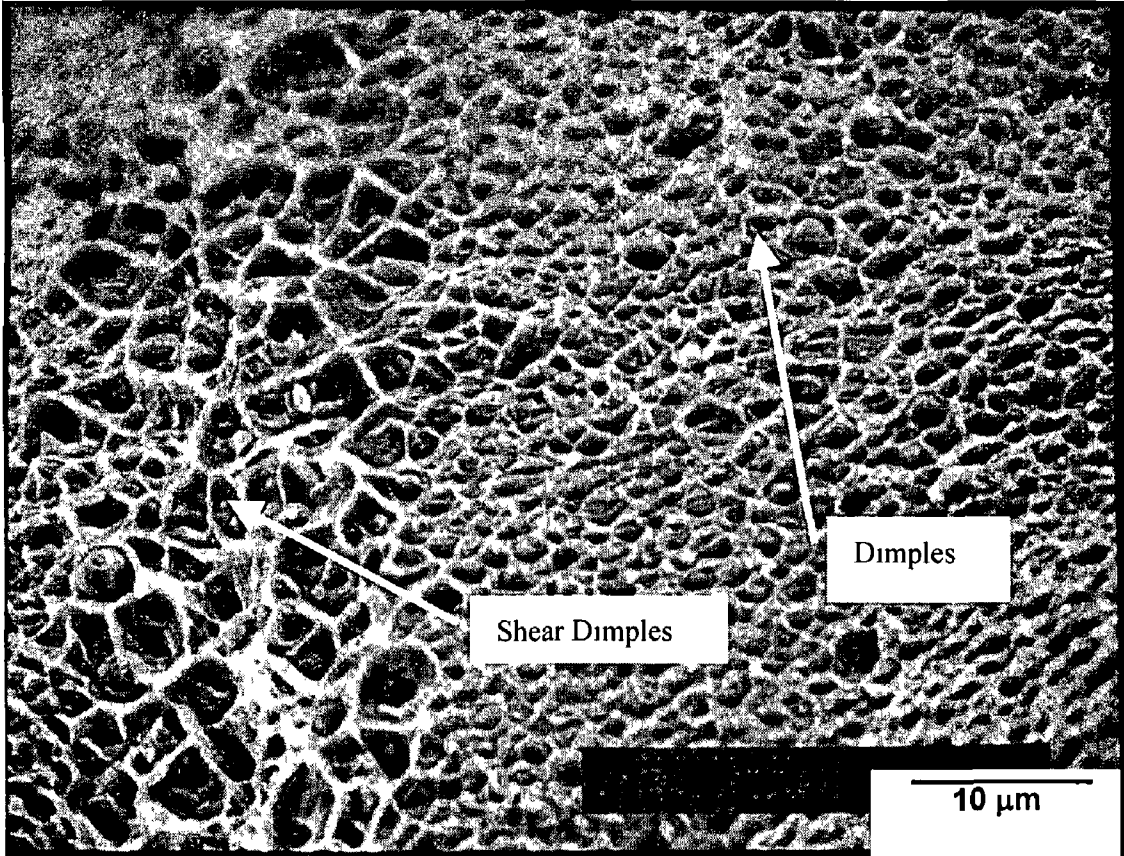
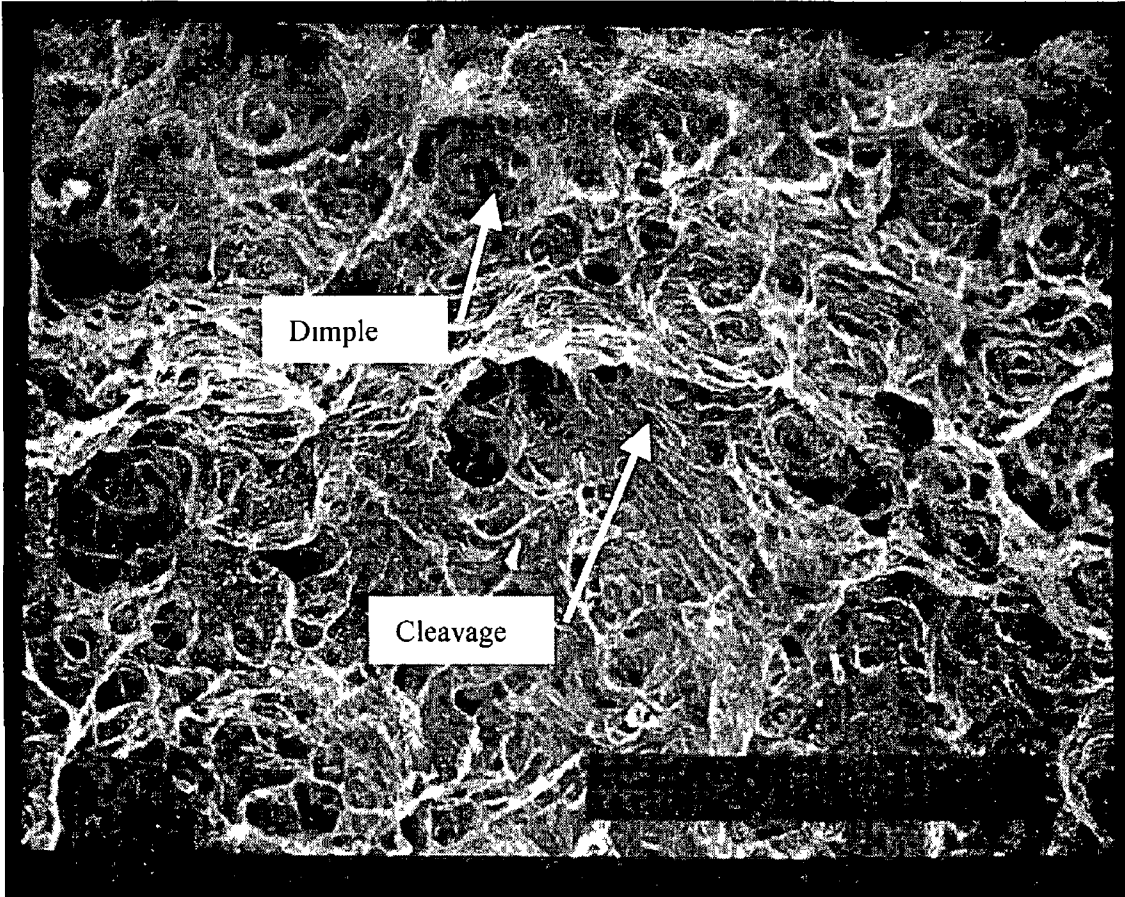
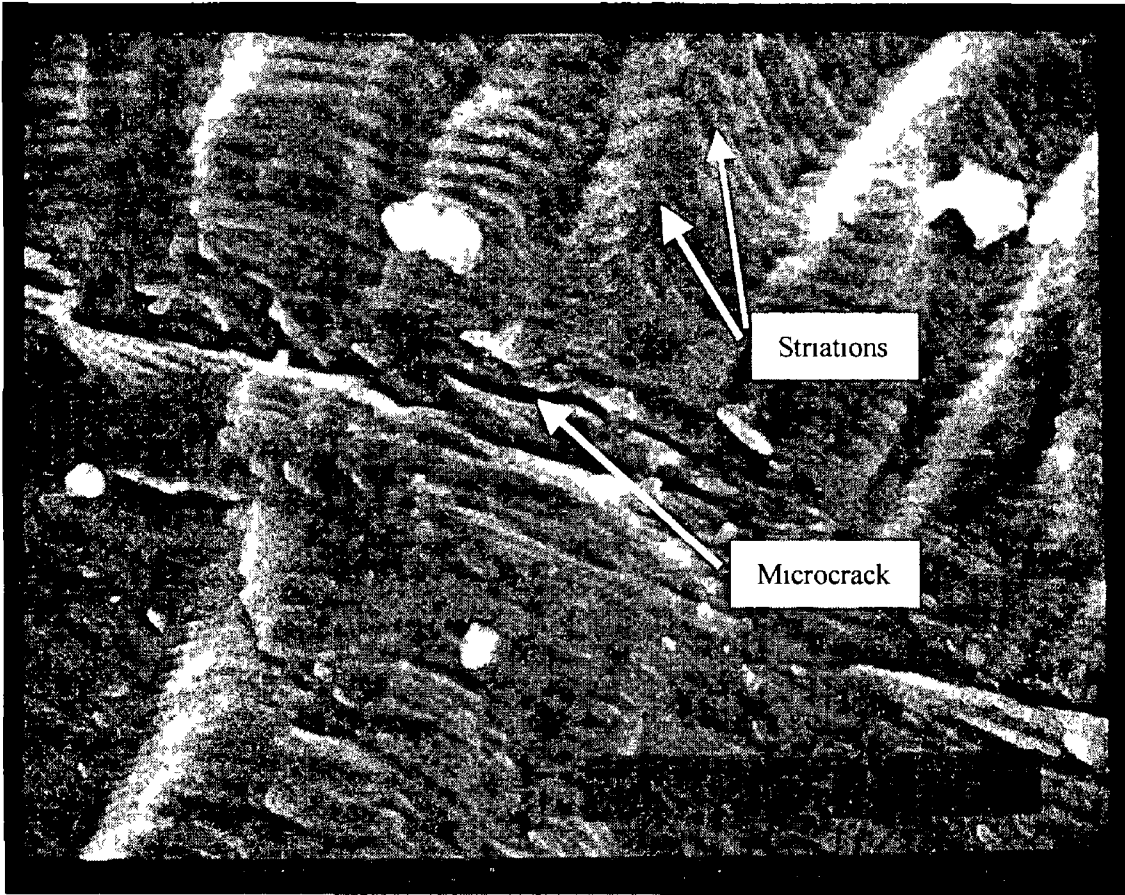


Figure 4 9b Dimples after tensile test of one hour heat treated workpiece



100 μm

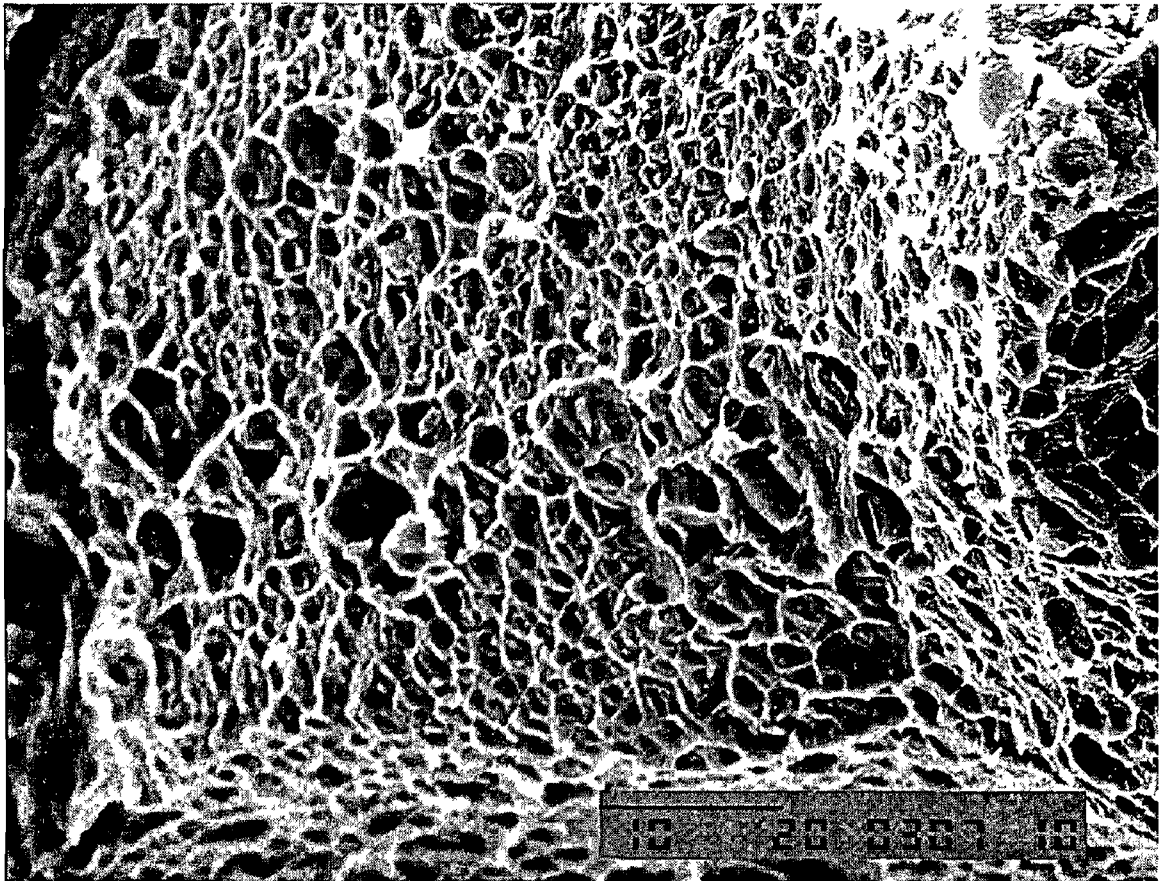
Figure 4 10a Fractured surface after fatigue test of one hour heat treated workpiece



10 μ m

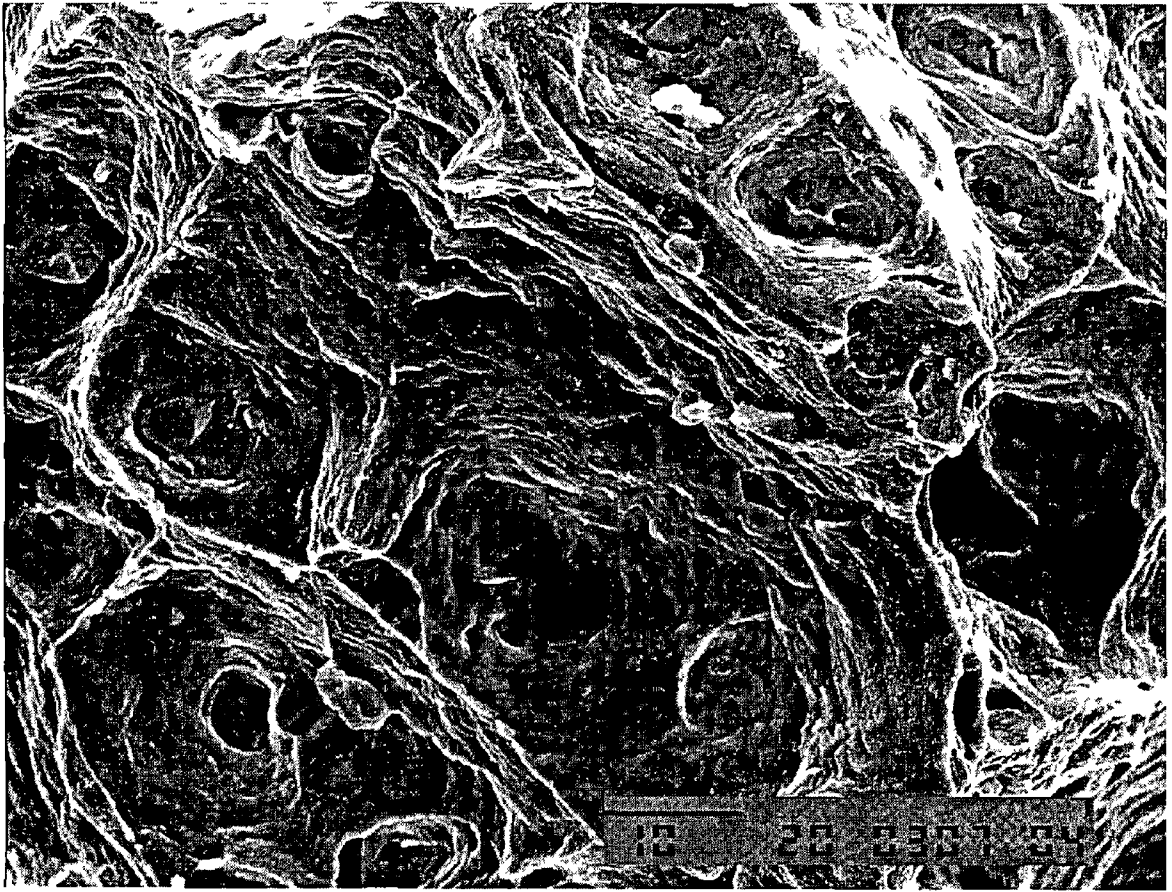
Figure 4 10b Dimples after fatigue test of one hour heat treated workpiece

Figure 4 11 shows the fractographs of the surface after fatigue and tensile tests of the electrochemically treated workpieces. The dimples, formed on the grain boundary facets, show the improved ductility of the workpieces after the heat treatment process. The dimple size varies, in which case micro-void coalescence produces unevenly distributed shear dimples with varying sizes. The large dimples are most likely formed at carbide particles, which is initiated by a large inclusion figure 4 12. Moreover, some fracture surface resembles cleavage facets, which result in low degree of flatness. It is also observed from high magnification fatigue fractured surfaces that the array of regular fatigue striations is evident at the transgranular facets figure 4 13a & b. In the region of electrochemically treated surfaces, dimples replace with the distorted surfaces, in which case oxide surface is seen figure 4 14.



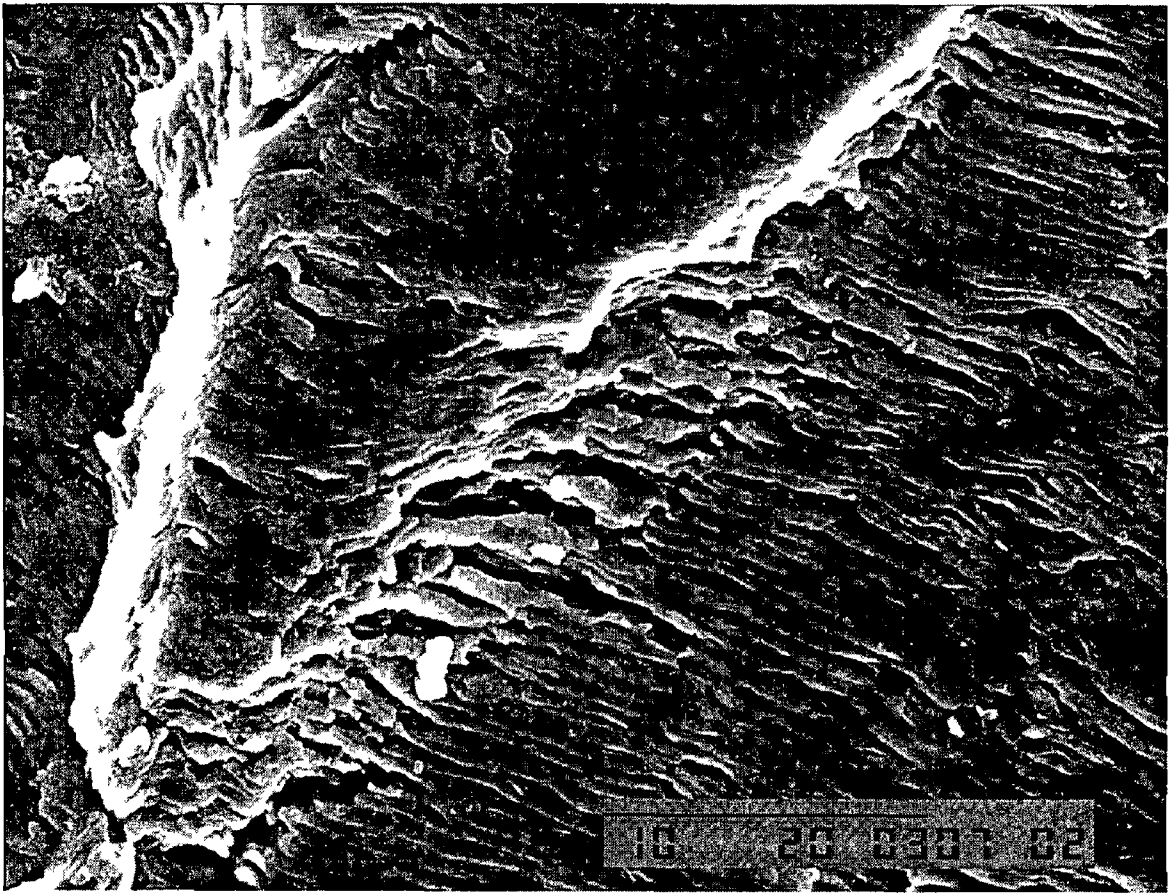
10 μ m

Figure 4 11 Fractographs of dimples after heat treatment and electrochemical test



10 μm

Figure 4 12 Fractographs of large dimples after one hour heat treated and electrochemical test



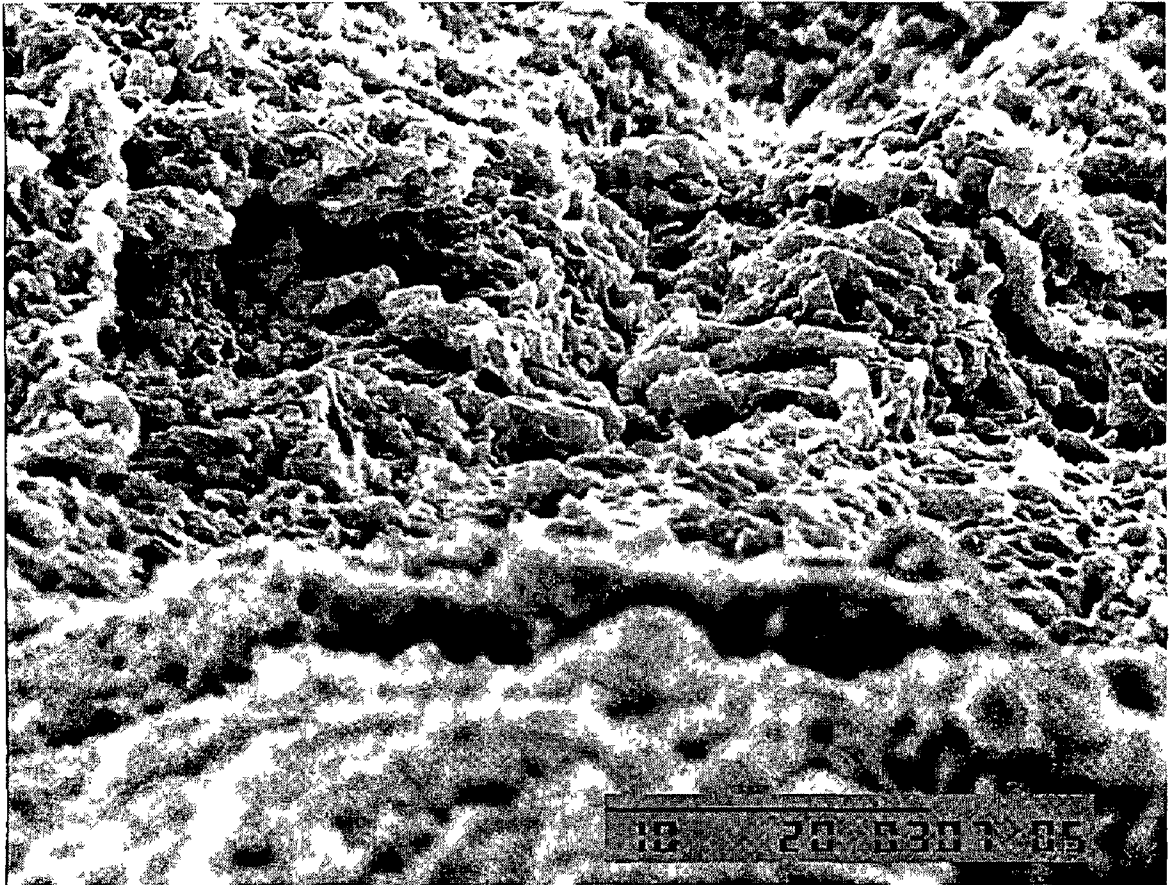
10 μm

Figure 4 13a Fractographs of striation patterns after one hour heat treated and electrochemical test



10 μ m

Figure 4 13 b Fractographs of striation patterns after one hour heat treated and electrochemical test



10 μ m

Figure 4 14 Fractograph obtained close to the workpiece surface after one hour heat treated and electrochemical test

The potentiodynamic polarization curves for untreated and heat-treated workpieces in 0.1 N H₂SO₄ and 0.005 N NaCl aqueous solution are shown in figure 4.15. The corrosion potential for one hour heat-treated workpiece is 132 mV, which is more noble than that of the untreated workpiece (190 mV). In addition, the corrosion current density for one hour heat-treated workpiece is almost half of that corresponding to the untreated surface. As the heat treatment duration is extended to two hours, the corrosion potential becomes higher than its counterpart corresponding to one hour heat-treatment, but it is less than that of untreated workpiece. These results indicate that the heat treatment reduces the anodic dissolution of the alloy either by forming an oxide layer at the material surface or slow down the removal of metal ions via complex ions formation.

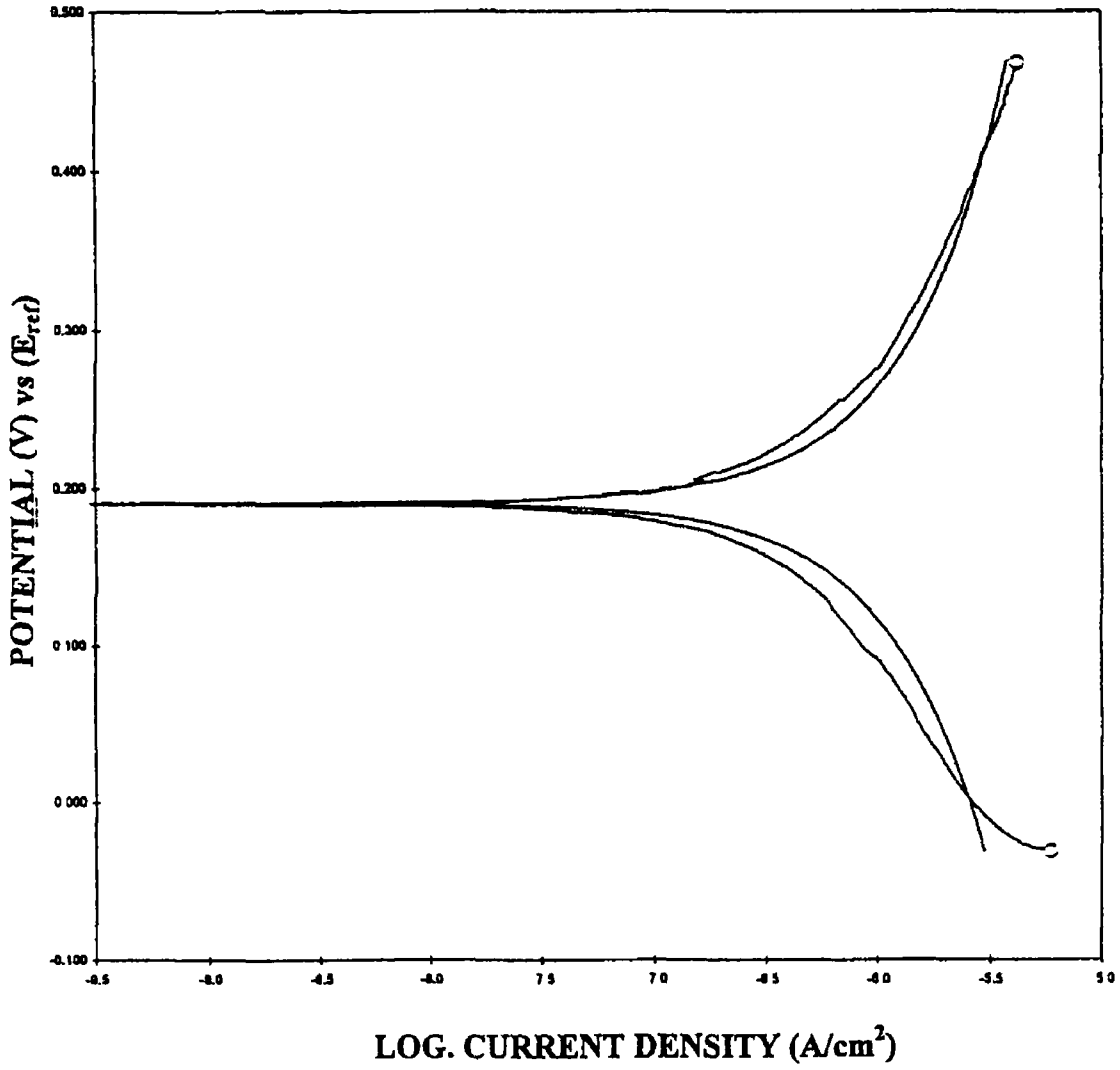


Figure 4 15a Polarization curve for untreated workpiece

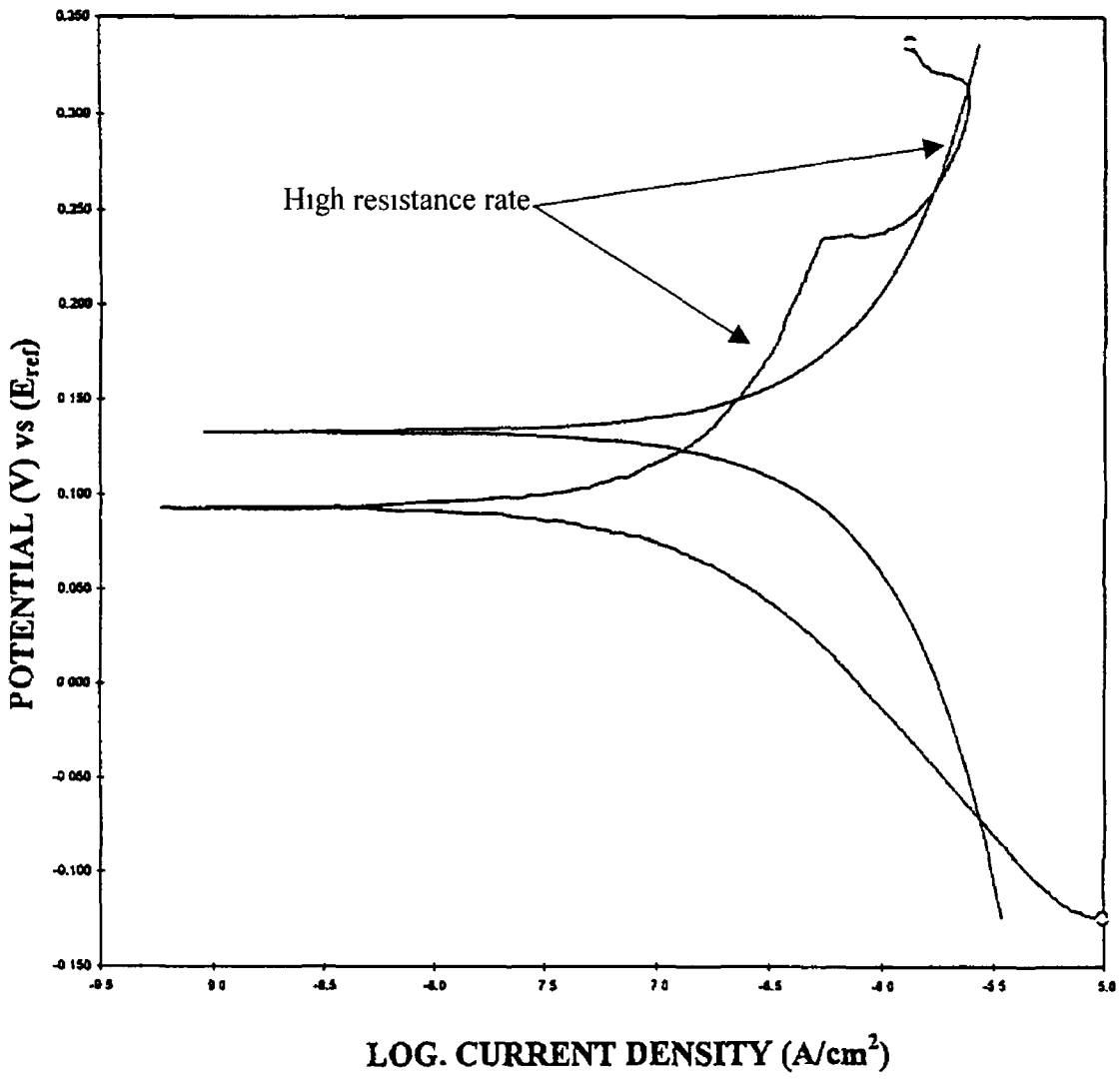


Figure 4 15b Polarization curve for one hours untreated workpiece

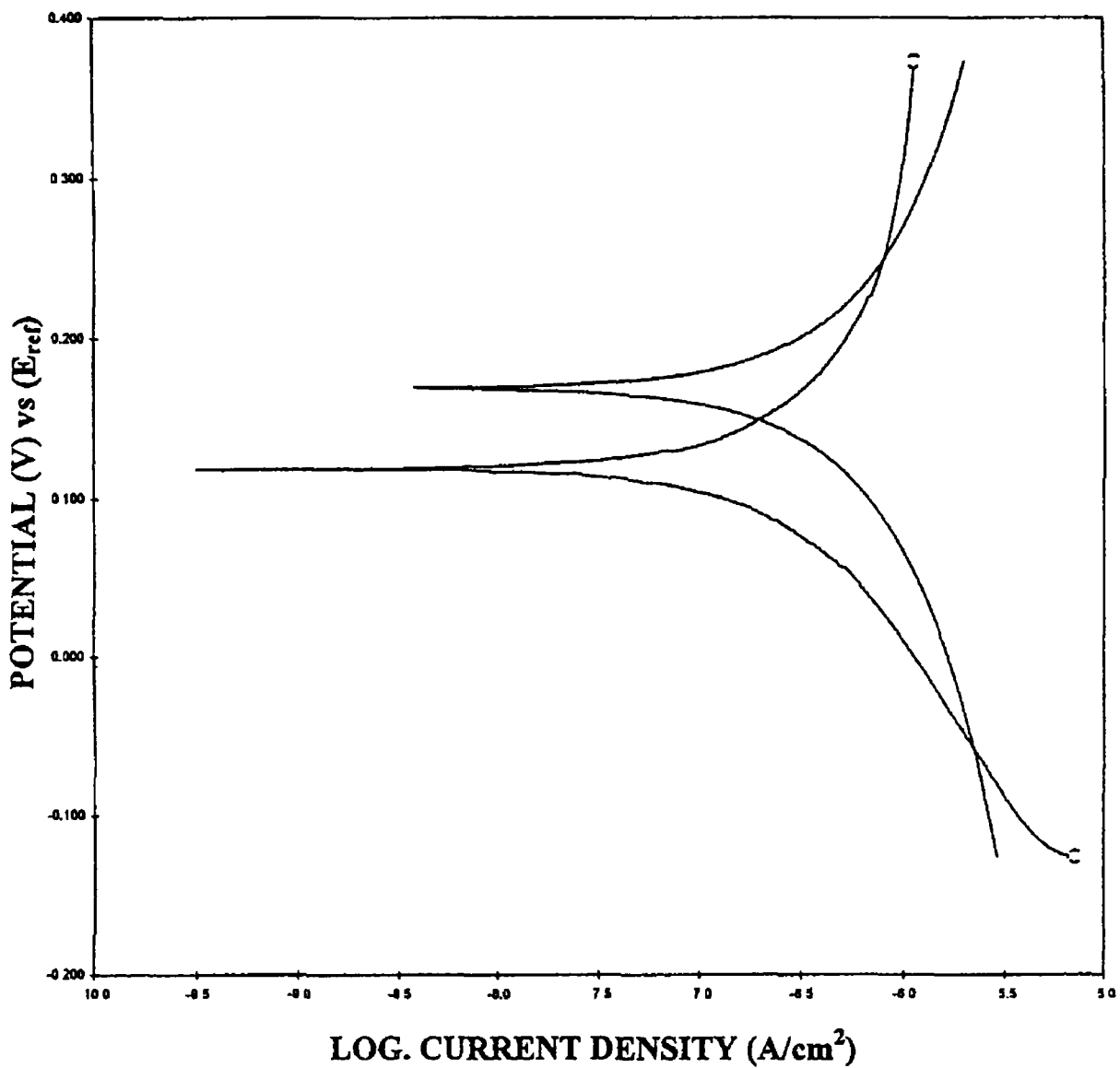


Figure 4 15c Polarization curve for two hours untreated workpiece

The TAFEL and polarization resistance results are given in tables 4.2 and 4.3. One hour heat-treated workpiece results in a minimum corrosion rate followed by two hours heat-treated workpiece and untreated workpiece in the increased order. The high corrosion rate of untreated workpiece is due to the partitioning out of solution of useful alloying elements after several thousands hours of operation. In this case, Cr, primary alloying element, depletes in the surface region of the workpiece, i.e. the protection of external surface of the alloy by forming Cr_2O_3 is suppressed, which is the primary reason for resistance to corrosion. Moreover, the workpiece before the heat treatment has segregated microstructure. This indicates that the material is no longer homogeneous as it was as new condition. The partitioned alloying elements combine with the residual carbon and form carbides. Once the alloying elements such as Cr and Mo form carbides, the grain boundary regions are depleted of these elements removing their passivation protection locally.

	E_{corr} mV	I_{corr} $A/cm^2 \times 10^{-7}$	Corrosion Rate (mpy)
Untreated	187	7.21	0.291
One Hour Heat-Treatment	96	1.51	0.157
Two Hour Heat-Treatment	115	5.25	0.31

Table 4.2 TAEFL results

	E_{corr} mV	I_{corr} $\text{A/cm}^2 \times 10^7$	Polarization Resistance $\Omega/\text{cm}^2 \times 10^4$	Corrosion Rate (mpy)
Untreated	191	9.61	7.49	0.381
One Hour Heat-Treatment	133	4.51	7.59	0.178
Two Hour Heat-Treatment	169	8.25	10.53	0.316

Table 4.3 Polarization resistance results

Figures 4.16, 4.17 and 4.18 show SEM microphotographs of workpiece surfaces after the electrochemical tests. The pit morphology gives the qualitative analysis of the corrosion product. The corrosion products in pits are being enriched in Cr and depleted in Ni and Fe. No specific pattern on the pit geometry is observed for the workpiece surfaces subjected to one hour heat-treatment (figure 4.17). In addition, the pit size is small and the pit density is less than the other workpieces. This indicates that higher Cr content in the alloy increases the acidification reaction in the pit and decreases the amount of precipitation. In this case, the mouth of pit serves as a cathode for the reduction of O_2 and it would attain a noble potential. In the case of untreated workpiece, the pit geometry shows significant lateral growth along the surface leading to elongated pits. The pit growth saturates after some time. This implies that the re-activation of pits being passivated, i.e., the secondary micropits play an important role in the re-activation process. Moreover, severe pitting over the grain boundary is evident from figure 4.16, in which case the formation of Cr and Mo oxides is unlikely in this region. In the case of two hours heat-treated workpiece (figure 4.18), localized deep pits are formed. In this case, during the pit growth the pit bottom acts as an anode galvanically coupled to the

external cathodic area leading to a steeper potential gradient in the pit. Consequently, the pit depth increases. In the later stage, ohmic resistance to current flow inside the pit is bound to develop due to formation of insoluble pit corrosion products causing polarization to a more noble potential and a lower corrosion current.

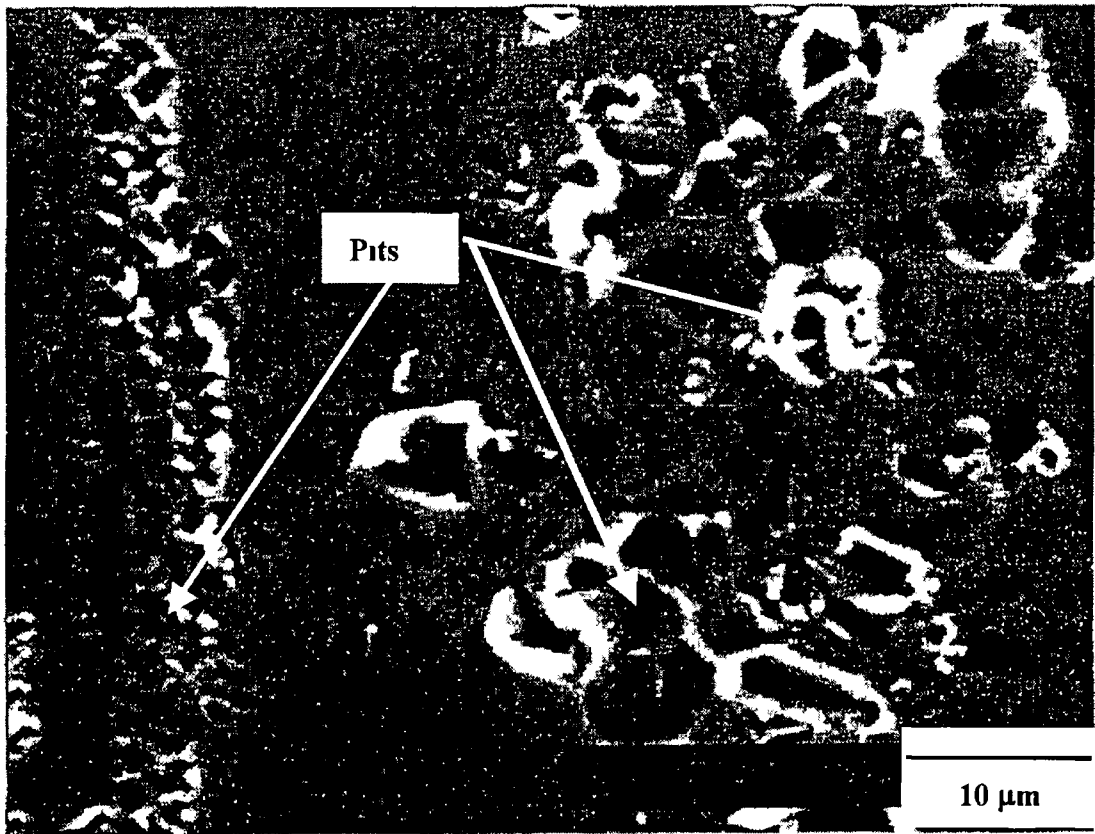


Figure 4 16 SEM microphotographs of pits developed on the surface of untreated workpieces

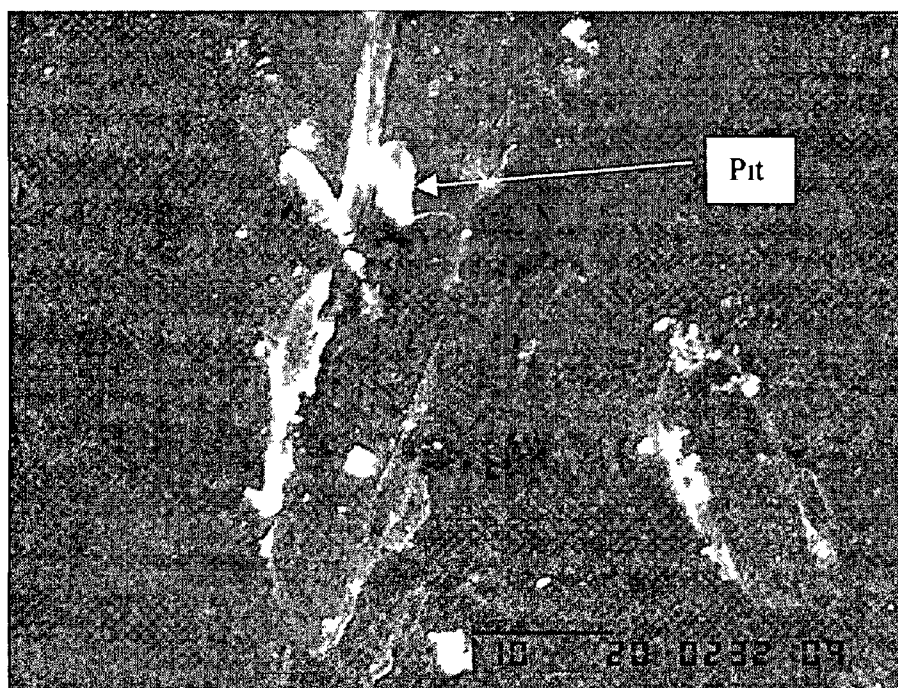
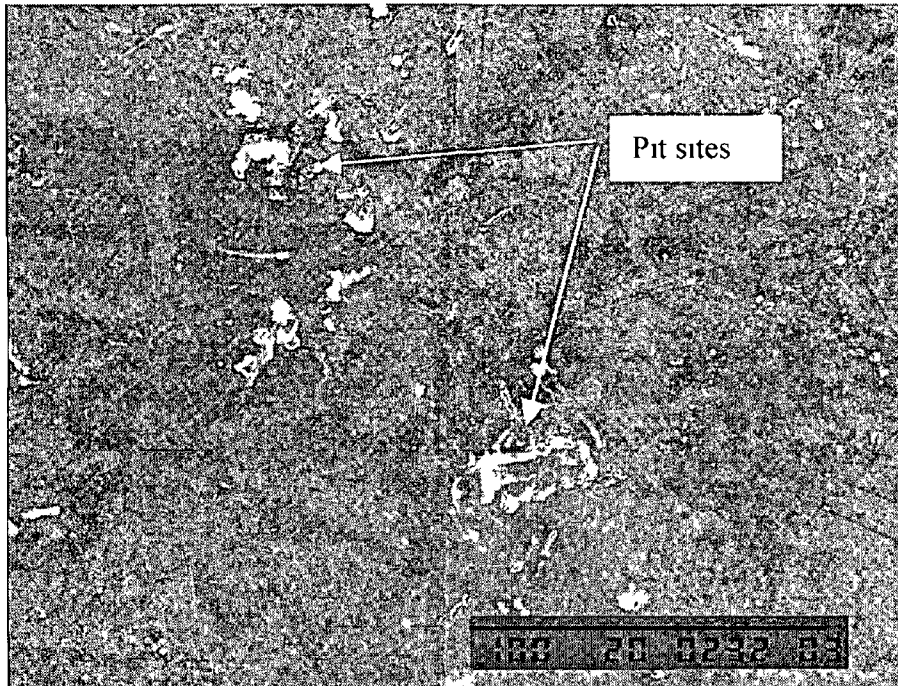
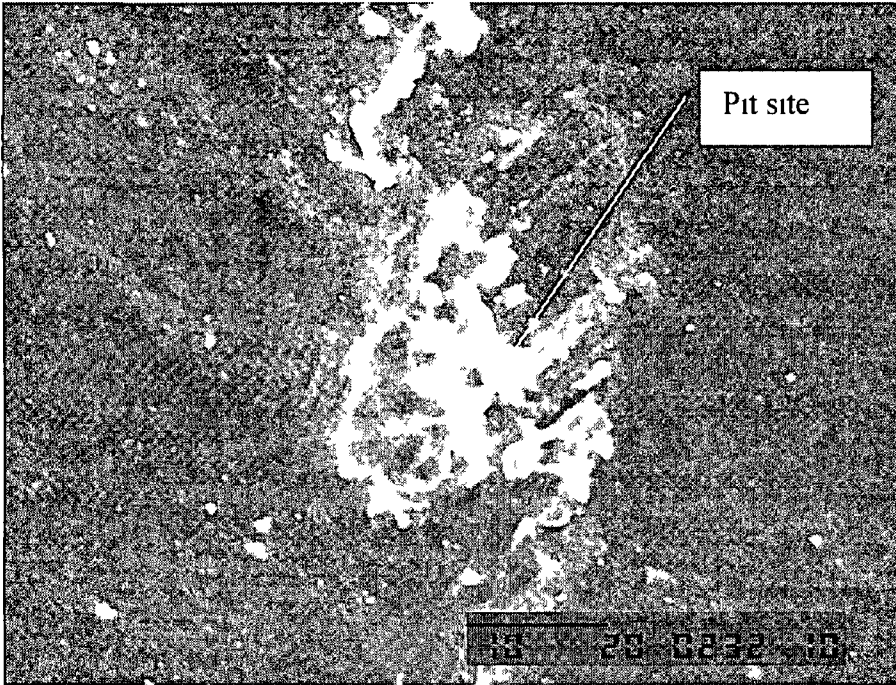


Figure 4 17 SEM microphotographs of pits developed on the surface of one hour treated workpieces



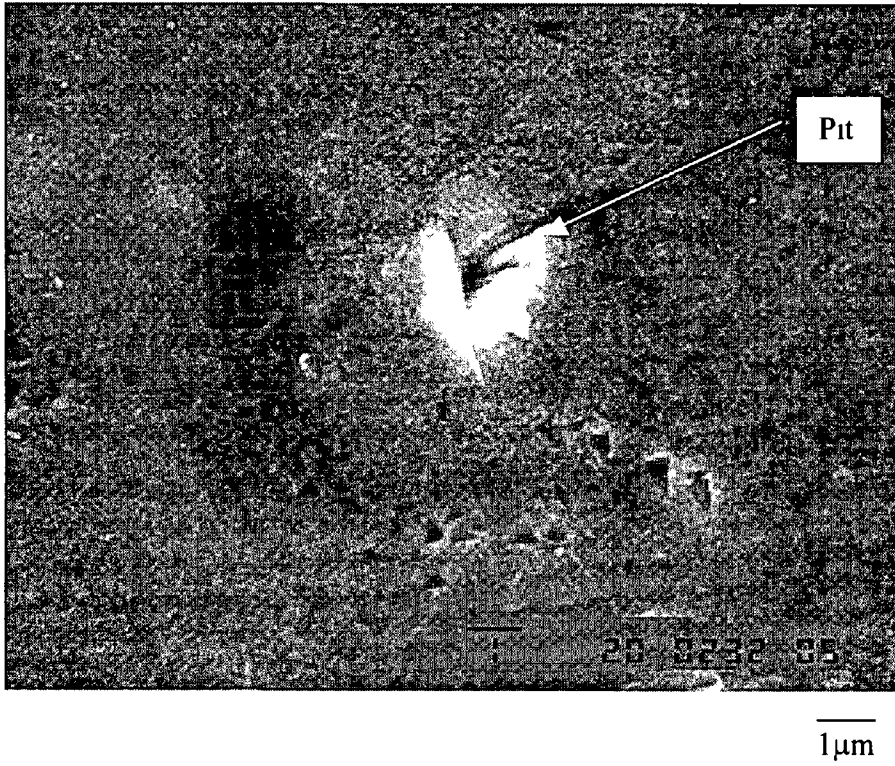


Figure 4 18 SEM microphotographs of pits developed on the surface of two hours treated workpieces

CHAPTER V

CONCLUSIONS AND RECOMMENDATION FOR FUTURE WORK

Inconel 617 alloy which was used for about 37000 hours of operation is examined through electrochemical and mechanical tests. The electrochemical tests are conducted using 0.1 N H_2SO_4 and 0.005 N NaCl aerated solution while fatigue and tensile tests are conducted for the evaluation of the electrochemical and mechanical properties of the heat-treated workpieces. The electrochemical response of the untreated and heat-treated workpiece surfaces is estimated through potentiodynamic measurements. It is found that the corrosion rate measured from TAFEL and polarization tests reduces for heat-treated workpieces. The depletion of Cr at the grain boundary increases the pitting density in this region. In general, it is found that heat treatment improves slightly corrosion resistance of the workpiece surface as well as tensile and fatigue properties of the alloy. Consequently heat treatment of the Inconel 617 alloy after long term of operation improves slightly its properties. Moreover, partial regaining of the alloy properties through heat treatment with temperature range and the duration employed in the present work is visible. The specific conclusions derived from the present work can be listed as follows

1. The cavitation along the grain boundaries is observed for the untreated workpieces. This reduces partially after the heat treatment process. The multiple discontinuous creep cracks are also observed. The depletion in Cr and Al contents at the grain boundary occurs for the untreated workpieces.

- 2 The fatigue response of the workpiece does not change considerably after the heat treatment process, since the heat treatment partly improves the grain boundary precipitation. Moreover, the grain boundary cracks are responsible for an increased effective stress and acceleration of fatigue failure. The existence of dimples at the fractured surfaces indicates the occurrence of the fast fracture. The fatigue property of the alloy slightly worsens after the electrochemical tests.

- 3 Heat treated surfaces are more noble than the untreated workpieces. This is because of forming oxide layer at the surface during the heat treatment process and removal of metal ions slows down due to complex ion formation. The depletion of Cr and Mo in the surface vicinity of the untreated workpieces accelerates the corrosion rate, i.e. the partitioning alloying elements are combined with the residual carbon forming the carbides.

- 4 One hour heat-treated workpiece results in a minimum corrosion rate and untreated workpiece in increased order. This is mainly because i) the partitioning out of solutions of alloying elements in the untreated workpiece after several thousand hours of operation, and ii) the microstructure of workpiece used for long hours is segregated, which in turn results in non-homogenous structure. Moreover, the alloying elements such as Cr and Mo form carbides at the grain boundary for the untreated workpiece, in which case, the passivation protection of these elements becomes less in this region.

- 5 The pit geometry does not yield any specific pattern. The pit size is small and its density is low for one hour heat-treated workpiece. In general, the shallow pits are observed at the workpiece surfaces. This suggests that the ohmic resistance to current flow inside the pit is bound to develop due to formation of insoluble pit corrosion products, which cause polarization to a more noble potential and a lower corrosion current.
- 6 The tensile tests show that the untreated workpieces have low strain, which occurs because of the grain boundary carbides, i.e. the brittleness of the alloy is enhanced. Heat treatment improves the ductility of the alloy slightly, in which case partial dissolution of carbide particles occurs and internal cavitation reduces. Exposure of the workpiece surfaces to aqueous solution lowers slightly tensile strength of the alloy. This is because of the partial surface oxidation and local pitting of the surface.
- 7 The dimples are observed on the grain boundary facets mainly for the heat treated workpieces. This indicates the improved ductility of the alloy after the heat treatment process. The dimple size varies and micro-void coalescence produces unevenly distributed shear dimples with varying size. The array of regular fatigue striations is observed at the transgranular facets. In the region close to the surface, where surface is subjected to chemical solution, dimples replace with distorted oxide surfaces.

RECOMMENDATION FOR FUTURE WORK

The heat treatment improves partially the metallurgical and mechanical properties of Inconel 617 after long term service. However, the surface degradation due to exposure to high temperature hostile environment influence considerably the properties of the alloy in the long term service. Therefore, protective coating or special treatment of the alloy surface will be expected to improve the life cycle of the alloy. Consequently two approaches can be proposed for the future study i.e

- 1 High velocity oxygen fuel coating (HVOF) of the transition piece surface. The investigation is then directed to examine the influence of the coating properties such as coating thickness and spraying powder composition, on the life cycle of the alloy.
- 2 Laser assisted melting of the alloy surface with high cooling rates. This provides formation of small grains in the surface region of the alloy. The properties of the alloy surface after the laser assisted processing need to be examined. In addition, the life time assessment of the alloy after the laser treatment process needs to be explored.

REFERENCES

- [1] N F Mott and F R Nabarro, Rep Conference Sol Phys Soc 1-9, 1948
- [2] Chester T Sims, Norman S Stoloff, William C Hagel, "Superalloys II page 66, 1987
- [3] P Ganesan, G D Smith, and D H Yates, "Performance of Inconel alloy 617 in Actual and Simulated Gas Turbine Environments", Material and Manufacturing Processes Vol 10 No 5 925-938, 1995
- [4] Sahn, P R and Speidel, M O , "High temperature materials in gas turbines" Elsevier , New York, 1 974
- [5] DeeL O L , "Engineering Data on New Aerospace Structural Material", AFMI -TR-75-97, Battel-Columbus Laboratories, June 1975
- [6] Mankins W L , J C Hosier, And T H Bassford, "Microstructure and Phase Stability of Inconel 617", Metallurgical Transaction Vol 5 pp 2579-2590, Dec 1974
- [7] Shigemitsu Kihara, John B Newkirk, Akira Ohtomo, and Yoshinori Saiga, "Morphological Changes of Carbides During Creep and Their Effects on the Creep Properties of Inconel 617 at 1000 °C", Metallurgical Transaction A 11A, pp 1019-1031, June 1980
- [8] Kazuaki Mino, Masaki Kitagawa, Akira Ohtomo and Yoshinori Saiga, "Effect of Thermal and Mechanical History on the Creep Rate of Inconel 617", Transaction Iron Steel Inst Japan, Vol 20, pp 826-832, 1980
- [9] Kazuaki Mino and Akira Ohtomo "Grain Boundary Migration and Recrystallization Creep Strength of Inconel 617", Transaction Iron Steel Inst Japan, Vol 18, pp 731-738, 1978
- [10] Whittenberger, J D, "Tensile properties of haynes alloy 230 and inconel 617 after long exposures to $\text{LiF}_{22} \text{CaF}_2$ ", Journal of Materials Engineering and Performance Vol 3 n 6 pp 763-774 Dec 1994
- [11] Whittenberger, J D, "77 to 1200 K tensile properties of several wrought superalloys after long-term 1093 K heat treatment in air and vacuum", Journal of Materials Engineering and Performance Vol 3, pp 91-103, Feb 1994

- [12] Pandey M C and Satyanarayana D V V , "Effect of gamma prime depletion on creep behavior of a nickel base superalloy (Inconel alloy x-750)", *Bulleting of Materials Science*, Vol 19, pp 1009-1015, 1996
- [13] Chavez S A , Korth G E , Harper D M and Walker T J , "High-temperature tensile and creep data for Inconel 600, 304 stainless steel and SA106B carbon steel", *Nuclear Engineering and Design*, Vol 148, pp 351-363, 1994
- [14] Komazaki S , Watanabe Y and Shoji T , "Changes in slip band etching characteristics of inconel 718 due to high-temperature low-cycle fatigue", *Transactions of Japan Society of Mechanical Engineers, Part A*, vol 63 A, pp 1481-1488, 1997
- [15] Swaminathan, V P , Owens, H B and Hicks, N , Evaluation of gas turbine transitions after 20,000 and 37,000 hours of service *International Gas Turbine and Aerospace Congress and Exposition Conference*, Cologne, Germany, 1992
- [16] Ennis P J , Long C J , Schulz B "Physical properties of carburized high-temperature alloys", *High Temperature High Pressure abbreviated journal*, Vol 15 No 4 pp 463-473, 1983
- [17] Venkatesh V and Rack H J , "Elevated temperature hardening of Inconel 690", *Mechanics of Materials*, Vol 30, pp 69-81, 1998
- [18] Ennis P J , Lupton D F , Nickel H , Schuster H , "Influence of carburization on the room temperature tensile properties of high-temperature alloys", Report, Kernforschungsanlage, Julich, West Germany, Pages 60, Many 1982
- [19] Solberg, J K and Thor, H , "Creep corrosion and thermal cycling of nickel alloys in combustion gas", Research Report, No,770160-2, The Norwegian Council for Scientific and Industrial Research, Norway, 1981
- [20] Hirose A , Sakata K and Kobayashi K F , "Microstructure and mechanical properties of laser beam welded Inconel 718", *Int J Materials and Product Technology*, Vol 13 pp 28-44, 1998
- [21] Kleinpass, Bernd Lang, Karl-Heinz Loehe, Detlef Macherauch, Eckard, "Influence of the mechanical strain amplitude on the in-phase and out-of-phase thermo-mechanical fatigue behavior of Ni Cr₂₂ Co₁₂ Mo₉", *ASTM Special Technical Publication n 1371 2000* ASTM, Conshohocken, PA, USA p 36-52, 2000

- [22] Boursier, J M, Desjardins, D, Vaillant, F, "The influence of the strain-rate on the stress corrosion cracking of alloy 600 in high temperature primary water", Corrosion Science v 37 p 493-508, Mar 1995
- [23] Sung, J K, "Effect of heat treatment on caustic stress corrosion cracking behavior of alloy 600", Corrosion v 55 no12 p 1144-54, Dec 1999
- [24] Popov, B N, Zheng, G, White, R E, " Surface treatment for inhibition of corrosion and hydrogen penetration of type 718 alloy", Corrosion v 50 p 613-19, Aug 1994
- [25] England, Diane M, Virkar, Anil V, "Oxidation kinetics of some nickel-based superalloy foils and electronic resistance of the oxide scale formed in air", Journal of the Electrochemical Society v 146 No 9 p 3196-202, Sept 1999
- [26] Dunn D S, Sridhar,N, Cragolino,G A ,” Effects of surface chromium depletion on localized corrosion of alloy 825 as a high-level nuclear waste container material” Corrosion v 51 p 618-24, Aug 1995
- [27] Shaikh, M A, Ahmad, M, Shoaib, K A , “ Precipitation hardening in Inconel 625”, Materials Science and Technology v 16 no2 p 129-32, Feb 2000
- [28] Chang, M, Koul, A K, Au, P, “Damage tolerance of wrought alloy 718 Ni-Fe-base superalloy”, Journal of Materials Engineering and Performance v 3 p 356-66, June 1994
- [29] Goods, S H, Bradshaw, R W, “Constant extension rate testing of Inconel 625 LCF in molten nitrate salt”, Corrosion Science v 41 no6 p 1119-37, June 1999
- [30] Tsai Ming Chang, Tsai Wen Ta, Lee Ju Tung, “ The effect of heat treatment and applied potential on the stress corrosion cracking of alloy 600 in thiosulfate solution” Corrosion Science v 34 p 741-57, May 1993
- [31] Heck,-K -A, Smith,-J -S, Smith,-R “INCONEL alloy 783 an oxidation-resistant, low expansion superalloy for gas turbine applications” Journal of Engineering for Gas Turbines and Power v 120 no2 p 363-9, Apr 1998
- [32] Yang I J “Localized corrosion of alloy 600 in thiosulfate solution at 25 °C” Corrosion v 49 p 576-84, July 1993

- [33] Szklarska Smialowska Z , Xia Z , Valbuena R R , “Mechanism of crack growth in alloy 600 in high-temperature deaerated water” *Corrosion* v 50 p 676-81, Sept 1994
- [34] Lim Yun Soo, Suh Jeong Hun, Kuk Il Hyun, “Microscopic investigation of sensitized Ni-base Alloy 600 after laser surface melting”, *Metallurgical and Materials Transactions Part A, Physical Metallurgy and Materials Science* v 28A p 1223-31, May 1997
- [35] Chen Z , Brooks J W , Loretto M H “Precipitation in Incoloy alloy 909”, *Materials Science and Technology* v 9 p 647-53, Aug 1993
- [36] McIntyre N S , Davidson R D , Walzak T L , “The corrosion of steam generator surfaces under typical secondary coolant conditions effects of pH excursions on the alloy surface composition”, *Corrosion Science* v 37 p 1059-83, July 1995
- [37] Acoff V L, Thompson R G, “Characterization of constitutional liquid film migration in nickel-base alloy 718”, *IBM Journal of Research and Development* v 44 no5 p 668-80, Sept 2000
- [38] Shankar, Vanı Rao, K Bhanu, Sankara Mannan S L, “Microstructure and mechanical properties of Inconel 625 superalloy”, *Journal of Nuclear Materials* V 288 N 2-3 p 222-232, Feb 2001
- [39] Wang J D , Gan D , “Effects of grain boundary carbides on the mechanical properties of Inconel 600”, *Materials Chemistry and Physics* v 70 n p 124-128 May 2001
- [40] Altın, Orhan Eser, Semih, “Analysis of carbonaceous deposits from thermal stressing of a JP-8 fuel on superalloy foils in a flow reactor”, *Industrial and Engineering Chemistry Research* v 40 n 2 p 589-595 Jan 2001
- [41] Antunes, F V , Ferreira J M , Branco C M , Byrne J , “High temperature fatigue crack growth in Inconel 718”, *Materials at High Temperatures* v 17 n 4 p 439-448, 2000
- [42] Dong, J X , Xie X S , Thompson R G , “Influence of sulfur on stress-rupture fracture in INCONEL 718 superalloys”, *Metallurgical and Materials Transactions A Physical Metallurgy and Materials Science* v 31 n 9 p 2135-2144, Sep 2000

- [43] Slama C , Abdellaoui M , “Structural characterization of the aged Inconel 718”, *Journal of Alloys and Compounds* v 306 p 277-284, 2000
- [44] Kleinpass Bernd, Lang Karl-Heinz, Loehe Detlef, Macherauch Eckard, “Influence of the mechanical strain amplitude on the in-phase and out-of-phase thermo-mechanical fatigue behaviour of $\text{NiCr}_{22}\text{Co}_{12}\text{Mo}_9$, Inconel 617”, *ASTM Special Technical Publication* n 1371 ASTM, Conshohocken, PA, USA p 36-52, 2000
- [45] Huang Jinfeng, Fang Hongsheng, Fu Xiaorong, Huang Fuxiang, Wan Hong, Zhang Qianfa, Deng Shiping, Zu Jisheng, “High-temperature oxidation behavior and mechanism of a new type of wrought Ni-Fe-Cr-Al superalloy up to 1300 degree C”, *Oxidation of Metals* v 53 n 3 p 273-287, 2000
- [46] England Diane M , Virkar Anil V , “Oxidation kinetics of some nickel-based superalloy foils and electronic resistance of the oxide scale formed in air Part I”, *Journal of the Electrochemical Society* v 146 n 9 p 3196-3202, 1999
- [47] Kusabiraki Kiyoshi, Maekawa Teruo, “Precipitation and growth of gamma double prime phase in a Ni-22Cr-9Mo-5Fe-4Nb superalloy”, *Tetsu-To-Hagane/Journal of the Iron and Steel Institute of Japan* v 85 n 3 p 241-248, 1999
- [48] Singh I B , “Effects of concentration and temperature on corrosion resistance of nickel base alloys in acidic environments”, *British Corrosion Journal* v 33 n 1 p 67-70, 1998
- [49] Kayano, Rinzo, Ishiguro Tohru, Nishimoto Kazutoshi, “Effect of Ni content on solidification cracking susceptibility of Ni-base superalloy Inconel 706”, *Yosetsu Gakkai Ronbunshu/Quarterly Journal of the Japan Welding Society* v 16 n 3 p 365-373, Aug 1998
- [50] Venkatesh Vasisht, Rack H J , “Elevated temperature hardening of Inconel 690”, *Mechanics of Materials* v 30 n 1 p 69-81, Sep 1998
- [51] Vishnudevan M , Venkatachari G , Muralidharan S , Rengaswamy N S , “Corrosion behaviour of Inconel 600 and 601 in orthophosphoric acid solutions”, *Anti-Corrosion Methods and Materials* v 45 n 4 p 248-251, 1998
- [52] Chen W , Chaturvedi MC , Richards NL , McMahon G , “Grain boundary segregation of boron in Inconel 718”, *Metallurgical and*

REFERENCE

- Materials Transactions A Physical Metallurgy and Materials Science v 29A n 7 p 1947-1954, Jul 1998
- [53] Patel Y, Tamboli D, Desai V H, Cheruvu N S, "Environmental degradation of gas turbine materials in steam", American Society of Mechanical Engineers (Paper) ASME, New York, NY, USA 15p 97-GT-293, 1997
- [54] Kawagoishi Norio, Chen Qiang, Tanaka Hideho, Maeno Ichiro, Kiyofuji Jun-ichi, "Characteristics of small crack growth in a nickel-base superalloy", Nippon Kikai Gakkai Ronbunshu, A Hen/Transactions of the Japan Society of Mechanical Engineers, Part A v 63A n 611 p 1398-1402, Jul 1997
- [55] Li Zhang, Gobbi S L, Fontana G, Richter H K, Norris J, "Investigation on the metallurgy and techniques in laser welding of wrought Inconel 718", Metallurgia Italiana v 89 n 5 p 41-47, May 1997
- [56] Chen W, Chaturvedi M C, "Dependence of creep fracture of Inconel 718 on grain boundary precipitates", Acta Materialia v 45 n 7 p 2735-2746, Jul 1997
- [57] Aleman B, Gutierrez I, Urcola J J, "Interface analysis on diffusion bonded bimetallic composites part II formation of intermetallics", Key Engineering Materials v 127-131 n Pt 1 p 703-710, 1997
- [58] Sun W R, Guo S R, Lu D Z, Hu Z O, "Effect of sulfur on the solidification and segregation in Inconel 718 alloy", Materials Letters v 31 n 3-6 p 195-200, Jun 1997
- [59] Gao Ming, Chen Shyuan-Fang, Chen Gim Syang, Wei Robert P, "Environmentally enhanced crack growth in nickel-based alloys at elevated temperatures", ASTM Special Technical Publication n 1297 p 74-84, 1997
- [60] Wen Juhua, Lu Jingju, Hu Zhihui, "Behavior of Inconel 600 and Inconel 690 in preoxidation processes with permanganate based (NP and AP)", Hedongli Gongcheng/Nuclear Power Engineering v 21 n 5 p 430-434, Oct 2000
- [61] Schwartz Adam J, Kumar Mukul, King Wayne E, "Influence of processing method on the grain boundary character distribution and network connectivity", Materials Research Society Symposium - Proceedings v 586 Materials Research Society, Warrendale, PA, USA p 3-14, 2000

- [62] Rong Yonghua, Chen Shipu, Hu Gengxiang, Gao Ming, Wei Robert P , “Prediction and characterization of variant electron diffraction patterns for gamma double prime and delta precipitates in an INCONEL 718 alloy”, *Metallurgical and Materials Transactions A Physical Metallurgy and Materials Science* v 30 n 9 p 2297-2303, Sep 1999
- [63] Hirose Akio, Liu Liufa, Kobayashi Kojiro F , “Laser surface annealing of Ni-base super alloy for enhancement of material performance in hydrogen environment”, *Proceedings of SPIE - The International Society for Optical Engineering* v 4088 Society of Photo-Optical Instrumentation Engineers, Bellingham, WA, USA p 236-239, 2000
- [64] Antunes F V , Ramalho A , Ferreira J M , “Identification of fatigue crack propagation modes by means of roughness measurements”, *International Journal of Fatigue* v 22 n 9 p 781-788, Oct 2000
- [65] Wu Xiaowei, Chandel R S , Li Hang, Seow H P , Wu Shichun, “Induction brazing of Inconel 718 to Inconel X-750 using Ni-Cr-Si-B amorphous foil”, *Journal of Materials Processing Technology* v 104 n 1 p 34-43 Aug 2000
- [66] Parker J D , Stratford G C , “Characterisation of microstructures in nickel based transition joints”, *Journal of Materials Science* v 35 n 16 p 4099-4107, Aug 2000
- [67] Khalid F A , Benjamin S E , “Effect of deformation substructure on the high-temperature oxidation of inconel 625”, *Oxidation of Metals* v 54 n 1 p 63-71 Aug 2000
- [68] Slama C , Servant C , Cizeron G , “Aging of the Inconel 718 alloy between 500 and 750 degree C”, *Journal of Materials Research* v 12 n 9 p 2298-2316 Sep 1997
- [69] Kim Jong Jip, Jung Jong Ho, Cho Seong Jai, Yoon Kyung Jin, “Solid particle erosion of Inconel 625 at elevated temperatures”, *Journal of Materials Science Letters* v 19 n 9 p 759 -761, 2000
- [70] Altın Orhan, Eser Semih, “Characterization of carbon deposits from jet fuel on Inconel 600 and Inconel X surfaces”, *Industrial and Engineering Chemistry Research* v 39 n 3 p 642-645, 2000
- [71] Kawaura Hiroyuki, Nishino Kazuaki, Saito Takashi, “New surface treatment using a fluidized bed for improving oxidation resistance of TiAl-base alloys”, *Nippon Kinzoku Gakkaishi/Journal of the Japan Institute of Metals* v 63 n 12 p 1584-1590, Dec 1999

- [72] Park Heung-Bae, Lee Byong-Whi, "Effect of specimen thickness on fatigue crack growth rate", *Nuclear Engineering and Design* v 197 n 1 p 197-203, 2000
- [73] Neville A , Hodgkiess T , "Characterisation of high-grade alloy behaviour in severe erosion-corrosion conditions", *Wear* v 233-235 p 596-607, Dec 1999
- [74] Chen Q , Kawagorishi N , Nisitani H , "Evaluation of fatigue crack growth rate and life prediction of Inconel 718 at room and elevated temperatures", *Materials Science and Engineering A Structural Materials Properties, Microstructure and Processing* v 277 n 1-2 p 250-257, Jan 31 2000
- [75] Yamamoto M , Ogata T , "Damage mechanisms of Inconel 738LC under creep-fatigue loading conditions", *Acta Metallurgica Sinica English Letters* v 11 n 6 p 470-476, 1998
- [76] Edris H, McCartney D G, Sturgeon A J, "Microstructural characterization of high velocity oxy-fuel sprayed coatings of Inconel 625", *Journal of Materials Science* v 32 p 863-72 Feb 15 1997
- [77] Lopez B, Gutierrez I, Urcola J J, "Microstructural analysis of steel-nickel alloy clad interfaces", *Materials Science and Technology* v 12 p 45-55 Jan 1996
- [78] Liu W C , Chen Z L , Yao M , "Effect of cold rolling on the precipitation behavior of delta phase in Inconel 718", *Metallurgical and Materials Transactions A Physical Metallurgy and Materials Science* v 30A n 1 p 31-40, Jan 1999
- [79] Liu Lin, Zhang Rong, Wang Liuding, Pang Shuxian, Zhen Baolin, "New method of fine grained casting for nickel-base superalloys", *Journal of Materials Processing Technology* v 77 n 1 p 300-3043, May 1 1998
- [80] Liu W C , Xiao F R , Yao M , Chen Z L , Jiang Z Q , Wang S G , "Influence of cold rolling on the precipitation of delta phase in Inconel 718 alloy", *Scripta Materialia* v 37 n 1 p 53-57, July 1 1997
- [81] Koterazawa Keiji, Inoue Shozo, Uchida Hitoshi, Kozono Yasushi, Tsurui Takafumi, "Intergranular corrosion and hydrogen embrittlement of sensitized SUS316 steel and Inconel 600", *Zairyo/Journal of the Society of Materials Science, Japan* v 46 n 9 p 1046-1050, Sep 1997

- [82] Cherian J T , Fisher R M , Castner D G , Dellwo R R , “Scanning AES and XPS analysis of a thin Au emissivity barrier on Ni alloy”, *Journal of Materials Science* v 36 n 17 p 4189-4194, Sep 1 2001
- [83] Ashour E A , “Crack growth rates of Inconel 600 in aqueous solutions at elevated temperature”, *Journal of Materials Science* v 36 n 3 p 685-692, 2001
- [84] Hong S J , Chen W P , Wang T W , “A diffraction study of the gamma double prime phase in INCONEL 718 superalloy”, *Metallurgical and Materials Transactions A Physical Metallurgy and Materials Science* v 32 n 8 p 1887-1901, August 2001
- [85] Yilbas B S , Khaled M , Gondal M A , “Electrochemical response of laser surface melted inconel 617 alloy”, *Optics and Lasers in Engineering* v 36 n 3 p 269-276, September 2001
- [86] Guoge Z , Chandel R S , Seow H P , “Solid-state diffusion bonding of Inconel alloy 718 to 17-4 PH stainless steel”, *Materials and Manufacturing Processes* v 16 n 2 p 265-279, March 2001
- [87] Cooper K P , Sledobnick P and Thomas E D , “Seawater corrosion of laser surface modified Inconel 625 alloy”, *Materials Science and Engineering*, Vol A206, pp 138-149, 1996
- [88] Ho J T and Yu G P , “Pitting corrosion of Inconel 600 in chloride and thiosulfate anion solutions at low temperature”, *Corrosion*, Vol 48, pp 147-156, 1992
- [89] Gonzalez-Rodriguez J G and Fionova L , “Effect of structural evolution in Inconel 601 on intergranular corrosion”, *Materials Chemistry and Physics*, Vol 56, pp 70-73, 1998
- [90] Chen W, Chaturvedi M C , Richards N L , “Effect of boron segregation at grain boundaries on heat affected zone cracking in wrought INCONEL 718”, *Metallurgical and Materials Transactions A Physical Metallurgy and Materials Science* v 32 n 4 p 931-939 April 2001
- [91] Rabbanı F , “Some observations on the morphology and structure of high temperature oxides formed on three superalloys as a result of the superficial application of $Ce(SO_4)_2$ ”, *Surface and Coatings Technology* v 140 n 2 p 67-75 May 30 2001

- [92] Zupanic F, Boncina T, Krizman A, Tichelaar F D, "Structure of continuously cast Ni-based superalloy Inconel 713C", *Journal of Alloys and Compounds* v 329 n 1-2 Nov 14 p 290-297, 2001

PAPERS IN CONFERENCES AND JOURNALS

- 1 Kewther M A , Hashmi M S J and Yilbas B S ,” Fatigue properties of refurbished Inco-617 alloy”, Proceeding of International Conference on Advances in Materials and Processing Technologies, AMPT’98, pp 963-969, Dublin, Ireland, 3-6, August 1999
- 2 Kewther M A , Yilbas B S , Hashmi, M S J , “Corrosion properties of Inconel 617 alloy after heat treatment at elevated temperature”, ASM, Journal of Materials Engineering and Performance v 10 p 108-113, Feb 2001
- 3 Kewther M A , Yilbas B S , Hashmi, M S J , “Tensile and fatigue testing of Inconel 617 alloy after heat treatment and electrochemical tests”, Industrial Lubrication and Tribology v 53 n 3 p 112-118, June 2001
- 4 Kewther M A , Yilbas B S , Hashmi, M S J , “Fatigue properties of refurbished Inco-617 alloy”, J Material Processing Technology, accepted for publication